AEDC-TR-66-212

ARCHIVE COPY
DO NOT LOAN

cy 1

MEASUREMENT OF GAS DENSITY BY ELECTRON SCATTERING

J. W. Cunningham and C. H. Fisher

ARO, Inc.

PROPERTY OF U. S. AIR FORCE
AEDC LIBRARY

February 1967

Distribution of this document is unlimited.

PROPULSION WIND TUNNEL FACILITY
ARNOLD ENGINEERING DEVELOPMENT CENTER
AIR FORCE SYSTEMS COMMAND
ARNOLD AIR FORCE STATION, TENNESSEE

AEDC TECHNICAL LIBRARY
5 0720 00031 3650

PROPERTY OF U. S. AIR FORCE
AEDC LIBRARY
AF 40(600)1200

NOTICES

When U. S. Government drawings specifications, or other data are used for any purpose other than a definitely related Government procurement operation, the Government thereby incurs no responsibility nor any obligation whatsoever, and the fact that the Government may have formulated, furnished, or in any way supplied the said drawings, specifications or other data, is not to be regarded by implication or otherwise, or in any manner licensing the holder or any other person or corporation, or conveying any rights or permission to manufacture, use, or sell any patented invention that may in any way be related thereto.

Qualified users may obtain copies of this report from the Defense Documentation Center.

References to named commercial products in this report are not to be considered in any sense as an endorsement of the product by the United States Air Force or the Government.

ERRATA

AEDC-TR-66-212, February 1967

MEASUREMENT OF GAS DENSITY
BY ELECTRON SCATTERING

J. W. Cunningham and C. H. Fisher, ARO, Inc.

Arnold Engineering Development Center
Air Force Systems Command
Arnold Air Force Station, Tennessee

The information on the reverse of this page should be substituted for the information on p. ii in AEDC-TR-66-212.

FOREWORD

The work reported herein was done for the Air Force Systems Command (AFSC), under Program Element 61440514, Project 8951, Task 895105.

The results of research which are presented in this report were obtained by ARO, Inc. (a subsidiary of Sverdrup & Parcel and Associates, Inc.), contract operator of the Arnold Engineering Development Center (AEDC), AFSC, Arnold Air Force Station, Tennessee, under Contract AF 40(600)-1200. The research was conducted from October 18, 1963, to September 30, 1965, under ARO Project No. PL2419, and the report was submitted by the authors on September 26, 1966.

Some of the information reported herein was presented at the 2nd International Congress on Instrumentation in Aerospace Simulation Facilities, August 29-31, 1966, held at Stanford University.

This work was funded partially by NASA under Project Super. These funds were used to extend the work beyond 50,000 v. A 350,000-v electron gun has been built, but test results using this gun are incomplete. Only the work at 50,000 v is reported here.

This technical report has been reviewed and is approved.

Fred W. Alles
1/Lt, USAF
Research Division
Directorate of Plans and Technology

Edward R. Feicht
Colonel, USAF
Director of Plans and Technology

MEASUREMENT OF GAS DENSITY BY ELECTRON SCATTERING

J. W. Cunningham and C. H. Fisher

ARO, Inc.

Distribution of this document is unlimited.

AF - AEDC
Arnold AFS Tenn

FOREWORD

The work reported herein was done for the Air Force Systems Command (AFSC), under Program Element 61440514, Project 8951, Task 895105.

The results of research which are presented in this report were obtained by ARO, Inc. (a subsidiary of Sverdrup & Parcel and Associates, Inc.), contract operator of the Arnold Engineering Development Center (AEDC), AFSC, Arnold Air Force Station, Tennessee, under Contract AF 40(600)-1200. The research was conducted from October 18, 1963, to September 30, 1965, under ARO Project No. PL2419, and the report was submitted by the authors on September 26, 1966.

Some of the information reported herein was presented at the 2nd International Congress on Instrumentation in Aerospace Simulation Facilities, August 29-31, 1966, held at Stanford University.

This work was funded partially by NASA under Project Super, Project 9514/951405. These funds were used to extend the work beyond 50,000 v. A 350,000-v electron gun has been built, but test results using this gun are incomplete. Only the work at 50,000 v is reported here.

This technical report has been reviewed and is approved.

Edward R. Feicht
Colonel, USAF
AF Representative, PWT
Directorate of Test

Leonard T. Glaser
Colonel, USAF
Director of Test

ABSTRACT

It is theoretically possible to infer the density of a gas from the rate at which particles are scattered out of a beam of subatomic particles which is passed through the gas. This technique offers the possibility of a probeless density measurement which is independent of the state of the gas. Previous research verified that this technique could be implemented using a gamma ray beam, but that the best spatial resolution and measuring time which could be achieved were inadequate to allow the technique to be applied to a low density test facility. In the research reported herein, the technique was applied using a 50,000-v electron beam. It was found that excellent spatial resolution and measuring time could be achieved at densities as low as 6×10^{-8} gm/cm^3. Density profiles were measured in a low density wind tunnel with a nozzle exit diameter of 18 in. and an open jet test section. A spatial resolution of about 1 cm was achieved, and measurements required 10 sec per point. This measuring time can probably be reduced by several orders of magnitude if necessary. The densities measured were repeatable within 1 percent. Accuracy, spatial resolution, and measuring time are found to be interrelated. The constraint on the combination is discussed in detail. The design of equipment is discussed.

CONTENTS

APPENDIXES

I. Illustrations

NOMENCLATURE

Units: cgs units are used with two exceptions: pressure is measured in torr, or microns of mercury, and electrical quantities are measured in practical units.

A	Atomic weight, atomic mass units
a	Spatial resolution along the beam, cm
b	Impact parameter, cm
b	Collimator dimension, cm (see Fig. 34a)
C	Number of electrons counted in time T
c	Average counting rate, electrons/sec
c	Collimator dimension, cm (see Fig. 34a)
D	Distance from sensitive volume to collimator entrance, cm
D(C)	Standard deviation of the variate, C
d	Collimator dimension, cm (see Fig. 34a)
E(C)	Expected (average) value of the variate, C
E_e	Rest energy of an electron, 510,984 ev
e	Charge of an electron, 1.60207×10^{-19} coulomb
$F(\beta)$	A function defined by Eq. (5)
f	Collimator dimension, cm (see Fig. 34a)
$G(\theta)$	A function defined by Eq. (6)
g	Collimator dimension, cm (see Fig. 34a)
$H(\beta, \theta, Z)$	A function defined by Eq. (4)
I	Beam current, amp
K	A constant, 12.362
ℓ	Beam length between gun and sensitive volume, cm
N_A	Avogadro's number, 6.02472×10^{23} particles/gm mole
n	Atomic number density, atom/cm^3
Q	A parameter defined by Eq. (9), cm
Q_ℓ	Q of a lens collimator, cm

Q_{opt}	Q of a slit collimator of optimum design, cm
r_b	rms beam radius, cm
r_e	Classical radius of an electron, 2.81784×10^{-13} cm
S_b	Cross-sectional area of electron beam, cm^2
s_ℓ	Lens area, cm^2
T	Measuring time, sec
t	Detector diameter, cm
V	Beam voltage, v
w	Width of detector which is visible, cm
x	Thickness of scattering medium, cm
y	Distance from axis of collimator, cm
Z	Atomic number
α_{ij}	Number of atoms of type i in molecule of type j
β	Ratio of speed of a particle to speed of light
β_j	Fraction by volume of molecules of type j in a mixture
γ	Dimensionless beam radius, r_b/ℓ
δ	Dimensionless spatial resolution, a/D
ϵ	Fractional statistical accuracy
θ	Scattering angle, radians
ν	Average number of atoms per molecule in a mixture
ρ	Mass density of a gas, gm/cm^3
σ	Scattering cross section per atom, cm^2
$\Phi(\beta, \theta, Z)$	Differential scattering cross section per atom, $d\sigma/d\Omega$, cm^2
Ω	Solid angle subtended by detector, steradians

SECTION I
INTRODUCTION

In 1961 Dr. John B. Dicks, acting as a consultant to ARO, Inc., investigated the possibility of applying the methods of the physics laboratory toward solving some of the measurement problems which were plaguing the aerospace field. His suggestions were presented in a report which was circulated within the Arnold Engineering Development Center. One of his proposals was that the density of a gas at a point could be inferred from measurements of the scattering of subatomic particles in the gas. The possibility is obviously attractive; first, because the gas flow need not be disturbed by material probes, and second, because the method is applicable to high enthalpy flows wherein the use of probes may be impossible.

The principle of measurement is indicated in Fig. 1. A beam of particles traverses the gas flow. The type and energy of the particles are chosen so that very nearly the entire beam reaches the collector without suffering collisions with gas molecules. All along the beam, however, such collisions occasionally occur, and the colliding particle is scattered out of the beam in a random direction. If a particle detector is fitted with a collimator so that it views a portion of the beam, it will intercept a fixed fraction of the particles which are scattered within this portion of the beam, the fraction being determined by the size and position of the detector. Since the probability that a collision will occur is proportional to the number of molecules exposed to the beam, the rate at which particles are detected is proportional to the gas density. The measurement is made in the volume defined by the intersection of the beam and the field of view of the detector.

The type and energy of the particles can be chosen to fit the circumstances; i.e., the density and composition of the gas, the physical size of the apparatus, the time available for measurement, and so forth. The choice is influenced by the following considerations:

1. The scattering cross section must be high enough so that a sufficient number of particles will be detected in the time available, and yet low enough so that the beam intensity will not vary appreciably between source and collector.
2. The particles must be easily detected.
3. It must be possible to collimate the particles into a well defined beam.

4. The particles must be available in sufficient numbers from a source which is convenient in terms of size, weight, cost, and safety hazard.
5. The source must in most cases produce particles of a well defined energy.

The initial work on this concept of measurement was done using gamma rays (photons) from a radioactive source (cesium 137) and is described in Ref. 1. Measurements were made in the flame of a propane torch which agreed with conventional aerodynamic measurements, and the counting rates observed were found to be in agreement with the assumed scattering mechanism, Compton scattering. Compton scattering is the process wherein photons are scattered out of a beam by collisions with atomic electrons. However, the source was found to be inconvenient to handle because of the safety hazard involved and the heavy lead shielding which was necessary. It was also extremely inefficient. Photons are emitted in all directions, and those which are emitted in the desired direction represent a minute fraction of the total. Furthermore, these particles were difficult to collimate, since they penetrate a half-inch of lead, the best shielding material available. Long measuring times were necessary (several minutes), and the prospects for reducing the required time were not bright. In retrospect, it appears that the method might be used with gamma rays at high densities (atmospheric and above) in applications requiring only modest spatial resolution.

In order to apply this method to an aerospace test facility, it was necessary to obtain significant improvements in spatial resolution and measurement time over those which could be achieved with gamma rays. These improvements were achieved by using electrons with 50-kev energy as the probing particle. Since the electrons carry a charge, it is possible to focus them in the desired direction, so that a smaller, far more intense beam can be obtained than is available from a gamma ray source. This intense beam, coupled with a scattering cross section which is several orders of magnitude larger than the cross section for gamma scattering, results in shorter measuring times at much lower densities than can be achieved with gamma rays. The safety hazard is reduced, because the electrons are much less penetrating than gamma rays and because the electron gun emits electrons only when actually in use. The electron beam does generate X-rays, however, and personnel radiation monitoring and some shielding must be used. It is a problem which has been easy to handle, but it is one which must be dealt with.

Electron beams have been used in the past for density measurements. In several instances, the attenuation of the beam in traversing the gas has been calibrated in terms of density (Refs. 2, 3, and 4). This technique suffers from several theoretical objections and also has one severe operational disadvantage: The density measured is a function of the gas density along the entire length of the beam, and if density gradients are present, the measurement is difficult to interpret.

The beam has also been used to induce fluorescence in the gas. Over a range of densities, the light output per unit length of beam is proportional to density. A photocell and collimator can be arranged to view a small portion of the beam and thus to make a point density measurement. This technique has been successfully applied in wind tunnels several times (Refs. 5, 6, and 7). The method fails at densities high enough so that excited molecules lose energy by processes other than radiation (e.g., collisions with other molecules). On the low density end, the method fails when sufficient light is no longer available from the beam or when background radiation becomes a problem. It presently appears that the scattering technique can be applied at both higher and lower densities than the fluorescence technique.

It is also possible to analyze the light from the beam spectroscopically. This technique offers exciting possibilities for determining the exact state of a nonequilibrium gas and perhaps even its velocity (Refs. 8, 9, and 10).

The possibility of using electron scattering for density measurements has been discussed (Refs. 11 and 12), and the method has been successfully applied in at least one instance to a shock tunnel (Ref. 13). In this application, individual electrons were not detected, but only the cumulative effect of many electrons striking the detector. The ultimate capabilities of the method for spatial resolution were not utilized, but the short measuring time capability was. Measurements were made in several microseconds.

An adequate theory to account for electron scattering has been available for many years: The deviation of the electron from its initial straight path is caused by the coulomb attraction between the electron and the positively charged atomic nucleus. This process is known as Rutherford scattering. The work reported here was not undertaken in order to learn anything basic about particle physics, and it came as no surprise that the Rutherford theory satisfactorily accounted for the detected counting rates. The work was done, on the other hand, to determine whether the mundane problems of generating the beam and detecting the scattered electrons could be solved, and to gain experience in these areas.

Most of the effort which went into this project was spent in these areas: First, generating a well focused beam (which must be done at a pressure on the order of 10^{-5} torr Hg) and injecting it into the test gas, which is at a pressure of 1 to 1000 μ Hg; Second, detecting the scattered electrons in the presence of amplifier noise, and verifying that they arrive with the correct numbers and energies; Third, measuring the effect of various parameters on beam spreading; that is, determining what spatial resolution can be achieved; and Fourth, applying the method to a low density wind tunnel.

SECTION II
THEORY OF RUTHERFORD SCATTERING

2.1 COLLISIONS OF ELECTRONS WITH ATOMS

When a beam electron encounters an atom of the scattering medium, the interaction between the two is described as a collision. Since the De Broglie wavelength of the beam electron is small (of the order of 5×10^{-10} cm) compared to the dimensions of an atom, the beam electron does not see the atom as a single particle but as a collection of inidividual electrons and a nucleus.

In a collision between the beam electron and an atomic electron, the atomic electron can acquire considerable energy, so that the atom is left excited or ionized. Such collisions are termed inelastic. In such a collision, the beam electron loses some of its energy, but because of its very large initial momentum, the change in its direction is very small (Ref. 14). When the atom returns to the ground state (or recombines with an electron) following the collision, the excess energy is radiated. This process is responsible for the fluorescence produced by the beam. The rate of energy loss from the beam is plotted in Fig. 2 (which is a plot of Eq. (8.3), page 63, Ref. 14). As Fig. 2 shows, the energy loss in the density and voltage range of interest is insignificant.

When a beam electron collides with an atomic nucleus, it loses very little energy since the nucleus is four orders of magnitude heavier than the electron, and thus is essentially immovable. Such collisions are termed elastic. If the electron passes some distance from the nucleus, its exact path is difficult to determine because it is influenced both by the nuclear field and by the field of the electron shell. If it is to be deflected through a significant angle, however, it must pass well within the electron shell, where it is completely exposed to the intense field of the bare nucleus. Since the radius of the orbit of the innermost electrons of the light elements is about 10^{-9} cm, whereas the nuclear radius is about 5×10^{-13} cm, it is evident that there is a vast region within the

atom wherein the effect of the electron shell on the beam electron is insignificant. The path of the electron in this region is determined solely by the coulomb attraction of the nucleus. This force has the same form as the gravitational attraction between bodies (the force is inversly proportional to the square of the distance), and the electron thus follows the same path as an orbiting astronomical body. In this case, the electron has too much energy to remain bound to the nucleus in a closed orbit, and its path is thus a hyperbola.

2.2 COLLISION CROSS SECTION OF A SINGLE ATOM

By solving for the path of the electron, one may determine the angle through which the electron is deflected (Ref. 15),

$$\text{Cot } \frac{\theta}{2} = \frac{\beta^2}{Z} \cdot \frac{b}{r_e} \tag{1}$$

The parameter β expresses the speed of the electron, which is a function only of beam voltage, and is given by

$$\beta = \left[1 - \left(1 + \frac{V}{E_e}\right)^{-2}\right]^{1/2} \tag{2}$$

The parameter b, which is known as the "impact parameter," is the distance by which the electron would miss the nucleus if it were not deflected (see Fig. 3). Equation (1) cannot be used directly because it is obviously not possible to determine b for each collision. In place of Eq. (1), it is more convenient to have an expression for the effective cross-sectional area of the nucleus, σ. The cross section is defined as the area presented by each atom through which an incident electron must pass if it is to enter a given detector. If a very small detector is used, which intercepts electrons scattered through an angle θ and which subtends a solid angle $d\Omega$, then the cross section presented by each atom is (Ref. 15)

$$d\sigma = \left(\frac{r_e}{2}\right)^2 Z^2 \frac{1}{\beta^4} \frac{1}{\sin^4 \frac{\theta}{2}} d\Omega \tag{3}$$

The physical significance of $d\sigma$ is shown in Fig. 4.

Equation (3) was derived using classical mechanics and requires two corrections. First, since the velocity of the beam electrons approaches the speed of light, a correction must be made for the increase of mass of the electron. This necessitates multiplying Eq. (3) by $(1 - \beta^2)$. Second, at high velocities and large angles, the electron

approaches the nucleus quite closely and a quantum mechanical correction for the spin of the electron must be made (Ref. 16). This necessitates multiplying Eq. (3) by the factor $H(\beta, \theta, Z)$, where

$$H(\beta, \theta, Z) = 1 - \beta^2 \sin^2 \frac{\theta}{2} + \pi \beta \frac{Z}{137} \left(1 - \sin \frac{\theta}{2}\right) \left(\sin \frac{\theta}{2}\right) \tag{4}$$

If functions $F(\beta)$ and $G(\theta)$ are now defined

$$F(\beta) = \frac{1 - \beta^2}{\beta^4} \tag{5}$$

$$G(\theta) = \frac{1}{\sin^4 \frac{\theta}{2}} \tag{6}$$

Equation (3) (with corrections) may then be expressed as

$$\Phi(\beta, \theta, Z) = \frac{d\sigma}{d\Omega} = \left(\frac{r_e}{2}\right)^2 Z^2 F(\beta) G(\theta) H(\beta, \theta, Z) \tag{7}$$

In order to facilitate the calculation of cross sections, the functions $F(\beta)$ and $G(\theta)$ are tabulated in Tables I and II and are plotted in Figs. 5 and 6. The function $H(\beta, \theta, Z)$ is plotted in Fig. 7 for hydrogen, air, and argon (atomic numbers of 1, 7.3, and 18). Finally, cross sections for a number of gases have been tabulated in Table III. The manner in which the figures for air were obtained is given in Section 2.4.

2.3 COUNTING RATE AT THE DETECTOR

Equation (7) describes the effect of a single atom on a single electron. It is easy to determine the effect of many atoms upon the beam, provided that multiple scattering can be neglected. That is, the probability that an electron will reach the detector by a single large angle scattering must be much larger than the probability that it will reach the detector by many small angle scatterings. This condition is probably met in this case. Multiple scattering is also accompanied by spreading of the beam (Ref. 17), and it is likely that beam spreading would obviate the measurement at densities so high that multiple scattering became a problem.

Assuming that single scattering prevails, let an electron beam of cross-sectional area S_b traverse a slab of scattering medium of thickness x. The volume of scattering medium exposed to the beam is then $S_b x$, and this volume will contain $\frac{N_A}{A} \rho \cdot S_b x$ atoms. Since each atom presents an area $d\sigma$ to the beam, the total area presented by these atoms

is $\frac{N_A}{A} \rho \cdot S_b x \cdot \Phi \cdot \Omega$. The probability that an electron traversing the medium will enter the detector is equal to the fraction of the beam area thus covered, $\frac{N_A}{A} \rho \Phi \Omega x$. The rate at which electrons will be detected is equal to this probability multiplied by the number of electrons per second in the beam,

$$c = \frac{I}{e} \frac{N_A}{A} \rho \Phi \Omega x \tag{8}$$

In most cases, the solid angle subtended by the detector will be a function of position along the beam. In this case, the product Ωx in Eq. (8) must be replaced by $\int \Omega(x)\, dx$, and the counting rate is given by

$$c = \frac{I}{e} \frac{N_A}{A} \rho \Phi Q \tag{9}$$

where $$Q = \int \Omega(x)\, dx$$

Geometry enters this expression through Φ and Q; beam voltage and current enter through Φ and I; gas composition enters through A and Φ; density enters directly as ρ; and the remaining factors are constants.

Since $\frac{N_A}{A} \rho$ is the atomic number density in the gas, it is possible to calibrate this instrument either in terms of number density, n, or of mass density, ρ. If the gas composition were fixed, this would be a matter of choice. However, Φ is nearly proportional to Z^2, so that if the calibration is made in terms of number density, sensitivity will vary as Z^2. On the other hand, if the calibration is made in terms of mass density, sensitivity varies as $\frac{Z^2}{A}$ and is less strongly influenced by changes in gas composition.

2.4 COUNTING RATE WHEN SEVERAL TYPES OF ATOMS ARE INVOLVED

Equation (9) is applicable if the gas contains a single type of atom only, but cannot be used directly if the gas molecules are composed of several types of atoms, or if the gas is a mixture of several types of molecules (e.g., air). In this case, each type of atom scatters electrons into the detector as if it alone were present.

Equation (9) may be used even in the case of a mixture, if appropriate definitions are adopted for an average atomic weight, A_{ave}, and an average cross section, Φ_{ave}, as follows. We may define the composition of the molecules present by a parameter α_{ij}, where α_{ij} is the number of atoms of type i contained in molecule type j. The mixture composition may similarly be defined by the parameter β_j, where β_j is

the fraction by volume of molecules of type j in the mixture. We also define $\nu = \sum_{ij} \beta_j \alpha_{ij}$, the average number of atoms per molecule (averaged over all types of molecules in the mixture). Then

$$\left.\begin{aligned} \Phi_{ave} &= \frac{1}{\nu} \sum_{ij} \beta_j \alpha_{ij} \Phi_i , \\ A_{ave} &= \frac{1}{\nu} \sum_{ij} \beta_j \alpha_{ij} A_i \end{aligned}\right\} \quad \text{and} \quad (10)$$

It is also convenient to define an average atomic number, Z_{ave}, and an average function, H_{ave}, so that Eq. (7) can be used directly to calculate Φ_{ave}. These are

$$\left.\begin{aligned} Z_{ave}^2 &= \frac{1}{\nu} \sum_{ij} \beta_j \alpha_{ij} Z_i^2 \\ H_{ave} &= \frac{1}{\nu} \sum_{ij} \beta_j \alpha_{ij} \left(\frac{Z_i}{Z_{ave}}\right)^2 H_i \end{aligned}\right\} \quad \text{and} \quad (11)$$

The cross sections given in Table III and the function $H(\beta, \theta, Z)$ plotted in Fig. 7 were calculated assuming the following composition for air:

Component	Fraction by Volume
N_2	0.7808
O_2	0.2095
A	0.0093
CO_2	0.0003
	0.9999

This composition results in

ν = 1.9908 atoms per molecule

A_{ave} = 14.5487 atomic mass units

Z_{ave} = 7.3105

Since large angle scattering requires that the beam electron penetrate deep within the electron shell of the atom, close to the nucleus, it is reasonable to suppose that the path of the electron will be independent of the state of the electron shell. The detected counting rate should then depend only upon the gas density and should not be affected by excitation, ionization, or dissociation of the gas. This is a very attractive possibility. It has not been possible to test it experimentally, however, because of the difficulty of producing a volume of ionized or dissociated gas of known density.

SECTION III
THE ELECTRON SOURCE

This measurement technique requires the use of an electron beam of roughly the same voltage and current as are used in some television tubes. These guns are available commercially and are complete with lenses so the user need not be concerned with the problems of electron optics. There are, however, other problems which are met in using these guns, such as providing high voltage insulation, injecting the beam into the relatively high pressure test gas, and supplying the several electrode voltages to the gun. Two electron gun assemblies have been built and used during the course of this work. Since some difficulty was experienced with them, their design and the problems encountered will be discussed. Both electron guns were operated at 50 kv, primarily because this appeared to be about the lowest voltage at which electrons could be reliably detected. The gun used[1] was manufactured as a replacement part for a Type 7NP4 TV projection tube, which is rated at 80 kv. Figure 8 is a photograph of one of these guns.

3.1 GENERAL DESIGN CONSIDERATIONS

Two points became clear early in the development. First, no insulating material may be exposed to the beam. Invariably, it will charge and discharge erratically because of secondary electron bombardment and the beam will be deflected and defocused randomly. In one case, random deflections were traced to an insulating deposit which formed on an orifice when the beam decomposed pump oil vapor.

The second point is that the oxide cathode which is normally supplied with these guns is unsatisfactory in this application. Although it will last for hundreds of hours in the projection tube (operating at pressures below 10^{-7} torr), its life is at most an hour or two at pressures in the 10^{-5} torr range, when it is exposed to water vapor and pump oil vapor. Fortunately, the supplier was able to furnish these guns with tungsten filaments. These filaments operate well at pressures somewhat above 10^{-4} torr (although focusing is poor at such a high pressure). At beam currents of 100 μa, the guns will last 25 hr or more. Beam currents of 500 μa have been obtained for short periods. The only difficulty which has been encountered with these guns is that the filaments are not

---

[1]The guns were supplied by the Superior Electronics Corp., Clifton, New Jersey, and are designated as Type 7NA.

accurately positioned as supplied. With some effort, the position of the filament can be checked and corrected before the gun is installed.

3.2 SEAL BETWEEN GUN AND VACUUM SYSTEM

The guns are supplied with a lead-glass header through which the leads are brought out and can be sealed to the vacuum system through a lead glass-to-metal seal. This provides an excellent vacuum seal but makes changing guns quite awkward, since the services of a glass blower are required. Furthermore, the seal sometimes cracks because of the heat generated by the filament. A method of sealing the gun which overcomes these objections is shown in Fig. 9. The header is sealed by a semi-flexible epoxy[2] into a stainless steel fitting which is, in turn, jointed to the vacuum system by an O-ring seal. Although the epoxy joint will occasionally leak, it represents a considerable improvement over a glass-to-glass seal. The epoxy joint is improved if the gun is placed in a bell jar and pumped to a low pressure for a few minutes before the epoxy sets up.

3.3 HIGH VOLTAGE INSULATION

Since the beam must emerge from the gun at ground potential, the cathode must be operated at a negative potential of 50 kv. This poses a design problem which cannot be entirely solved analytically. A considerable volume of literature on high voltage breakdown is available, but most of it is applicable only to special geometries, usually to the case of uniform fields. Nevertheless, Refs. 18 through 21 are quite useful.

Generally, an electron gun is designed so that the insulator which supports the high voltage components also serves as a wall of the vacuum enclosure. High voltage breakdown usually occurs along the surface of this insulator. If air at atmospheric pressure is used on one side of the insulator, breakdown usually occurs in the air. However, if high pressure air, or a gas such as sulfur hexafluoride is used, breakdown occurs on the vacuum side of the insulator. The breakdown voltage is very sensitive to the shape and texture of the insulator surface, and the material of which it is made. The junction between the insulator and the metal electrode is also critical.

---

[2]EC-2216, manufactured by 3-M Company.

Even if the high voltage insulator does not break down, a small leakage current is inevitable. This current flows along the surface of the insulator, or through the insulating gas as a corona discharge (the last traces of corona being very difficult to eliminate). It is important that this current be supplied directly from the power supply and not from one of the gun electrodes, since most of the electrodes are supplied from a fairly high impedance source. This can be accomplished by mounting the gun within a metal tube which is supported by the high voltage insulator and is connected electrically to the gun cathode and to the power supply (refer to Section 3.6). Of course, the gun electrodes must be insulated from this tube, but since the electrode voltages (with respect to the cathode) are much smaller than the total accelerating voltage, leakage from the electrodes is not a serious problem.

3.4 VACUUM SYSTEM

A major consideration in designing an electron gun assembly is that of injecting the beam into a relatively high pressure gas while maintaining the gun volume at low pressure. This is usually accomplished by providing a small orifice through which the beam emerges into the higher pressure gas. The gun housing must then be connected to pumps large enough to maintain the desired pressure in spite of the influx of gas through the orifice. The size of the orifice should of course be as small as possible and is determined by the minimum diameter to which the beam can be focused. If pumps of exorbitant size would be required to obtain the desired pressure drop in one stage, then the beam can be made to pass through two or more orifices in succession (Fig. 10). By pumping the gun housing and the space between each pair of orifices, enormous pressure ratios can be obtained with small pumps.

The design of these "dynamic" pumping systems is discussed in detail in Ref. 22. The procedures described in this reference have been found to be accurate, but the charts used in the design are in a rather inconvenient form. In Appendix III, the design procedure is discussed, and charts are presented in a modified form which is perhaps more convenient to use.

3.5 POWER SUPPLY

The guns used are of the electrostatic focusing type and require, in addition to the 50-kv anode voltage, filament, bias (G1), accelerating (G2), and focusing (G3) voltages. The anode voltage can be obtained from any of a number of commercially available 50-kv, 1-ma supplies.

The filament voltage can be obtained from a commercially available transformer, or one can be constructed by winding a number of turns of RG-58-U core on a toroidal primary[3]. The other voltages are more difficult since they must be supplied with respect to the cathode, and the supplies must be insulated from ground for 50 kv. The bias and accelerating electrodes require only a few hundred volts at very low current and so can be obtained from batteries and can be adjusted by potentiometers. The focus electrode must be biased about 10-kv positive with respect to the cathode and can be connected to a voltage divider across the 50-kv supply. The focus voltage can be varied by switching resistors into one leg of the voltage divider.

Any corona current which flows to the gun electrodes will alter the electrode voltages randomly and cause the operation of the gun to be erratic. The focus voltage is especially vulnerable because of the high impedance of the source from which it is obtained. It is useful to enclose all of the high voltage components within an enclosure which is connected electrically to the cathode. Components within the enclosure are then exposed only to the electrode voltages and not to the entire anode voltage.

The calibration of the density measuring apparatus is sensitive to variations in beam voltage and current (see Section 6.4). Some form of beam voltage and current regulation would be very desirable, although it would undoubtedly be expensive.

3.6 DESCRIPTION OF TWO ELECTRON GUN ASSEMBLIES

Two electron gun assemblies which have been designed on these principles will now be discussed. The first gradually evolved to the form shown in Figs. 10 and 11. It was designed to inject a beam into gas at pressures up to 1 torr. The differential pumping system consists of two stages. The low pressure stage contains an orifice 0.060-in. diameter by 0.75 in. long; the high pressure orifice is 0.040-in. diameter by 0.75 in. long. Both are pumped by 2-in. diffusion pumps. The vacuum system performance is shown in Fig. 12.

Both an angular and a lateral adjustment must be provided in order to align the beam with the axis of the orifices. These adjustments are

---

[3]Superior Electric Company, Bristol, Connecticut, Type TP-150.

made by sliding O-ring seals. For the lateral adjustment, the O-ring slides on a plane surface, whereas for the angular adjustment, it slides on a spherical surface with the entrance to the first orifice at the center of the sphere. In principle, these two adjustments should be independent; actually they interact somewhat because of the flexibility of the O-rings. The adjustment is mechanically stable, and the alignment is not difficult to perform. However, the necessary machine work was expensive, and the length of exposed O-ring raises the ultimate pressure in the vacuum system.

High voltage insulation for the gun is provided by a cylindrical insulator of Vycor® glass 3.0-in. OD by 2.75 in. long. According to Refs. 20 and 22, this insulator should support well over 50 kv. However, it often flashed over on the outer surface at voltages as low as 30 kv, probably because it is exposed to a nonuniform field. The difficulty was remedied by surrounding it with transformer oil.

The distance from the gun to the orifice is the same as the distance from the gun to the fluorescent screen in the TV projection tube. The beam diameter has not been measured, but it is small enough so that the orifices intercept less than 1.0 percent of the beam current. The orifices are insulated from ground so that the current which they intercept can be measured. This measurement is almost indispensible in aligning the beam with the orifices.

The second gun assembly (shown in Figs. 13 and 14) was designed for use in an 18-in. arc heated tunnel at pressures up to 100 μ. The vacuum system consists of a single orifice 0.050-in. diameter by 0.100 in. long, pumped by a 2-in. diffusion pump. The pump exhausts to the tunnel plenum and, thus, requires no backing pump. The system maintains a pressure of 2×10^{-4} torr in the gun when the plenum pressure is 100 μ.

The high voltage insulator is a 4.0-in.-diam Vycor disk. Since the housing is mounted in the tunnel plenum, the high pressure side of the insulator is enclosed by a cap, which is filled with sulfur hexafluoride to atmospheric pressure. This gas has three times the dielectric strength of air, is noncorrosive and nontoxic, and is relatively inexpensive. The connections between the gun and the power supply are made with five lengths of shielded high-voltage cable having a jacket over the shield. Vacuum seals are made to the cable jacket where it penetrates the cap and the tunnel plenum. Since both ends of the high voltage cable are at atmospheric pressure, leakage of gas along the braided shield is not a problem. RG-58/U was originally used for the high voltage cable but was found to be unsatisfactory. Although it will support 130 kv in

short tests, its life at 50 kv is only a few hours. Fortunately, a similar cable rated at 50 kv is available although it is relatively expensive.

Since the vacuum orifice is quite short, a considerable angular misalignment of the beam can be tolerated, and no angular adjustment is provided. The beam is deflected by a pair of centering coils[4] to pass through the orifice. The use of an electrical adjustment simplifies the construction of the gun and makes alignment of the beam much more convenient.

The distance from the gun to the orifice was shortened by 6.9 in. in this design. This has caused no difficulty in focusing the gun. The orifice is again insulated from ground, so that intercepted current can be measured.

The housing was initially constructed of thin-walled aluminum tubing. However, the tubing was porous enough to interfere with the operation of the vacuum system, and the housing was subsequently rebuilt of stainless steel.

The same power supply is used with both of these electron gun housings. Figure 15 is a photograph of the supply, and Fig. 16 is the schematic diagram. The supply reached its present condition after a process of evolution and is now in accordance with the general principles discussed earlier in this section. A number of changes were made in attempting to eliminate corona discharges in the supply. Halfway methods such as the use of corona dope and the installation of makeshift corona shields were only partially effective, and the difficulty was not eliminated until all of the high voltage components were enclosed in the cage seen in Fig. 15. The last traces of corona were finally eliminated by surrounding the course focus switch (Fig. 16) with a cup of transformer oil. The top and bottom of the high voltage cage are made from toroidal corona shields[5]. The high voltage connections to the gun are made through an octal socket which is mounted in the center of the top toroid. Since the focus voltage is too high to be brought through this socket, one pin of the socket is drilled out. The core of the cable passes through the socket and terminates in a pin jack mounted about an inch below the socket.

---

[4]Constantine Engineering Laboratories Company, Mahwah, New Jersey, Type KC-403.

[5]Available from Universal Voltronics Corporation, White Plains, New York.

The schematic diagram (Fig. 16) is self-explanatory. The surge limiting resistor in series with the anode voltage supply is necessary to protect the supply during flash-overs which occur occasionally. The spark gaps similarly protect the potentiometers. The power supply common bus is isolated, and the electron gun itself is insulated from ground. The beam current alone flows to ground and is measured as it returns to the common bus. Any leakage currents (except perhaps corona within the power supply) flow directly to the common bus. This arrangement is an aid in obtaining an accurate beam current measurement.

SECTION IV
DETECTION OF SCATTERED ELECTRONS

Electrons which are elastically scattered in the gas will arrive at the detector with the full beam energy. These are not the only electrons which will enter the detector, however. Electrons which rebound from the collector may eventually enter the detector, after being scattered about by metal surfaces in the test section (see Section 5.1). These latter electrons may be identified because they will have lost a fraction of their initial energy in inelastic collisions. For this reason, it is desirable that the detector have the capability of measuring the energy of the electrons which strike it.

Electrons arrive at the detector at random time intervals, and an estimate of the average rate of arrival will necessarily involve a statistical error. In order to attain a probable error of 1.0 percent in this estimate, it is necessary to collect at least 4560 electrons. (This is discussed more fully in Section 6.3). If measurements are to be made in a reasonable length of time, it is thus necessary for the detector to be able to handle hundreds or thousands of electrons per second. In addition to these rather well defined capabilities, which the detector must possess, it must also be "convenient" to use and must survive exposure to the vacuum environment.

4.1 TYPES OF DETECTORS

The most commonly used particle detectors are the Geiger-Muller tube, the scintillation detector, and the silicon surface barrier detector. Geiger-Muller tubes do not provide energy discrimination and are limited to rather low counting rates, and so cannot be used in this application. A scintillation detector with an anthracene crystal was used in some initial experiments. Such detectors provide adequate energy resolution,

can handle very high counting rates, and provide a relatively large electrical output signal. However, the photomultiplier must be shielded from magnetic fields and must see no light whatever. Furthermore, the antracene crystal has a rather high vapor pressure and is damaged by exposure to low pressures. The scintillation detector was abandoned in favor of a silicon surface barrier detector, although it might serve well in some applications, especially if fitted with a plastic scintillator in place of the anthracene crystal.

The silicon surface barrier detector consists of a wafer of n-type silicon on which a very thin p-type layer is formed by an evaporated layer of gold (Ref. 23). When the p-n junction is reverse-biased, a depletion layer 50 to 500 μ thick is formed. An incident particle striking the detector dissipates its energy almost entirely in ionizing silicon atoms within the depletion layer. The free electrons and holes which result drift to the electrodes in a few nanoseconds and cause an output current pulse. The total charge in this pulse is proportional to the number of atoms ionized, which is proportional to the particle energy. These detectors are very small, are unaffected by magnetic fields, and withstand exposure to a vacuum environment. Although they are somewhat sensitive to light, they are not nearly so critical in this respect as are scintillation detectors. Their energy resolution, which is determined primarily by noise in the subsequent electronics, is perhaps not as good as that of a scintillation detector, but is adequate for this purpose. A photograph of a surface barrier detector is shown in Fig. 17.

4.2 DETECTOR INSTRUMENTATION

The instrumentation which follows these detectors is shown in Fig. 18. The preamplifier converts the extremely low level charge output from the detector into a higher level voltage signal. Because the preamplifier noise is adversely affected by capacitance across the detector, the preamplifier must be mounted near the detector and connected to it by the shortest possible cable (no more than a few inches long). The signal from the preamplifier (about 25 mv) is transmitted to the main amplifier by a cable of any desired length. In the main amplifier, the signal is amplified to the 50- to 100-v range, and pulse shaping is accomplished. This amplifier is especially designed for good linearity and fast recovery from overload.

The signal from the main amplifier is examined by the pulse height analyzer, which can be used in either of two modes. In the integral mode, the pulse height analyzer delivers an output pulse for each input pulse which exceeds a set voltage (known as the baseline voltage). In the

differential mode, the unit delivers an output pulse for each input pulse which exceeds the baseline voltage by less than a set voltage (known as the window width). The pulse height analyzer is used to determine the amplitude distribution of the input pulses. The counter, which follows the analyzer, measures the rate at which pulses in a given amplitude range arrive.

4.3 EFFECT OF AMPLIFIER NOISE

The accuracy with which the number and energy of particles striking the detector can be determined is limited primarily by the noise which is added to the signal in the preamplifier. This noise has two effects. First, it degrades the energy resolution of the detector by adding the instantaneous value of the noise voltage to the output pulse amplitude. Thus, even if all input pulses were of the same amplitude, the output pulses would not be. Second, since peaks of the noise voltage cannot be distinguished from current pulses from the detector, the noise causes extraneous pulses to be counted by the pulse height analyzer.

Figure 19 shows a differential pulse height spectrum which illustrates the effect of noise. The input to the preamplifier was obtained in this case from a pulse generator. Without the effects of the noise, all of the output pulses would have occurred at a baseline voltage of 42 v. The noise, however, causes the output pulse height to vary from pulse to pulse over a range of several volts. Since the noise has a gaussian distribution, the output pulse amplitude spectrum does also. (The gaussian distribution curve, which is "bell-shaped" on linear paper, plots as a parabola on semi-logarithmic paper.) The high counting rate at low baseline voltages is caused by the detection of peaks in the noise voltage itself. These peaks also have a gaussian amplitude distribution centered at zero baseline volts (Ref. 24).

Any pulse shaping which is performed ahead of the pulse height analyzer influences the effect of the noise. By reducing the high frequency response of the main amplifier, the rms noise voltage can be reduced at the expense of increasing the pulse length. It is thus necessary to compromise between good energy resolution (which requires low noise level) and high counting rate capability (which requires fast pulse response). The data presented in this report were taken using a differentiation with a 1.6 μsec time constant, followed by a 1.0 μsec delay line shaper. Neither of these limits the bandwidth of the amplifier, and it is quite possible that a considerable improvement in energy resolution could be obtained by adding some form of low-pass filter.

SECTION V
VERIFICATION OF THE THEORY

5.1 MEASUREMENTS IN A SMALL TEST CHAMBER

As has been mentioned, the first objective of this work was to verify that the electrons scattered by the Rutherford process could be detected, and that they would not be obscured by electrons from other sources or by electronic noise. To accomplish this, the electron gun shown in Fig. 10 was mounted on a tank 30 in. in diameter by 16 in. high (inside dimensions). A small collector was mounted on the opposite side of the tank, and a collimator and silicon surface barrier detector were mounted at 90 deg to the beam axis. The general arrangement of the equipment and the important dimensions are shown in Fig. 20. The tank was pumped by a two-stage 15-cfm mechanical pump and could be evacuated to 10μ in 20 min. The ultimate pressure in the tank was about 2μ. The pressure in the tank was controlled by valving off the pump and bleeding in air to the desired pressure.

Details of the detector and collimator are shown in Fig. 21. The field of view of the detector was limited by a slit at the front of the collimator (the slit being perpendicular to the beam axis) and by the dimensions of the detector itself at the rear of the collimator. The collimator was aligned so that its axis intersected the beam axis. This alignment is not critical, however, since the detector field of view is fan-shaped. The value of Q (Eq. (9)) for this detector was determined graphically to be 4.1×10^{-5} cm. The detector was at least partially visible over a beam length of 1.29 cm.

Using this experimental arrangement, differential energy spectra of the scattered electrons were measured as the pressure in the tank was raised from 10 to 1000μ. These spectra showed very high counting rates and did not have the expected peak at 50-kev energy. The counting rate increased with density, though not linearly. This anomalous behavior was found to be caused by electrons which were escaping from the collector, rebounding at random from the walls of the tank, and eventually entering the detector. Since these electrons had lost part of their energy, they filled in the valley which was expected in the spectrum. The importance of completely attenuating the beam at the collector became clear at this point.

To eliminate these stray electrons, a larger, more efficient collector was installed, and a baffle plate was added opposite the collimator. A hole was cut into this baffle plate, which was slightly larger than the detector field of view, so that the detector viewed only the tank wall behind

the baffle. For a stray electron to enter the detector, it was necessary for it to enter the hole in the baffle, then to be scattered so that it struck the wall opposite the detector, and then to be scattered into the detector. The cavity behind the baffle acts as a "black body" for electrons in the same manner that a cavity in a mass of gray metal radiates heat as a black body. Finally, the entire interior of the tank and collector and both surfaces of the baffle were coated with Aquadag[6]®. Aquadag is nearly 100-percent carbon and produces only about one-tenth as many fast secondary electrons as steel (Ref. 25). The baffle and the new collector are indicated by dashed lines in Fig. 20 and are shown in Fig. 22.

After these changes were made, the spectra of Fig. 23 were obtained, using a 50-kev, 78-μa beam. Although there was still no peak in the spectra, they did flatten out in the area where the peak was expected. Furthermore, counting rates increase nearly linearly with gas density. The apparatus was calibrated in terms of density, assuming that all electrons with energy greater than 45 kev were scattered in the gas; electrons with lower energy were assumed to be stray electrons. Counting rates were measured in the integral mode at a baseline voltage corresponding to 45 kev over a range of pressure, resulting in the calibration curve shown in Fig. 24. (This curve could also have been obtained by measuring the area under the curve of Fig. 23 above 45 kev.) Figure 24 shows that counting rate increases linearly with density, except at high densities. The deviation is probably caused by beam spreading, which was so severe at these densities that part of the beam may have been outside the detector field of view. The counting rates obtained agreed with the prediction of Eq. (9) within the accuracy with which the geometry was known.

5.2 MEASUREMENTS IN THE LOW DENSITY WIND TUNNEL

A density measuring apparatus was then fabricated and installed in a low density, arc-heated wind tunnel. This tunnel consists of an 18-in. exit diameter conical nozzle with a 0.200-in.-diam throat, a free jet test section and a diffuser, all enclosed by a 6-ft-diam plenum chamber. It is powered by a 1/4-Mw arc heater, and the diffuser is pumped by a six-stage steam ejector. Air is used as the test fluid. Figure 25 is a drawing showing the major components of the tunnel. The tunnel is well suited to the use of this measurement technique, because ample room is available

---

[6]Available from Atchison Colloids Company, Port Huron, Michigan.

for the installation of a large collector and because the plenum walls are more than twice as far from the point of measurement as were the walls of the tank previously used.

The entire equipment was mounted on a yoke which was attached to the tunnel pitot probe mechanism so that the measurement could be made at any point in a vertical plane through the axis of the flow. The installation is shown in Figs. 26 and 27. The electron gun used was that shown in Fig. 13. The collector was 9.0 in. in diameter by 24.0 in. long, with an entrance hole 4.0 in. in diameter. The detector and collimator were mounted at the top of the yoke, and the preamplifier was enclosed within a pressure-tight box through which cooling air was passed. Both front and rear slits were used in the collimator, which viewed a 1.0-cm length of the beam. No black body was used opposite the detector, and only the interior of the collector was coated with Aquadag. The distance from the electron gun orifice to the collector entrance was 20 in., and the distance from the beam to the collimator entrance was 19 in.

An improved preamplifier and a detector with a wider depletion layer were used in these tests, and the cable between the detector and preamplifier was shortened. These changes resulted in a considerable reduction in the preamplifier noise.

A number of differential spectra were taken at plenum pressures from 10 to 100 μ (without flow), of which Fig. 28 is typical. This spectrum was taken at 10 μ using a 48-kev, 100-μa beam. The peak at the beam energy is well defined and is of the proper shape. The counting rate in the valley is nearly an order of magnitude below the peak counting rate, although it is not as low as it would be if no stray electrons were present. The improvement in the shape of the spectrum is caused in part by the reduced preamplifier noise and in part to the reduction in the number of stray electrons. The calibration curve shown in Fig. 29 was made in the integral mode, using a baseline voltage of 26 v. The box around each data point denotes an estimate of the maximum possible error in the measurement, taking into account errors in pressure measurement, voltage and current measurements, and statistical counting errors.

The counting rates indicated in Fig. 29 are close to (61 percent of) the rates predicted by Eq. (9). Furthermore, the great majority of the electrons enter the detector with the beam energy (Fig. 28). These two observations are deemed to be sufficient evidence for accepting Rutherford scattering as the process responsible for the scattered electrons. The discrepancy between predicted and measured counting rates

is not surprising since the geometry (slit widths, etc.) is not accurately known. It is also possible that the calibration was performed in gas containing a large percentage of water vapor, perhaps caused by backstreaming from the steam ejector, (which might occur without flow). The cross section of water vapor is 60 percent of the cross section of air.

The apparatus was also used to measure the density profile in the tunnel. This work is described in Section VIII.

The most significant outcome of this work (aside from the agreement with Rutherford theory which was demonstrated) was the realization of the importance of thoroughly absorbing the beam at the collector. Although there seems to be a very small probability that a given electron will escape from the collector and will enter the detector after several bounces from metal surfaces, the probability that a given electron will collide with a nucleus in the gas and be scattered into the detector is also very small (e.g., 350 in 6×10^{14} at 10μ). In many applications, these stray electrons will probably determine the ultimate accuracy which can be achieved with the technique.

SECTION VI
SPATIAL RESOLUTION AND ACCURACY

In this section, the factors which affect spatial resolution and accuracy will be discussed. The measurement is made in a volume defined by the cross-sectional area of the beam and the field of view of the detector. The spatial resolution is thus influenced by spreading of the electron beam and by the design of the collimator. Errors in measured density originate from at least three sources. Most basic is the statistical error due to the random nature of the scattering process. Then, there are errors imposed by the limitations of the equipment used, such as errors in voltage and current measurements and errors caused by electronic noise in the preamplifier. Finally, there are errors caused by defects in the scattering process itself, primarily because of the stray electrons. Each of these subjects will be discussed in turn.

6.1 BEAM SPREADING

The electron beam can spread after it leaves the vacuum system orifice because of several causes: electron optics, space charge forces, and multiple scattering. The optics of the electron gun cause the beam to converge to a minimum section at the orifice and to diverge

after passing through for purely optical reasons. If this effect is large enough to be objectionable, it can be corrected by installing a lens beyond the orifice, so as to reconverge the beam at the point of measurement. The mutual repulsion of the beam electrons (space charge) can also cause the beam to spread, but this effect is only important at high currents or low voltages (Ref. 26).

The dominating cause of beam spreading is multiple small angle scattering of the beam electrons. Equations (6) and (7) show that the probability of small angle scattering is far larger than the probability of large angle scattering. There are two net effects of many random small angle scatterings. First, the beam becomes broader as distance from the gun increases. Second, individual electrons no longer travel exactly parallel to the beam axis. Rossi and Greisen show in Ref. 17 that the electron density at any distance from the gun has a gaussian distribution. Furthermore, the angles which individual electron paths make with the beam axis have a gaussian distribution. In particular, they show that the rms beam radius at any distance from the gun is

$$r_b = K\left(\frac{r_e}{2}\right)\left(\frac{N_A}{A}\rho\right)^{1/2} \ell^{3/2} \; Z\, F(\beta)^{1/2} \tag{12}$$

where

$$K = 8\left[\frac{\pi}{6}\right]^{1/2}\left[\ell n(183 \cdot 7^{-1/3})\right]^{1/2} = 12.362$$

However, they derived this relationship under the assumption that the scattered particles have very high energy - much higher energy, in fact, than has been used in this application.

In order to test Eq. (12), the spreading of the electron beam was actually measured at energies from 30 to 50 kev, over beam lengths up to 60 cm using a 60 μa beam. Two means were used to measure beam size. First, the current density in the beam was surveyed by allowing the beam to impinge upon a Faraday cage with a very small entrance hole. A current density map obtained by this means is shown in Fig. 30. These plots were tedious to obtain and had to be integrated graphically before they could be compared with Eq. (12). Subsequent measurements were made by collecting the entire beam in a Faraday cage, and then measuring the variation in current collected as a metal vane was inserted to various distances into the beam. Figure 31 shows a group of plots obtained in this manner. It is shown in Ref. 17 that the current density measured in this manner should have a gaussian distribution, and plots such as Fig. 31 were found to approximate quite closely the cumulative gaussian distribution. The beam radius was taken as the standard

deviation of the distribution, which is half of the distance from the 16-percent to the 84-percent ordinate on the plot.

The results of these measurements are summarized in Fig. 32 and are compared with Eq. (12) in Fig. 33. It is evident that the agreement is only fair and that in all cases Eq. (12) is pessimistic. The lack of agreement might be because of the assumption of high energy in deriving Eq. (12), or it might be a result of space charge effects. It is known that under certain conditions a core of positive ions will form in a beam and will reduce its spreading. In any case, it is conservative to assume that the discrepancy is caused by space charge. One would then use Fig. 32 to predict the size of the electron beam, but would use Eq. (12) to predict spreading between the sensitive volume and the detector, where current density is very small and space charge presumably negligible.

The primary effect of beam spreading is to degrade the spatial resolution of the measurement. There is no first-order effect on counting rate, because, as Eq. (9) shows, counting rate depends only on total beam current and not on current density. There might be a second-order effect on counting rate, however, for two reasons. First, beam spreading will cause some electrons to cross the detector field of view closer to the detector where the detector solid angle, Ω, is larger. Second, the scattering angle, θ, will no longer be 90 deg for all electrons, since the electron paths will be inclined at a small angle to the beam axis. This effect might cause the counting rate to increase because the scattering cross section is a strong function of scattering angle.

Beam spreading will also have an effect on scattered electrons between the point of measurement and the detector. That is, it will cause some electrons which should strike the detector to miss it and conversely. Reasoning loosely, it seems that these two effects should cancel, and that there should be no first-order effect on counting rate. Further analysis is needed to show whether this is, in fact, true. In any event, it is pointless to design a collimator which attempts to attain spatial resolution beyond the limit imposed by beam spreading.

6.2 DESIGN OF COLLIMATORS

The purpose of the collimator is to restrict the field of view of the detector to a small length of the beam. This can be accomplished by mounting a pair of slits between the detector and the beam, the slits being perpendicular to the beam axis. The slits produce a fan-shaped field of view, which is narrow in a direction parallel to the beam, but wide in a direction perpendicular to the beam (see Fig. 1).

The geometry of the collimator is shown in Fig. 34a for the case of a scattering angle of 90 deg. Over a length of beam f, the detector width is determined by the rear slit, and the detector solid angle is the same from any point in this region. At least some part of the detector is visible over the beam length g. Within the region g, but outside of f, the detector width is determined by one edge of the front slit and the opposite edge of the rear slit. Over this region, detector width varies linearly with distance along the beam, as is shown in Fig. 34b.

The front slit should, of course, be placed as close to the beam as possible so that the dimension D is normally determined by the radius of the flow. The dimension g is determined by the spatial resolution desired. The problem is then to determine what values of the dimensions b, c, and d will yield the desired value of g, and at the same time maximize Q (Eq. (9)). The problem may be solved as follows: Assuming that b and d are fixed, find the value of c which yields the desired value of g. Then, using this value of c and letting b remain fixed, find the value of d which maximizes Q. This results in

$$\left.\begin{aligned} c &= \frac{b\,g}{2\,D} \\ d &= \frac{b\,g}{2(D+b)} \\ Q &= \frac{t\,b\,g^2}{4\,D(D+b)^2} \\ f &= 0 \end{aligned}\right\} \tag{13}$$

where t is the length of detector exposed (which may be taken to be the detector diameter). Q may now be maximized with respect to b, resulting in

$$\left.\begin{aligned} b &= D \\ c &= \frac{g}{2} \\ d &= \frac{g}{4} \\ Q_{opt} &= t\left(\frac{g}{4D}\right)^2 \end{aligned}\right\} \tag{14}$$

The maximum with respect to b is very broad, however, and little is lost by shortening the collimator appreciably. The value of Q/Q_{opt} is

$$\frac{Q}{Q_{opt}} = \frac{4\,b\,D}{(D+b)^2} \tag{15}$$

which is plotted in Fig. 35.

The collimator just discussed is wasteful of detector area since most of the detector is masked by the rear slit. All of the detector area can be used if the slits are replaced by a "venetian blind" arrangement, as shown in Fig. 36. This would, of course, be more difficult to construct than a simple slit collimator.

A most attractive possibility for increasing Q is to replace the collimator by an electron lens (Fig. 37) and to image a segment of the beam onto the detector. The solid angle, Ω, would then be determined by the lens area and the distance from the lens to the beam. Q would be given by

$$Q_\ell = \frac{g\, S_\ell}{D^2} \tag{16}$$

Since lenses up to 5 in. in diameter are available, Q could be increased several orders of magnitude by replacing a slit collimator by a lens. A lens has not been tried in connection with this work, and problems might arise. For instance, it would be difficult to determine when the lens was properly focused.

If the scattering angle is not 90 deg, this derivation remains valid, except that the path length over which each beam electron is in view of the detector is increased by $(\sin\theta)^{-1}$, and Q must be multiplied by this factor. Furthermore, the spatial resolution (measured along the beam) is no longer the dimension g, but is greater by the same factor $(\sin\theta)^{-1}$. Spatial resolution is denoted by a. If Q is expressed in terms of spatial resolution, a, and if the factor $(\sin\theta)^{-1}$ is included, Eqs. (14) and (16) become

$$Q_{opt} = t\left(\frac{a \sin\theta}{4D}\right)^2 \frac{1}{\sin\theta} = t\left(\frac{a}{4D}\right)^2 \sin\theta \tag{17}$$

and

$$Q_\ell = \frac{a \sin\theta\, S_\ell}{D^2} \quad \frac{1}{\sin\theta} = \frac{a\, S_\ell}{D^2} \tag{18}$$

The definition of a is perhaps not consistent with the definition of r_b, since r_b denotes the rms beam radius, and some scattering takes place beyond r_b. On the other hand, a denotes the absolute limits on the field of view, and no electrons scattered beyond a are detected (neglecting small angle scattering). The definition of a is useful, however, if this is kept in mind.

6.3 STATISTICAL COUNTING ERRORS

Since the arrival of the electrons at the detector is a random process, one would not expect to detect exactly the same number of electrons during each period of, say, 10 sec. The probability of detecting a given number of electrons in a given time interval is described mathematically by the Poisson probability distribution. The important features of this distribution are that for large numbers of electrons it approaches a gaussian distribution, and that the standard deviation of the number of electrons detected in the given time interval is equal to the square root of the average number detected in this interval. That is,

$$D(C) = [E(C)]^{1/2} \tag{19}$$

We may define a parameter ϵ as the ratio of the deviation in the number of electrons detected to the average number detected

$$\epsilon = \frac{D(C)}{E(C)} = [E(C)]^{-1/2} \tag{20}$$

Thus, to attain a standard deviation of 1.0-percent error, one must count long enough to detect 10,000 electrons on the average. The probable error (the error which is exceeded on half of the measurements) is equal to 0.675 D(C), so that one must count 4560 electrons on the average to attain a probable error of 1.0 percent. Figure 38 is a plot of standard deviation and probable error in the measurement versus average number of electrons detected. These statistical considerations determine the length of time required to attain measurement of a given precision.

6.4 CALIBRATION AND ERRORS IN VOLTAGE AND CURRENT MEASUREMENT

If Eq. (7) were absolutely accurate and if the geometry of the equipment were exactly known, then it would be possible to make absolute density measurements with this technique. This would require accurate absolute measurements of beam voltage and current. This, of course, is not the case. Equation (7) can be used to estimate the counting rate to be expected under given conditions, but one measurement must then be made on gas at a known density in order to remove the uncertainty in cross section and geometry. Thereafter, if beam voltage and current are held constant, the counting rate should be accurately proportional to gas density. There is then no requirement for absolute accuracy in measuring voltage and current, but only for repeatability. The current measurement must be repeatable within the accuracy expected of the overall density measurement. The error in the voltage measurement can be only half as large, because cross section is nearly inversely proportional to the square of beam voltage (Eqs. (5) and (7)).

In order to achieve an accurate beam current measurement, it is necessary to give careful attention to the arrangement of grounds in the power supply and electron gun, so that corona and leakage currents will not be mistaken for beam current. This has been mentioned in Section 3.6. It would appear to be possible to make an accurate beam current measurement at the collector, but this has failed mysteriously in one case (see Section 8.3). In order to obtain an accurate voltage measurement, it is necessary to use a stable and reliable multiplier resistor and to protect it from corona and surface leakage.

It should be remarked in passing that obtaining the one calibration point may be a formidable task. It is difficult by any means to measure gas density at low pressures to within 1.0-percent accuracy.

Ths use of the procedure outlined above requires that the nuclear composition of the gas remain fixed between the calibration and the subsequent density measurements. This could present a problem in some facilities, although a correction might be made for small, known changes in gas composition.

6.5 PREAMPLIFIER NOISE AND STRAY ELECTRONS

As was mentioned in Section 4.3, preamplifier noise has two effects. First, since peaks in the noise voltage are indistinguishable from pulses from the detector, the noise causes extra counts to be recorded when no electron has struck the detector. Second, since the instantaneous value of the noise voltage is added to the height of the pulse from the detector, the noise causes an error in the measurement of the energy with which an electron strikes the detector. The first effect was entirely insignificant in the measurements which were made in the 18-in. tunnel. Most of the noise peaks occur at low energies, and the number which occurs at energies in the range of interest (30 kev or more) is only of the order of one per second. The second effect would also be insignificant, if all electrons were known to strike the detector with the same energy. However, stray electrons have less than the beam energy, and it is desired to use this energy difference to avoid counting stray electrons. For this reason, the effect of noise on energy discrimination becomes important. This will be discussed in the next section.

6.6 ERRORS CAUSED BY STRAY ELECTRONS

The most persistent source of error which has been encountered in this work is that caused by stray electrons. In Section 5.1, it was shown that under unfavorable conditions these electrons can completely mask the single scattered electrons and make density measurements impossible.

The problem of eliminating stray electrons may be attacked from several angles. The largest, most efficient collector possible can be used. A black body can be used opposite the detector (Section 5.1), an Aquadag coating may be applied to surfaces from which stray electrons may rebound, and finally, it is possible to eliminate the effect of some stray electrons even after they have struck the detector. If the energy difference between the stray and single scattered electrons is sufficient, the stray electrons can be rejected by the spectrum analyzer.

The spectrum of Fig. 28 may be used as an example. The peak at 40 v is very nearly gaussian in shape on the high energy side but deviates somewhat on the low energy side. By fitting a parabola to the high energy side of the peak, the spectral distribution of the single scattered electrons may be estimated. The spectrum of noise peaks may of course be measured. By subtracting these two components from the measured spectrum, an estimate of the spectrum of the stray electrons is obtained. This process was carried out on the spectrum of Fig. 28, with the results shown in Fig. 39. The stray electrons apparently arrive with about 30-kev energy.

The spectrum analyzer may be set to reject electrons with less than a given energy and thus to avoid counting some of the stray electrons. The selection of the baseline energy involves a compromise, however. As the baseline energy is increased, more and more stray electrons will be rejected. Eventually, however, an appreciable number of single scattered electrons will also be rejected. When this occurs, the counting rates are reduced somewhat, but worse, the calibration factor of the apparatus (counts per second per unit of density) becomes dependent upon the baseline setting, which is not entirely stable. The best baseline setting is probably the highest energy for which stability is not a problem.

A reduction in preamplifier noise will make the peak at the beam energy taller and narrower. This will allow an increase in the baseline energy, which will reduce the number of stray electrons counted. A modest improvement in preamplifier noise might provide a considerable improvement in discrimination against stray electrons.

Experience thus far indicates that the problem of stray electrons can be handled in a spacious environment such as a wind tunnel with an open jet test section but that it becomes more difficult in cramped quarters. It remains to be seen whether the problem can be solved at all when the gas flow is entirely enclosed within walls.

SECTION VII
COMPROMISE BETWEEN RESOLUTION, ACCURACY, AND MEASURING TIME

In Section VI, the factors which affect spatial resolution, accuracy, and measuring time were discussed individually. It is evident that they are interrelated, and that it is not possible to improve resolution, for instance, without degrading either accuracy or measuring time. This interrelation is not surprising since both beam spreading (resolution) and counting rate depend upon the scattering cross section. In this section, the nature of the compromise will be determined, and a suggested design procedure will be given. The quantum-mechanical correction to the scattering cross section ($H(\beta, \theta, Z)$, Eq. (4)) will be neglected since only approximate results are needed.

7.1 DERIVATION OF THE CONSTRAINING EQUATION

Consider first the case in which a slit collimator is used. We assume that beam length, ℓ, collimator distance, D, and detector diameter, t, are known. The expressions from which the constraint is derived are as follows: First, the relationship between statistical accuracy and total number of electrons counted (from Eq. (20))

$$\epsilon^2 = \frac{1}{cT}; \tag{21}$$

second, the expression for beam radius, Eq. (12); third, the expression for counting rate (from Eqs. (7) and (9), using Q from Eq. (17))

$$c = \frac{I}{e} \frac{N_A}{A} \rho \left(\frac{r_e}{2}\right)^2 Z^2 F(\beta)\ G(\theta)\ t\left(\frac{a}{4D}\right)^2 \sin\theta \tag{22}$$

We have expressed statistical accuracy as a dimensionless ratio, ϵ, and it is convenient to do the same with the two components of spatial resolution. We define $\gamma = r_b/\ell$ and $\delta = a/D$. Using these definitions, Eqs. (12) and (22) become

$$\gamma^2 = K^2 \frac{N_A}{A} \rho \left(\frac{r_e}{2}\right)^2 Z^2 F(\beta)\ \ell \tag{23}$$

and

$$c = \frac{I}{e} \frac{N_A}{A} \rho \left(\frac{r_e}{2}\right)^2 Z^2 F(\beta)\ G(\theta)\ \sin\theta\ t\left(\frac{\delta}{4}\right)^2 \tag{24}$$

We now combine Eqs. (21), (23), and (24) to obtain the equation of constraint for a slit collimator

$$\gamma^2 \delta^2 \epsilon^2 \frac{IT}{e} = 16 \cdot K^2 \frac{\ell}{t} \frac{1}{G(\theta) \sin\theta} \tag{25}$$

A similar derivation for a lens collimator yields

$$\gamma^2 \delta \epsilon^3 \frac{IT}{e} = K^2 \frac{\ell D}{S_\ell} \frac{1}{G(\theta)} \tag{26}$$

Equations (25) and (26) show explicitly the trade-off which is possible between spatial resolution, accuracy, beam current, and measuring time. There are, of course, limits on the resolution, accuracy, etc., which can be achieved, regardless of what one is willing to trade. For instance, measuring time can be reduced by increasing beam current. Measuring time cannot be reduced indefinitely, however, because the counting rate will eventually exceed the capability of the pulse detection equipment. Thereafter, measuring time can only be reduced at the expense of statistical accuracy. Again, the smallest beam radius which can be achieved is limited ultimately by the highest voltage which one is willing to use on the electron gun.

Equations (25) and (26) must be viewed with some skepticism, since they involve the beam radius as determined by Eq. (12), which was found to be none too accurate in the voltage range of interest. They can be used with some confidence, however, to predict the tradeoffs which can be made with an existing set of equipment. The constant, K, would then be replaced by an unknown, which could be evaluated experimentally under a known set of conditions. Equations (25) and (26) could then be used to predict the effect of changing collimator design or beam voltage, etc.

These equations indicate that a large improvement in performance can be achieved by reducing the scattering angle from 90 deg to, say, 45 deg. Such a change causes more than a tenfold increase in cross section, with only a modest sacrifice in resolution. This change would presumably not affect the stray electron counting rate and so would also offer a tenfold reduction in the effect of the stray electrons.

7.2 DESIGN PROCEDURE

The procedure which must be used to select the equipment dimensions and operating conditions will obviously depend upon the constraints which are imposed on the solution. The following procedure assumes that complete freedom can be exercised in choosing operating conditions; that is, that one need not be restricted by the characteristics of any existing piece of equipment.

1. Establish the necessary values of ℓ and D. Select a collimator design and tentative values of t (or S_ℓ) and θ.

2. Select desired values of γ, δ, ϵ, and T.

3. Determine the beam voltage which is necessary to achieve the desired value of γ, by the use of Eq. (12) or Eq. (23). Equation (12) is plotted in Fig. 33, for the case of spreading in air. If this voltage is prohibitive, there is no choice but to relax the requirement on γ.

4. Determine the beam current which is necessary by the use of Eq. (25) (or Eq. (26)). If this current is prohibitive, it may still be possible to achieve the desired results by changing θ or t or by using a different collimator design. If the current remains prohibitive, there is no choice but to relax the requirements on γ, δ, ϵ, or T.

5. Determine the counting rate which the detection equipment must handle by the use of Eq. (21).

6. Determine the collimator dimensions by use of Eq. (14).

Adherence to this procedure obviously cannot guarantee the success of the measurement because no consideration was given to stray electrons or to physical constraints (e.g., on the size of the collector, collimator, etc.) or to problems of electrical noise pickup. The procedure will, however, indicate whether the method is at all promising in the proposed application.

SECTION VIII
TESTS IN THE LOW DENSITY WIND TUNNEL

Reference has already been made to tests of this method which were carried out in the low density wind tunnel (Section 5.2). The tests were performed to determine whether the method, which looked promising theoretically, would have operational problems which could not be solved and also to provide a rough check on the accuracy of the measurements. Considerable difficulty was experienced with the equipment, but nothing was encountered for which a clear-cut solution was not available. Most of these difficulties have already been discussed in Section III.

The tunnel and the installation of the measuring equipment have already been described in Section 5.2. In these tests, the arc heater was run at a chamber pressure of 10 atm and a stagnation temperature of 3800°K. Free-stream Mach number was estimated to be 14.8 and static pressure 17 μ Hg, based on nonequilibrium flow calculations. Cold-flow data were taken at a chamber pressure of 2.7 atm, which resulted in the same mass flow as was obtained with the arc heater operating.

Several tests were performed with no flow in the tunnel. These included a number of calibrations made over a period of time, a test in which beam current was varied while pressure was held constant, and a test in which density measurements were made with a metal plate placed near the sensitive volume. Tests were also made with flow under cold-flow conditions and also with the arc heater operating. In both cases, density profiles were measured, and electron energy spectra were obtained under all conditions.

8.1 TESTS WITHOUT FLOW

One of the static calibrations has already been discussed (Section 5.2, Fig. 29). A group of such calibrations is presented in Fig. 40. These calibrations were made over a period of about two weeks, and the fact that they were consistent lends some confidence to the measurements. Each point plotted in Fig. 40 is the average of five individual measurements. The standard deviation of each group of measurements was calculated and is plotted in Fig. 41. If only statistical fluctuations contributed to these deviations, one would expect the deviation to approximate $\sqrt{C}$. This seems to be the case for low counting rates, where the statistical fluctuations are relatively large (percentage-wise), but at higher counting rates the deviations are larger than expected. Actually, the deviation appears to be roughly proportional to counting rate. This probably indicates that not only statistical fluctuation, but also fluctuation in current, voltage, and pressure contribute to the deviations.

The difficulty of obtaining an absolute density calibration has been mentioned in Section 6.4. This difficulty might be compounded if it were found that the beam heated the gas during a calibration without flow. A test was therefore run in which beam current was varied while pressure was held constant. The results are presented in Fig. 42. These data tend to indicate that the beam does in fact heat the gas (without flow). They are not considered to be conclusive, however, because the accuracy of the current and pressure measurements was not as high as was desired.

It has been shown that current density in the beam falls to a few percent of its maximum value, a few millimeters from the beam axis (Fig. 30). This information is sufficient to define the sensitive volume if all scattering is caused by collisions with gas molecules. However, if a solid object (e.g., a test model) is placed near the sensitive volume, it will scatter an appreciable number of electrons if it is struck by even a minute fraction of the total beam current. To document this effect, a metal plate was mounted in the tunnel test section, and apparent gas

density was measured at varying distances from it. These measurements are shown in Fig. 43. No appreciable effect is noticeable until the beam axis is within 3 cm of the plate. At a distance of 2 cm, the effect is not overwhelming, and measured densities might be corrected for the presence of the plate. These results tend to indicate that the method would be most useful in an empty test section, and that it would not be applicable, for instance, for studying shock waves in the vicinity of a model.

8.2 MEASUREMENT OF DENSITY PROFILES

The ultimate use for which this technique was developed was that of measuring density profiles in low density wind tunnels. Two such profiles were measured and are shown in Figs. 44 (cold flow) and 45 (arc heater operating). The "horned" profile is often encountered in conical nozzles with thick boundary layers and is also observed in pitot pressure profiles (Fig. 46). Each point plotted is the average of three individual measurements. The standard deviation of each group of measurements was calculated and found to be roughly that expected for the existing counting rate. It was found that if the apparatus was returned to a previous position, the measurement could be repeated within 1.0 percent, the statistical error being somewhat less than this. One such repeated point is shown in Fig. 44.

Because the flow in the nozzle is not in equilibrium, the density in the uniform core is not accurately known. The density during arc-heated runs was estimated by nonequilibrium flow calculations which were begun in the reservoir and were continued until the calculated pitot pressure matched the measured centerline pitot pressure (Fig. 46). These calculations predicted a density of 7.45×10^{-8} gm/cm^3, which is 10 percent higher than the density which was actually measured (Fig. 45). No density estimate was attempted under cold-flow conditions because of complications caused by liquifaction.

There was some question beforehand as to whether a hot-flow profile could be obtained at all, as it was quite possible that noise pickup from the arc heater would completely obliterate the extremely low level signal from the detector. Some noise was in fact picked up, but not enough to affect the measurements seriously. The noise counting rate was about 12 percent of the total counting rate over the uniform core. Since it remained quite constant over the period during which the profile was taken, the measurements were corrected by merely subtracting the noise counting rate. Although the problem of noise pickup from the arc heater is a difficult one, it appears that it can be overcome by scrupulous attention to shielding and grounding.

8.3 EFFECT OF FLOW ON BEAM CURRENT MEASUREMENT

One completely unexpected phenomenon was observed when these profiles were made. Up to this time, beam current had been measured at the collector by connecting a meter between the collector and ground. This was considered to be more accurate than measuring the current in the grounded power supply lead, since this latter measurement included some leakage and corona current. However, as soon as flow was established, with or without operating the arc heater, the collector current dropped drastically and fluctuated between one-third and two-thirds of the power supply current. The profiles were taken by measuring power supply current and subtracting the leakage current, which was small but not negligible. The fact that the density measurements were repeatable verifies that this was a valid measure of beam current. No explanation for the drop in collector current is available. It is inconceivable that the stream velocity (3000 m/sec) could have any effect on the beam electrons, which travel at four-tenths of the speed of light. The effect must certainly be caused by positive ions formed by the beam, but to say more than this would be conjecture.

8.4 SPECTRA OF DETECTED ELECTRONS

The energy spectrum which was discussed in Section 6.6 (Fig. 28) is representative of most of those which were taken throughout these tests. They were resolved into single scattered electrons, stray electrons, and preamplifier noise peaks, by the method described in Section 6.4, and the results (except on arc heated runs) were quite similar. The counting rate caused by preamplifier noise peaks was found to be entirely negligible. During an early run, the valley in the spectrum occurred at 26 v. During subsequent calibrations and measurements, this value was arbitrarily used as the baseline voltage. This was a moderately poor choice and by choosing a higher baseline voltage, say 31 v, one could have rejected almost all of the stray electrons, while rejecting only 1.7 percent of the single scattered electrons. However, this choice did not seriously compromise the measurements.

Many of the spectra taken during the calibrations were resolved into components, and it was found that the number of stray electrons varied from about 3 percent of the total counted at low densities (10 μ) to about 7 percent at high densities (100 μ). The number of stray electrons is a function of beam spreading and apparently increases faster than the density in this case. Had the percentage of stray electrons remained constant as density varied, one would be tempted to say that they caused no error. This is not the case, however, since

the number of stray electrons is a function of density all along the beam, not just in the sensitive volume. Regardless of these considerations, it is safe to say that in this application the error caused by stray electrons can be made less than 1.0 percent by properly choosing the baseline voltage, even without using a black body opposite the detector.

The spectrum of the arc heater noise (Fig. 47) was interesting. It was obtained by measuring the integral noise spectrum with the arc heater operating, but with the beam off. The salient feature of this spectrum is that, in contrast to the case of stray electrons, little reduction in arc heater noise counting rate can be achieved by increasing the baseline voltage. Evidently, the only means available for reducing this counting rate is to improve shielding so as to reduce the pickup.

SECTION IX
CONCLUSIONS

It seems well established that the principle of density measurement by radiation scattering can indeed be applied using high-speed electrons as the probing particle. Moreover, the spatial resolution and measuring time which can be achieved at low density using electrons are far superior to those available using photons. The Rutherford theory satisfactorily explains the counting rates which were observed.

The most significant conclusion which can be drawn from the tests in the low density wind tunnel is that measurements made by this technique can be repeatable within 1.0 percent. It was found that the error caused by stray electrons could, with ease, be made negligible. Noise pickup from the arc heater was significant but not devasting, and means for reducing this noise source are probably available. It was found that valid density measurements could be made within about 2 cm of a metal object in the flow at a pressure of 11μ. This is about one-twentieth of the test section diameter. Although this figure might be improved somewhat, it appears that the technique could not be used, for instance, for studying shock structure near a model.

The most important limitations on the precision of the density measurement are presently imposed by the beam voltage and current measurements, and by the stray electrons in the test section. There seems to be no reason why the voltage measurement cannot be improved as much as desired, merely by using more sophisticated instrumentation. This is probably also the case with the current measurement, although the curious behavior of the collector current (Section 8.3) still needs to be explained. The stray electrons are probably electrons which have

escaped from the collector. The methods which are available for eliminating the effects of stray electrons have been discussed. In a facility with an open jet test section, these effects can be reduced to insignificance; if the flow is enclosed in a channel, perhaps they cannot.

Some further development work needs to be done. The Rutherford theory predicts that a large improvement in performance can be achieved by using a scattering angle of 45 deg in place of 90 deg. It also appears that another large improvement can be made by using a lens collimator in place of a slit collimator. It would be interesting to make these changes and see if the promise is fulfilled. Further analytical and experimental work is necessary to explain (or at least to document) the discrepancy between the predicted and measured beam spreading. The spatial resolution which is quoted in this report was determined only indirectly. It would be useful to confirm these values by direct measurement, if a technique for doing so can be devised.

A direct comparison between the capabilities of this technique and the fluorescence technique for density measurement (which is already an established diagnostic method) would be very informative. It appears that the scattering measurement might hold the advantage in measuring time and might be applicable at both lower and higher densities than the fluorescence measurement. The fluorescence measurement may hold some advantage in spatial resolution, since no beam spreading occurs between the sensitive volume and the detector. More important, however, the scattering measurement offers the possibility of being entirely independent of the state of the gas, and this may not be the case with the fluorescence measurement. This predicted independence has of course not yet been confirmed.

REFERENCES

1. Shepard, J. E. and Dicks, J. B. "A Technique for Measuring Local Gas Density Using Scattered Gamma Radiation." AEDC-TDR-63-187 (AD423150), November 1963.

2. Hurlbut, F. C. "An Electron Beam Density Probe for Measurements in Rarefied Gas Flows." WADC-TR-57-644 (AD155537), January 1958 (University of California).

3. Ballard, H. N. and Variable, D. "Shock-Front-Thickness Measurements by an Electron Beam Technique." Physics of Fluids, Vol. 1, No. 3, 1958, p. 225.

4. Wada, I. "Studies of the Flow in a Low Pressure Hypersonic Shock Tunnel Using an Electron-Beam Densitometer." NAL TR-37T, 1963.

5. Gadamer, E. O. "Measurement of the Density Distribution in a Rarefied Gas Flow Using the Fluorescence Induced by a Thin Electron Beam." UTIA Report 83, March 1962.

6. Budell, MacArthur, and Stevenson, L. M. "Flow Visualization and Quantitative Gas Density Measurements in Rarefied Gas Flows." ASD-TDR-62-793, December 1962 (Cornell Aero Lab).

7. Zempel, R., Mallin, J., and Muntz, E. "An Electron Beam Excitation Technique for the Measurement of Low Densities in Hypersonic Shock Tunnel Flows." G. E. Document No. 63SD707 (AD412726), August 1963.

8. Muntz, E. P. "Measurement of Rotational Temperature, Vibrational Temperature and Molecule Concentration in Non-Radiating Flows of Low Density Nitrogen." UTIA Report 71, 1961.

9. Muntz, E. P. "Static Temperature Measurements in a Flowing Gas." Physics of Fluids, Vol. 5, No. 1, 1962, p. 80.

10. Muntz, E. P. and Marsden, D. J. "Electron Excitation Applied to the Experimental Investigation of Rarefied Gas Flows." Third International Rarefied Gas Dynamics Symposium, Vol. 2, Academic Press, New York, 1963.

11. Falckenberg, H. R. and Schumacher, B. W. "The Possibilities for Gas Density Gauging by Single Scattering of Electrons." Canadian Journal of Physics, Vol. 40, 1962, p. 1521.

12. Rupp, A. K. "An Investigation of the Use of Radiation from Radioisotopes to Measure Density Altitude." Thesis, USAF Institute of Technology, GA/Phys/62-13, August 1962.

13. Camac, M. "Argon and Nitrogen Shock Thicknesses." AVCO Everett Research Laboratory, Research Report 172, BSD-TDR-63-257, December 1963.

14. Birkhoff, R. D. "The Passage of Fast Electrons through Matter." Encyclopedia of Physics, Vol. XXXIV, Springer-Verlag, Berlin, 1958, p. 53, edited by S. Flugge.

15. Shankland, R. S. Atomic and Nuclear Physics. The Macmillan Company, New York, 1960, p. 60 (Second Edition).

16. McKinley, W. A., Jr., and Feshback, H. "The Coulomb Scattering of Relativistic Electrons by Nuclei." Physical Review, Vol. 74, No. 12, December 1948.

17. Rossi, B. and Greisen, K. "Cosmic Ray Theory." Review of Modern Physics, Vol. 13, October 1941, p. 240.

18. Trump, J. G., Safford, F. J., and Cloud, R. W. "D-C Breakdown Strength of Air and of Freon in a Uniform Field at High Pressures." AIEE Transactions, Vol. 60, 1941, p. 132.

19. Trump, J. G. and Andrias, J. "High-Voltage D-C Flashover of Solid Insulators in Compressed Nitrogen." AIEE Transactions, Vol. 60, 1941, p. 986.

20. Trump, J. G. and Van de Graaff, R. J. "Insulation of High Voltages in Vacuum." Journal of Applied Physics, Vol. 18, 1947, p. 327.

21. Gleichauf, P. H. "Electrical Breakdown over Insulators in High Vacuum." Journal of Applied Physics, Vol. 22, 1951, p. 766.

22. Schumacher, B. W. "The Design of Dynamic Pressure Stages for High-Pressure/High-Vacuum Systems." UTIA Report 78, August 1961.

23. Instruction Manual, Silicon Surface Barrier Detector. Oak Ridge Technical Enterprises Corporation, Oak Ridge, Tennessee, 1964, Section 2.2.

24. Chang, S. S. L. Synthesis of Optimum Control Systems. McGraw-Hill Book Company, Inc., New York, 1961, p. 47.

25. Trump, J. G. and Van de Graaff, R. J. "The Secondary Emission of Electrons by High Energy Electrons." Physical Review, Vol. 75, 1949, p. 44.

26. Spangenburg, K. R. Vacuum Tubes. McGraw-Hill Book Company, Inc., New York, 1948, p. 440.

APPENDIX I
ILLUSTRATIONS

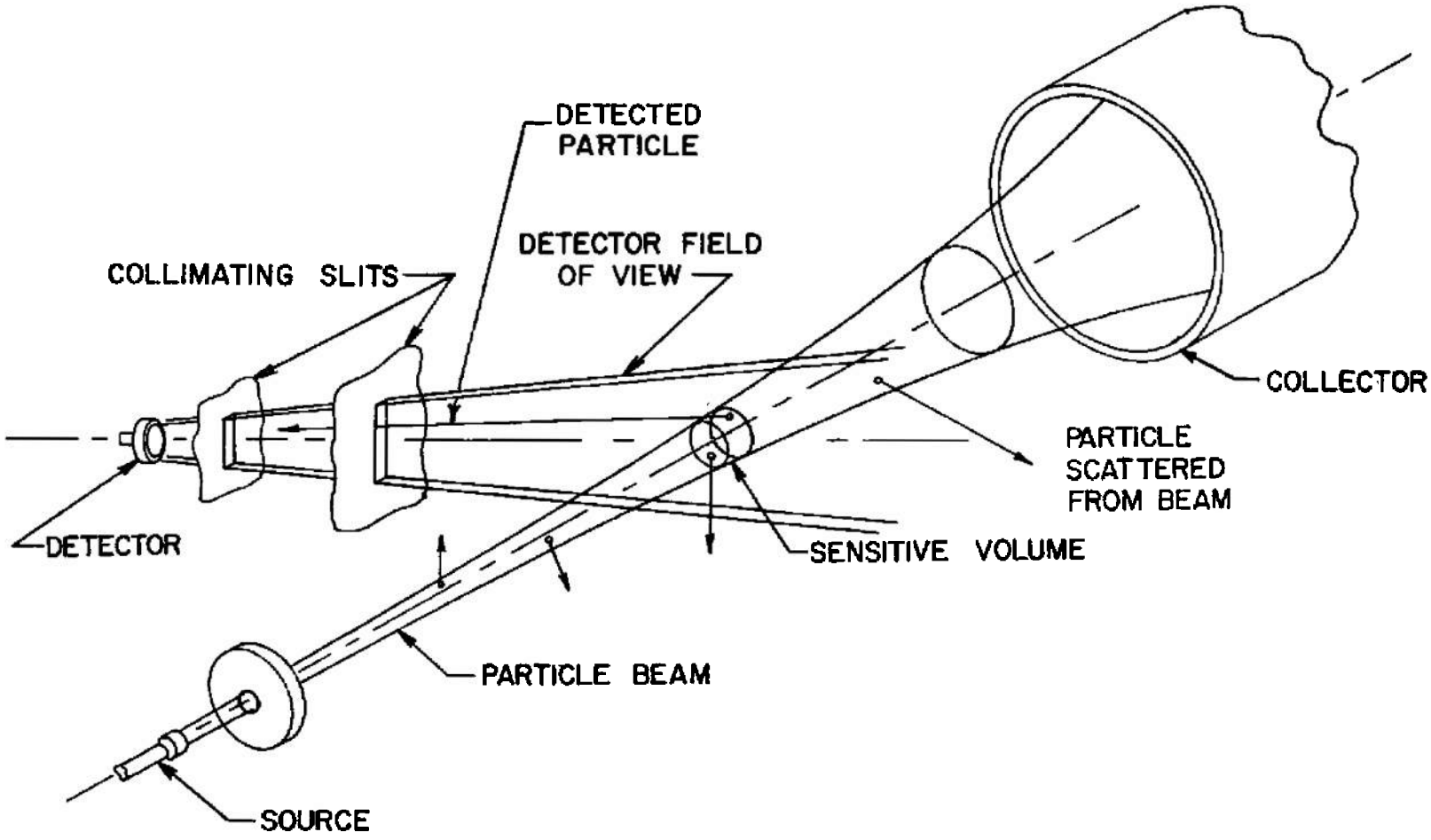

Fig. 1 Principle of Density Measurement by Radiation Scattering

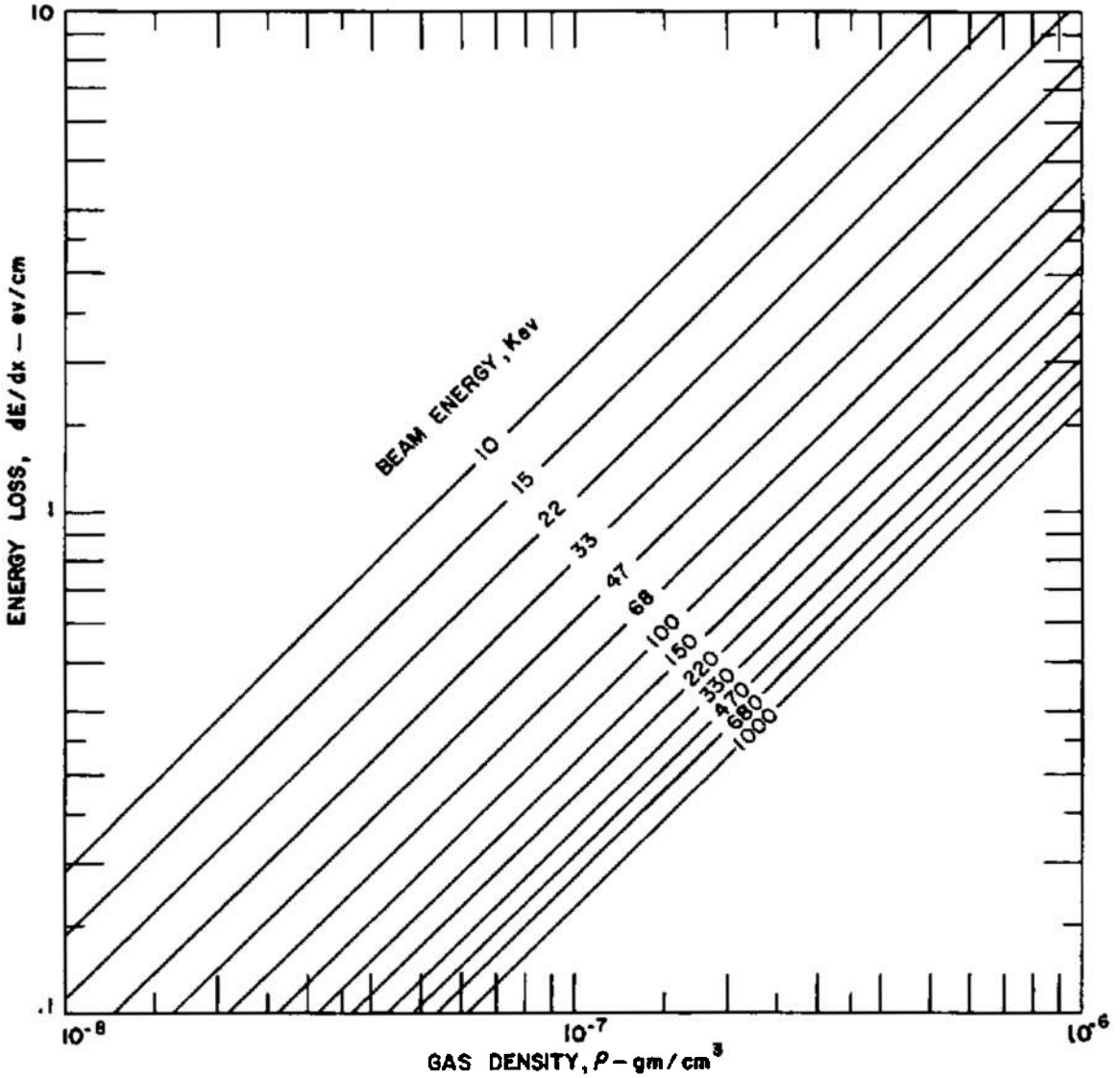

Fig. 2 Energy Loss of Electrons Caused by Inelastic Collisions

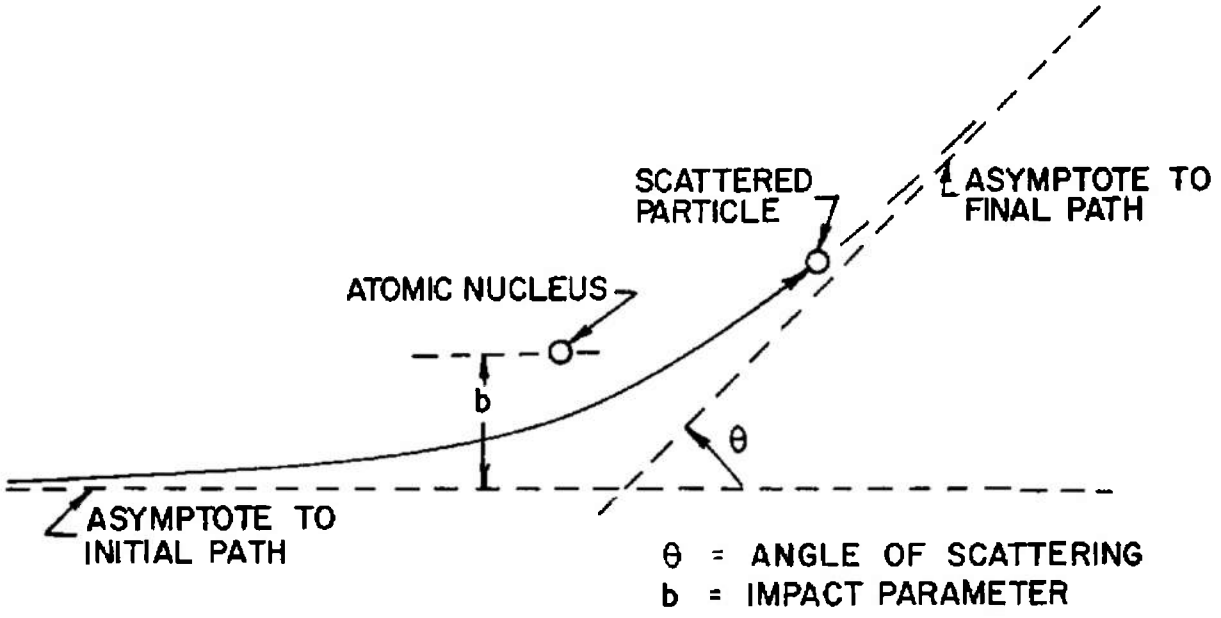

Fig. 3 Geometry of Rutherford Scattering

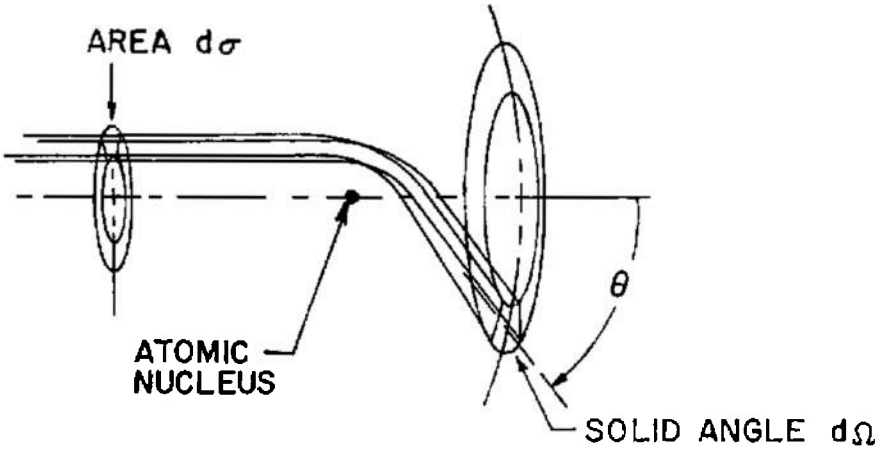

Fig. 4 Physical Significance of Differential Cross Section

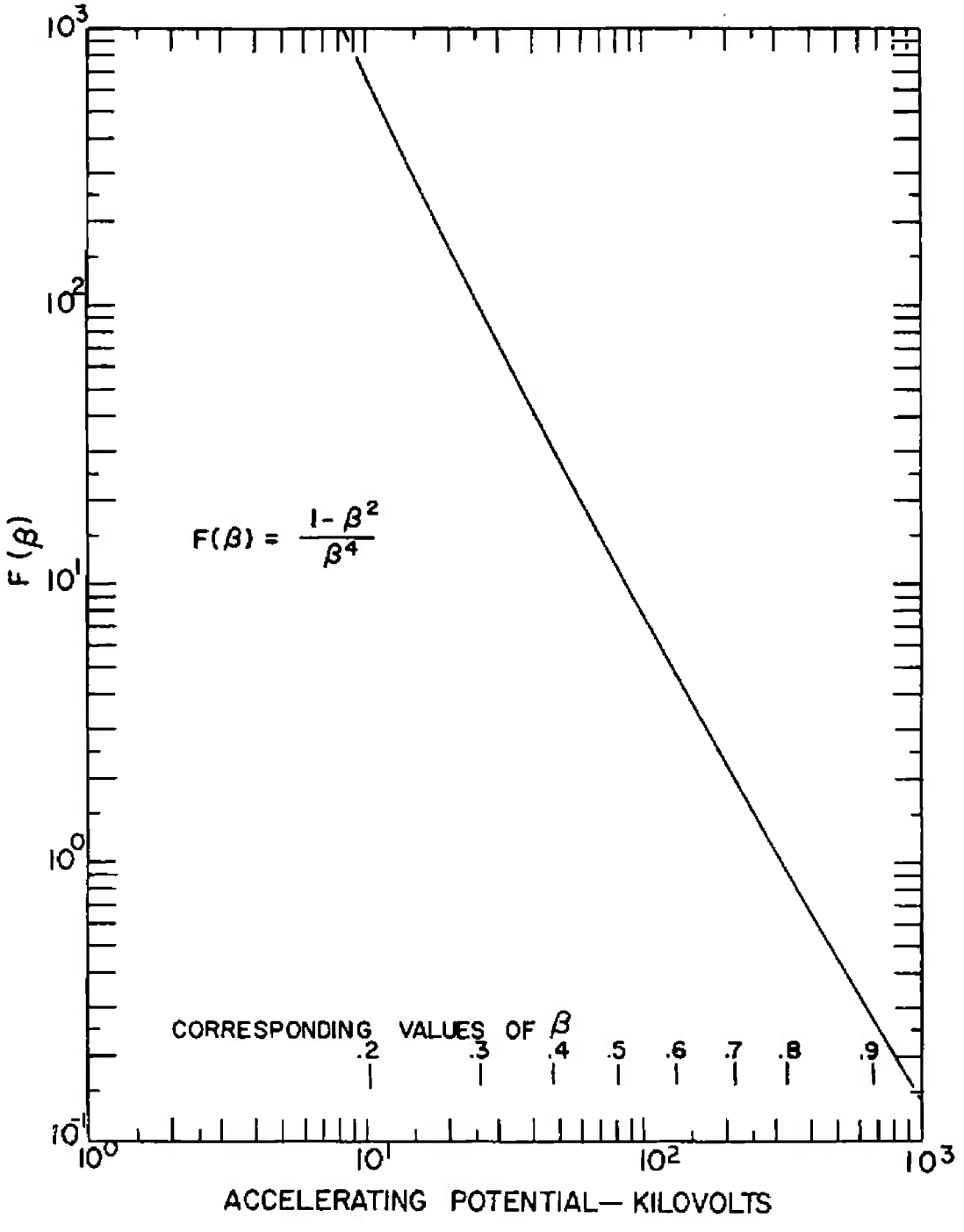

Fig. 5 Function F (β)

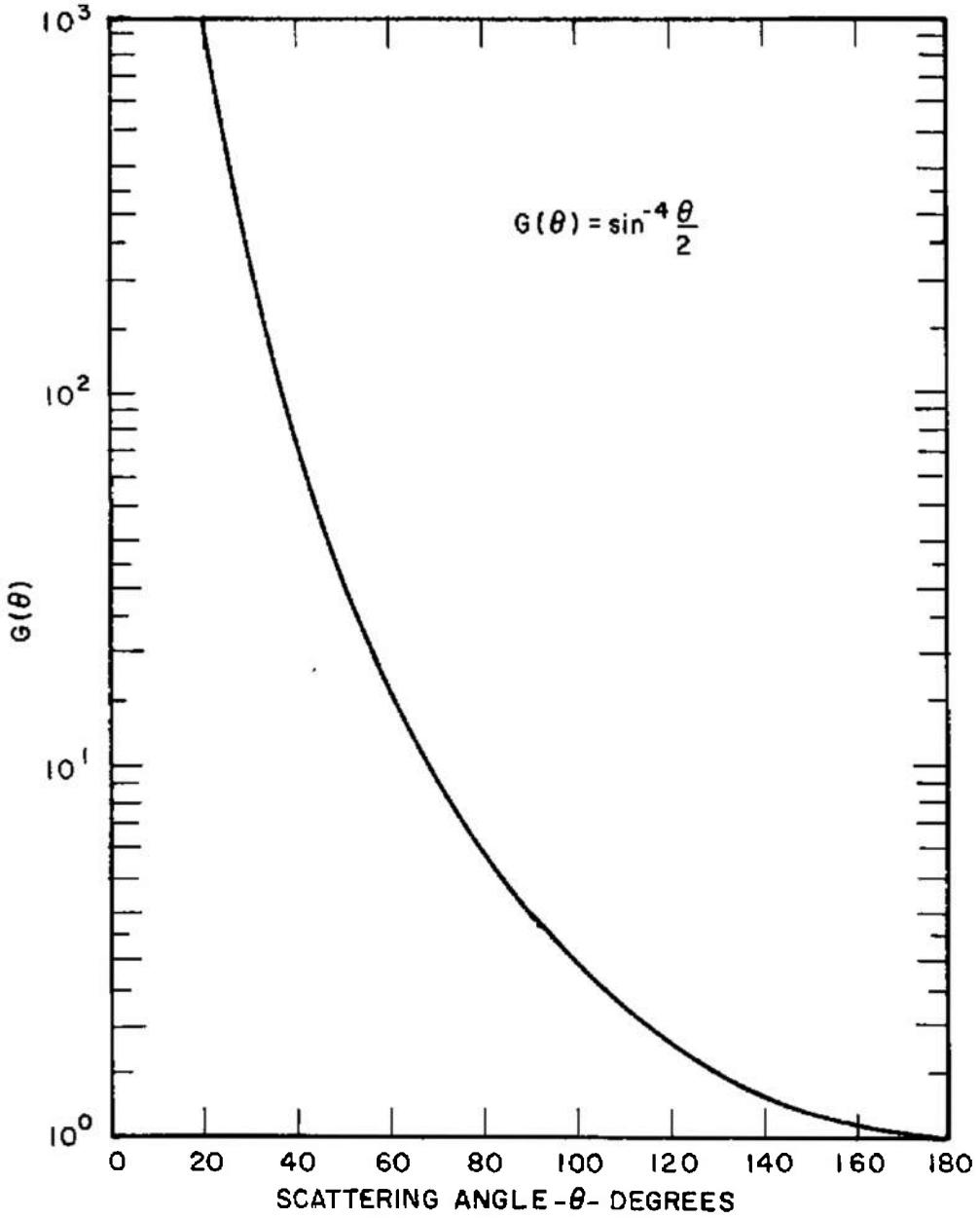

Fig. 6 Function $G(\theta)$

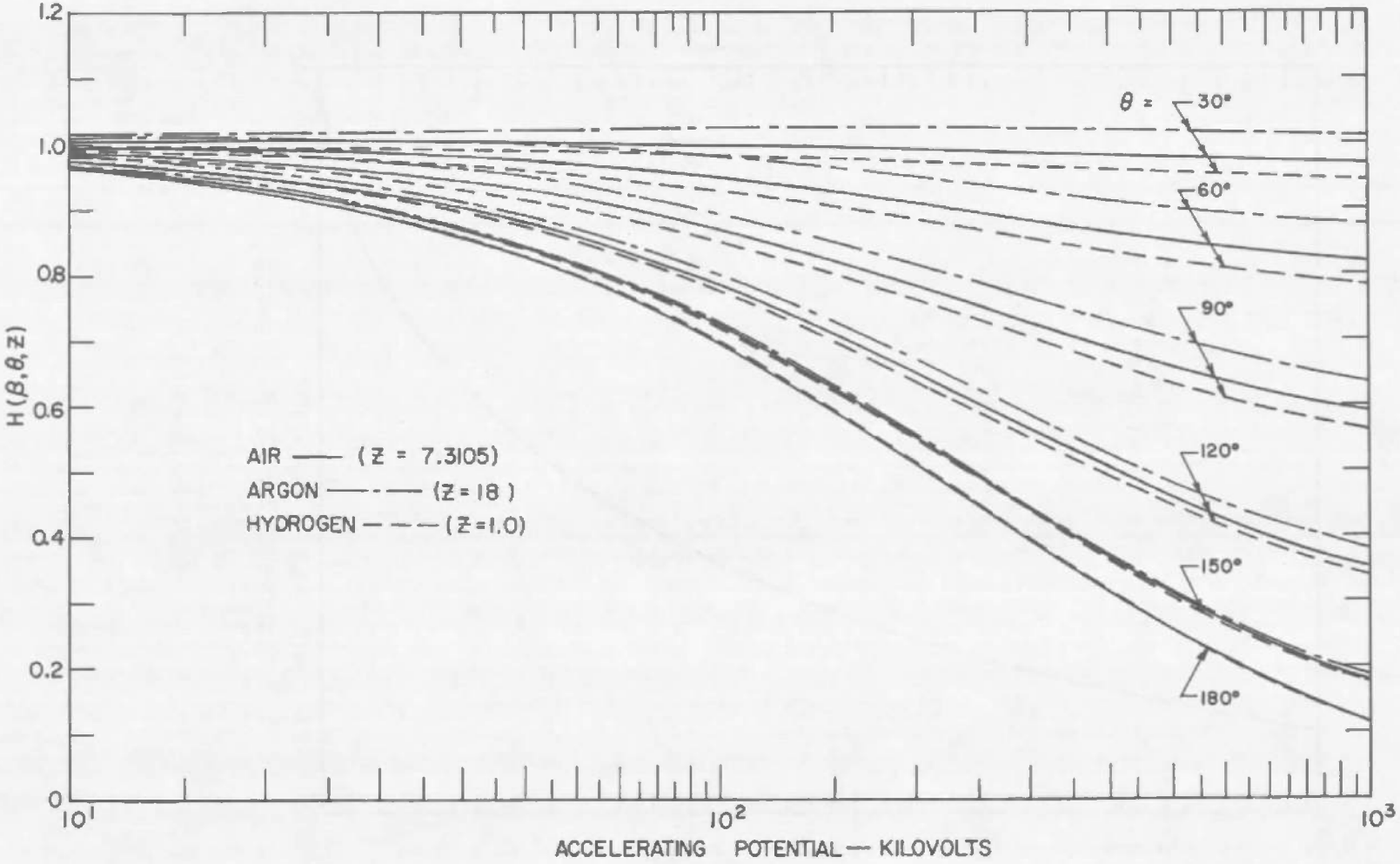

Fig. 7 Function H(β, θ, Z)

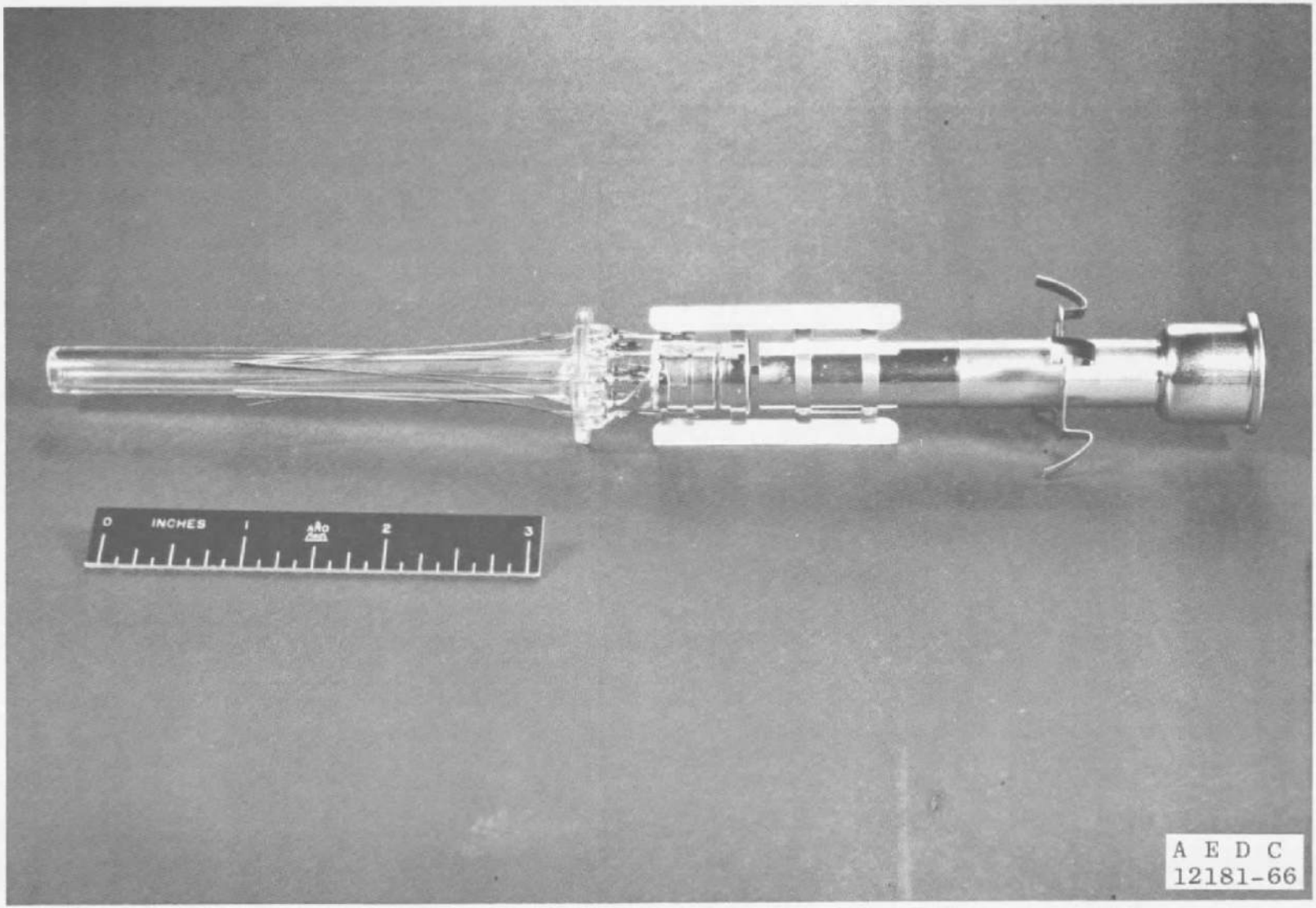

Fig. 8 Photograph of Type 7NA Electron Gun

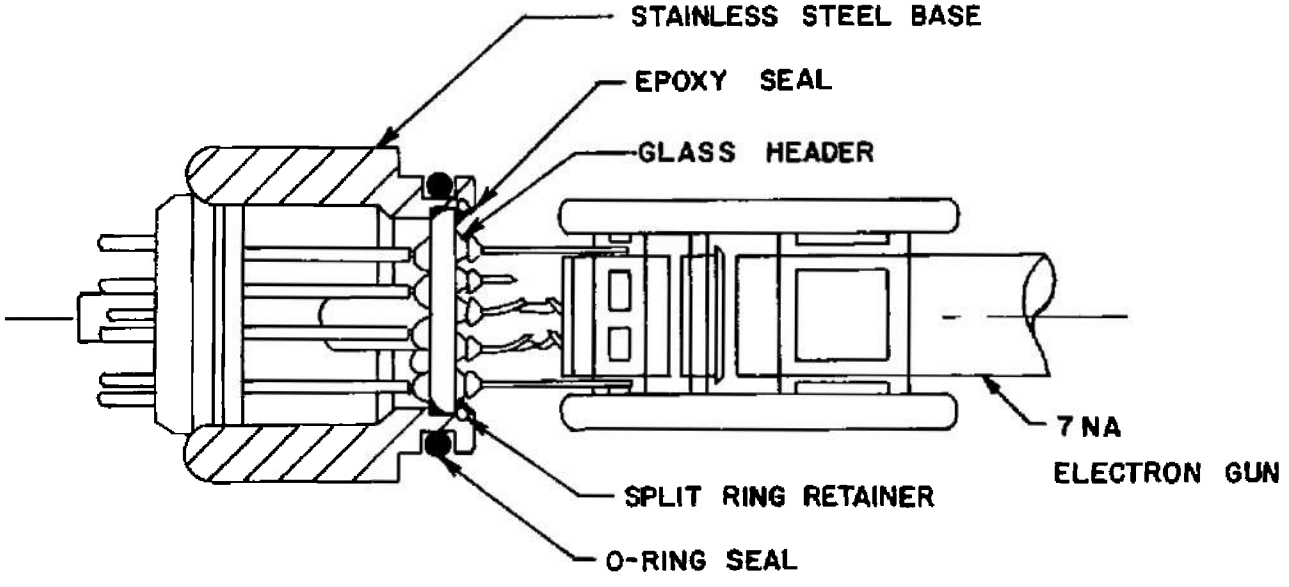

Fig. 9 Method of Sealing the Gun Header to the Vacuum System

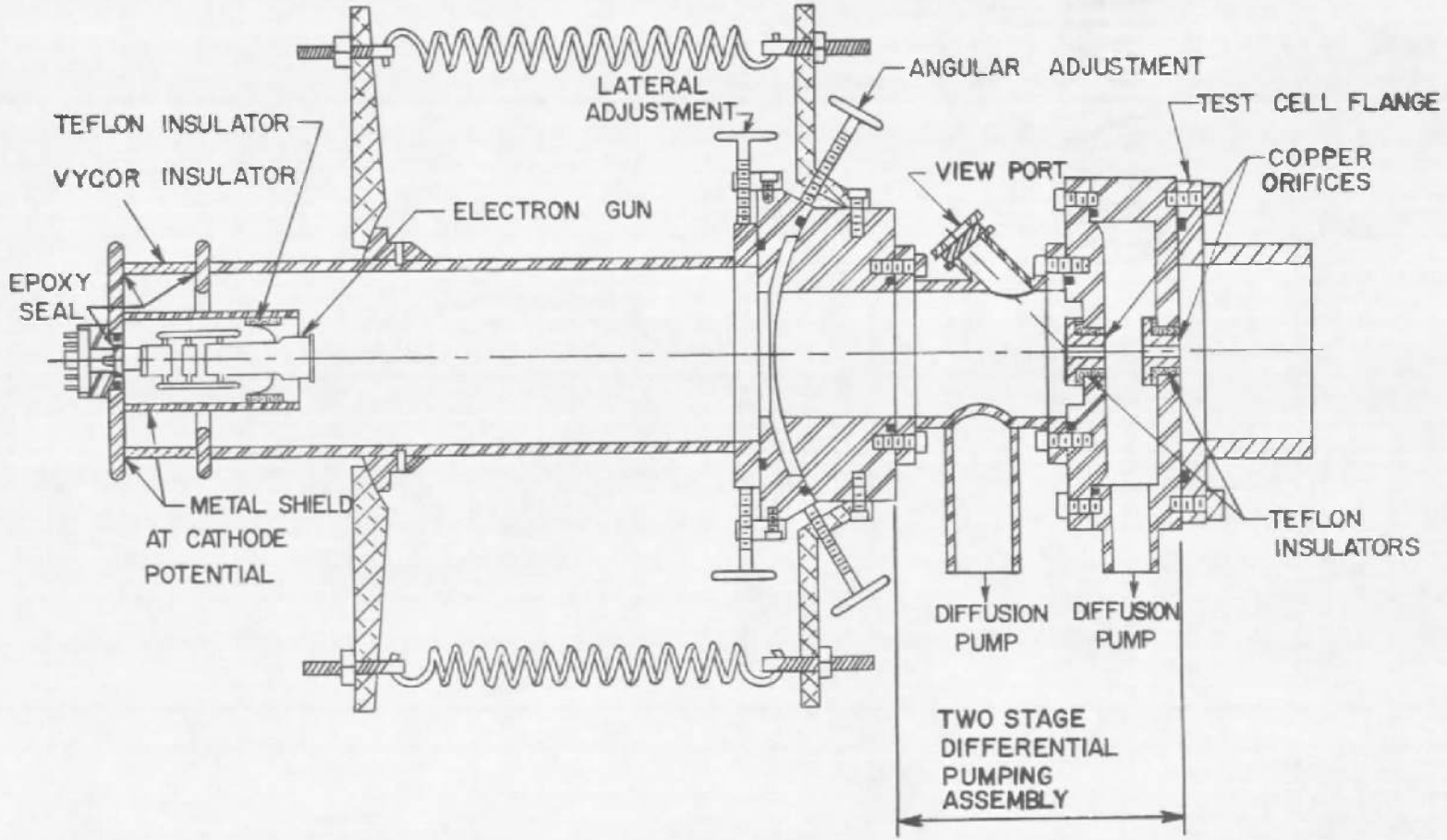

Fig. 10 Electron Gun Housing Using Mechanical Alignment

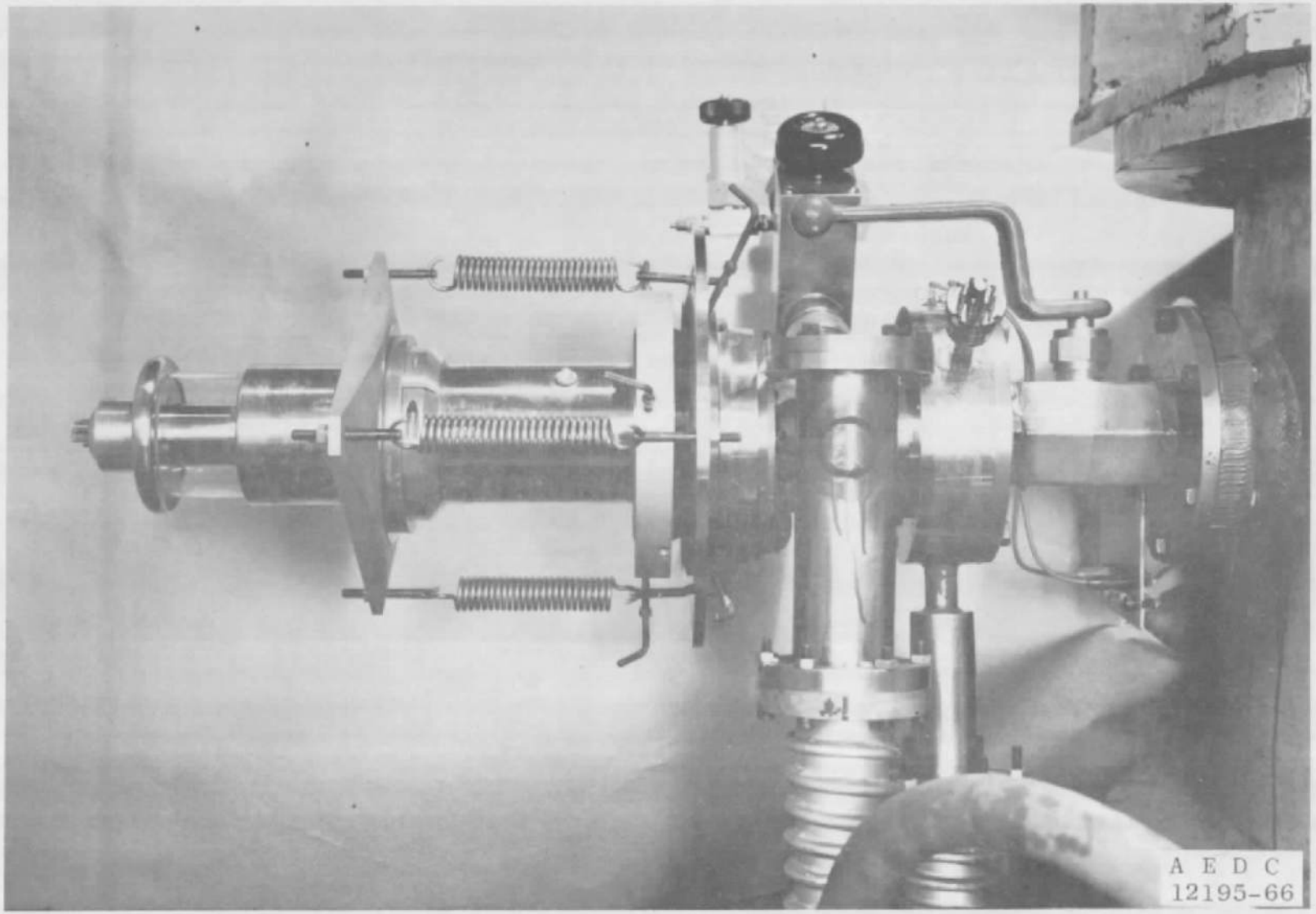

Fig. 11 Photograph of Electron Gun Housing with Mechanical Alignment

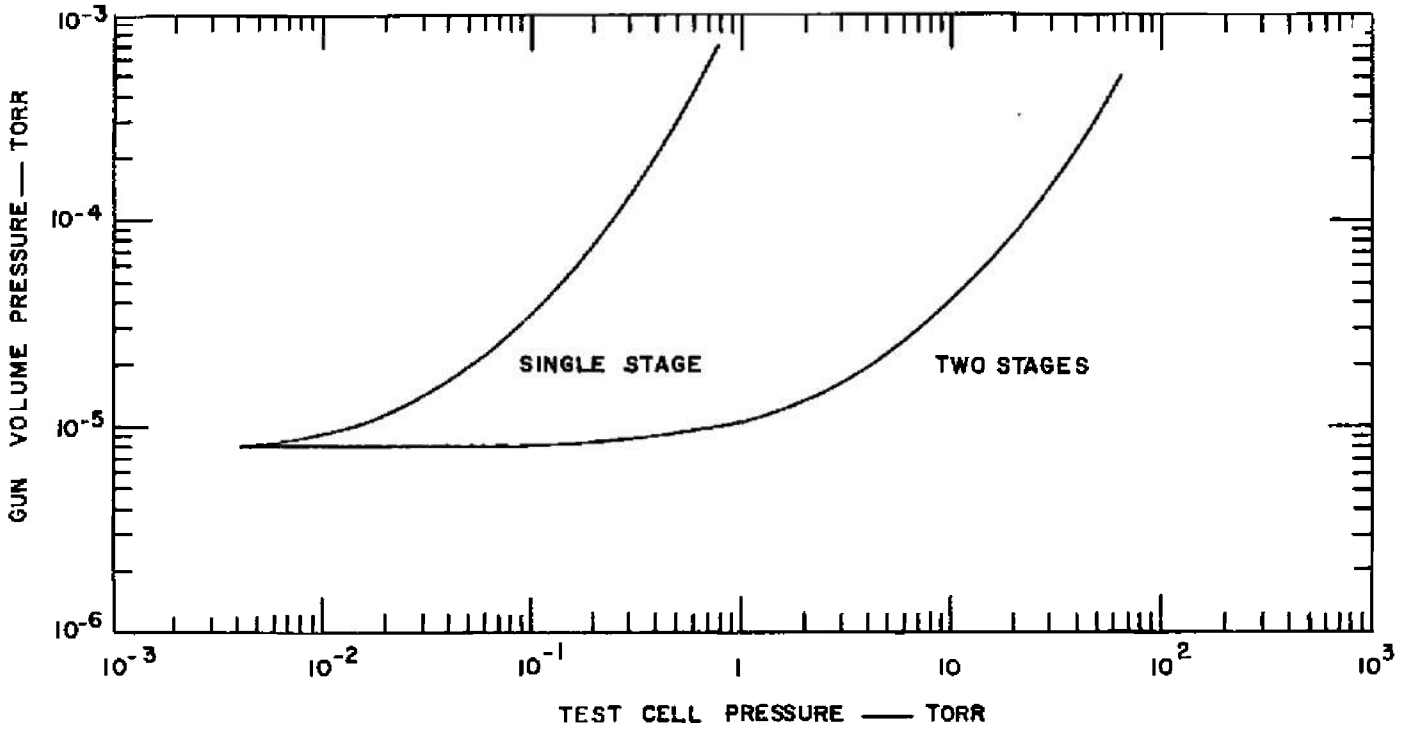

Fig. 12 Vacuum System Performance for Assembly Shown in Fig. 10

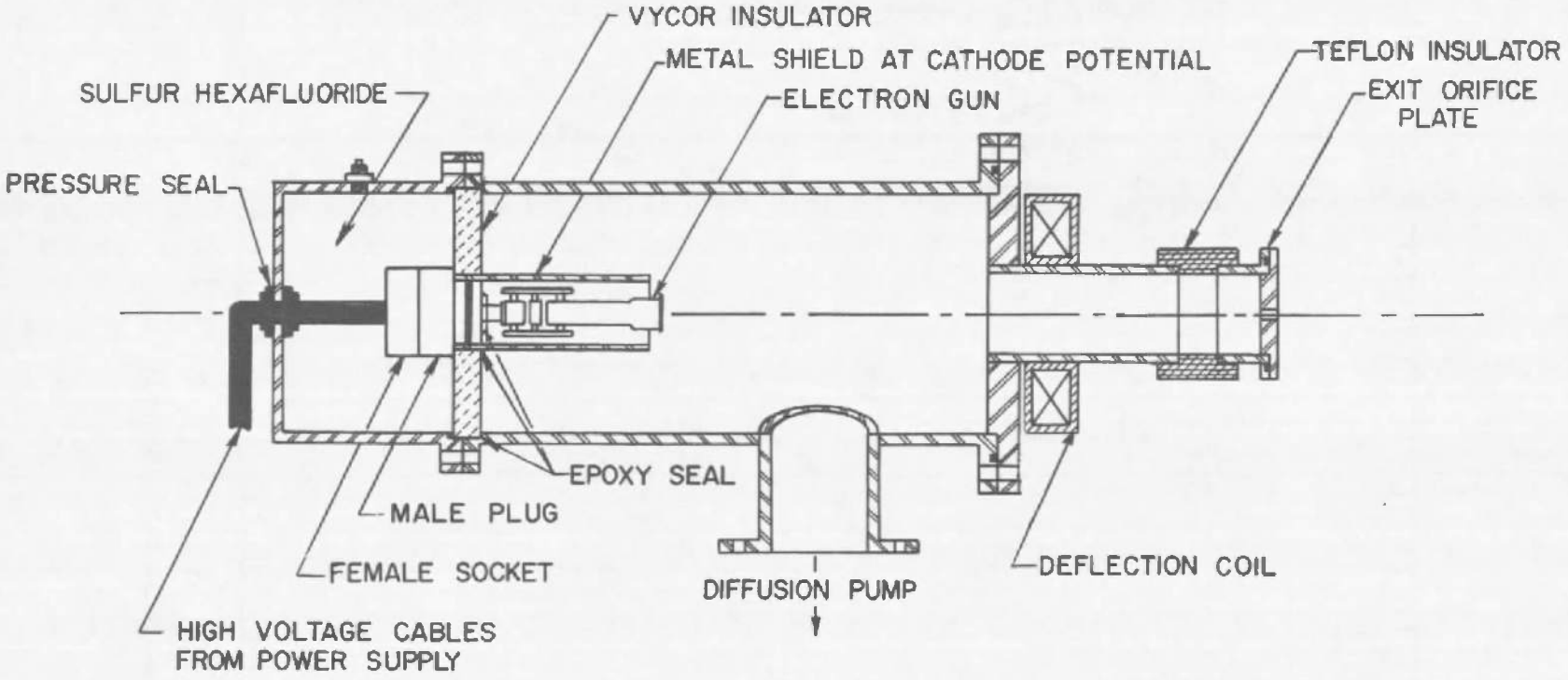

Fig. 13 Electron Gun Housing Using Deflection Coils for Alignment

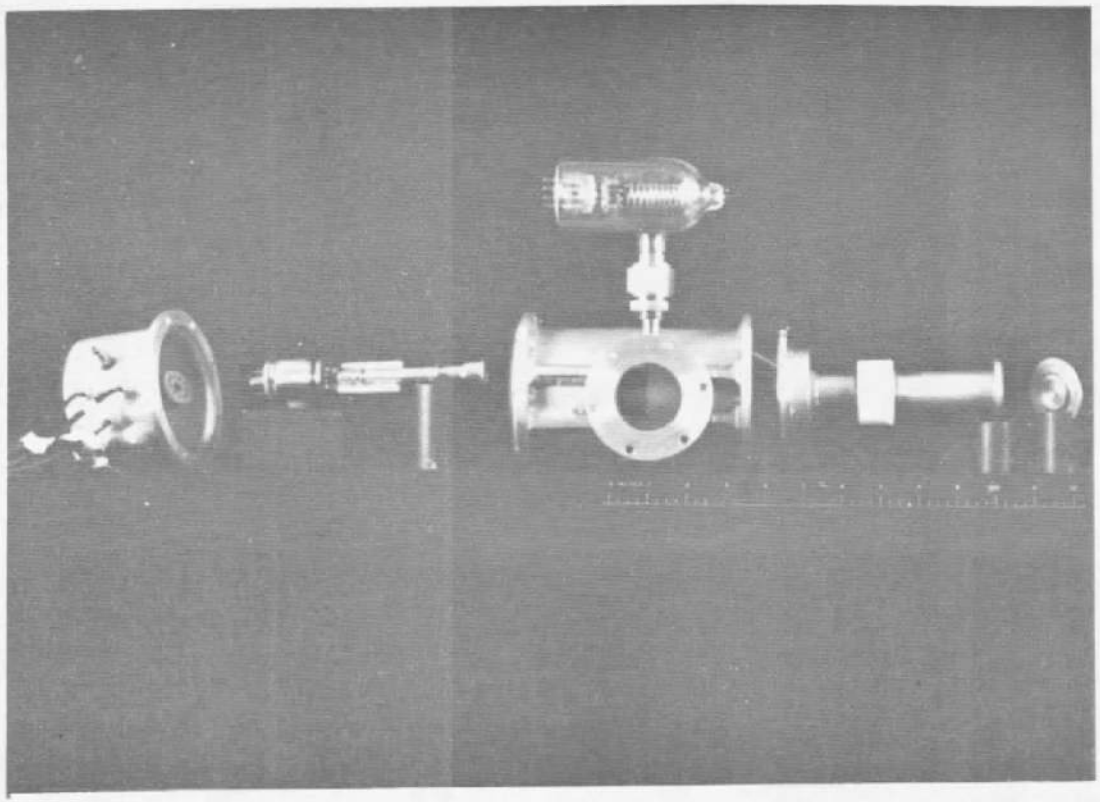

Fig. 14 Photograph of Electron Gun Housing Using Deflection Coils for Alignment

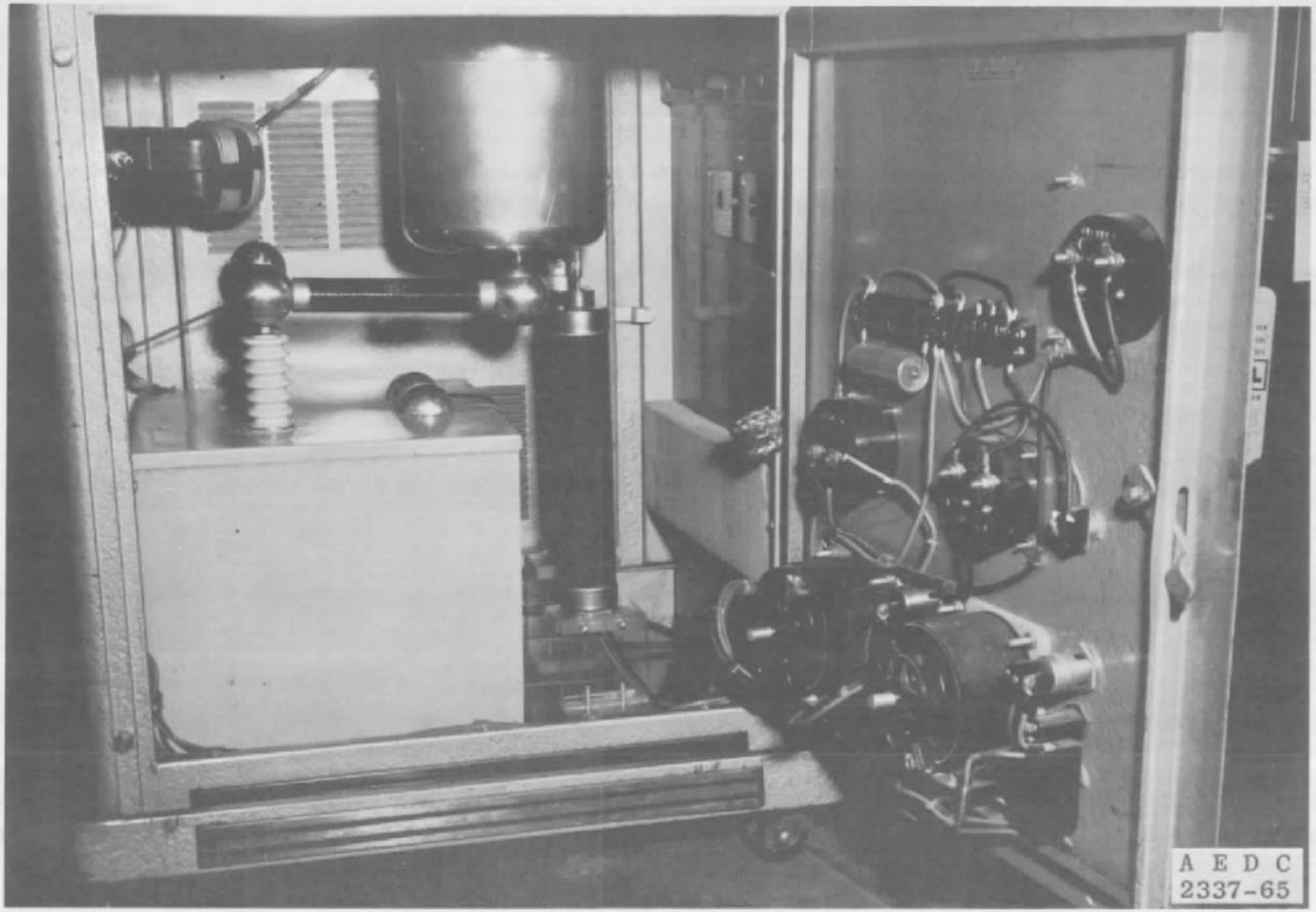

Fig. 15 Photograph of 50-kv Power Supply

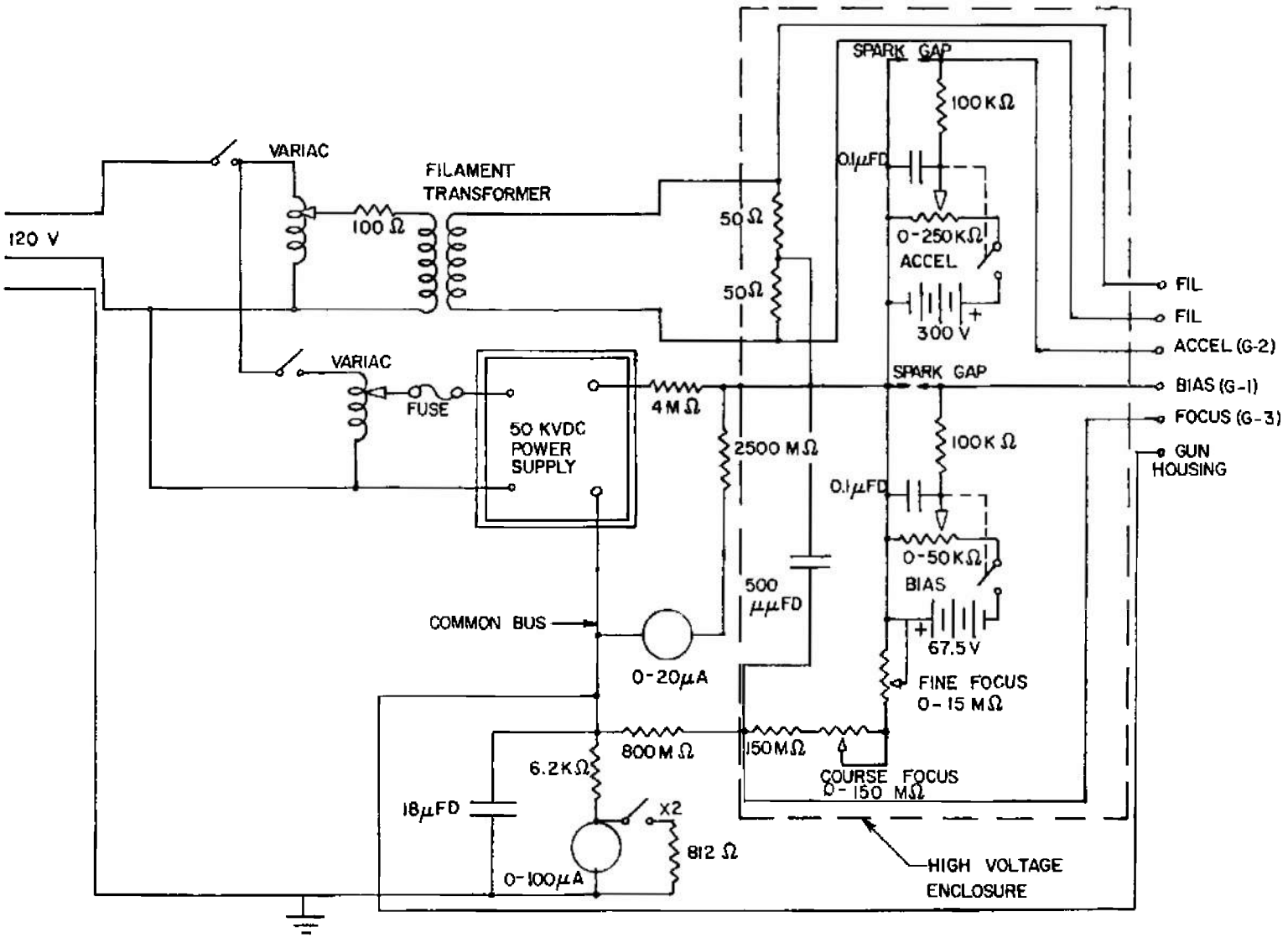

Fig. 16 Schematic Diagram of 50-kv Power Supply

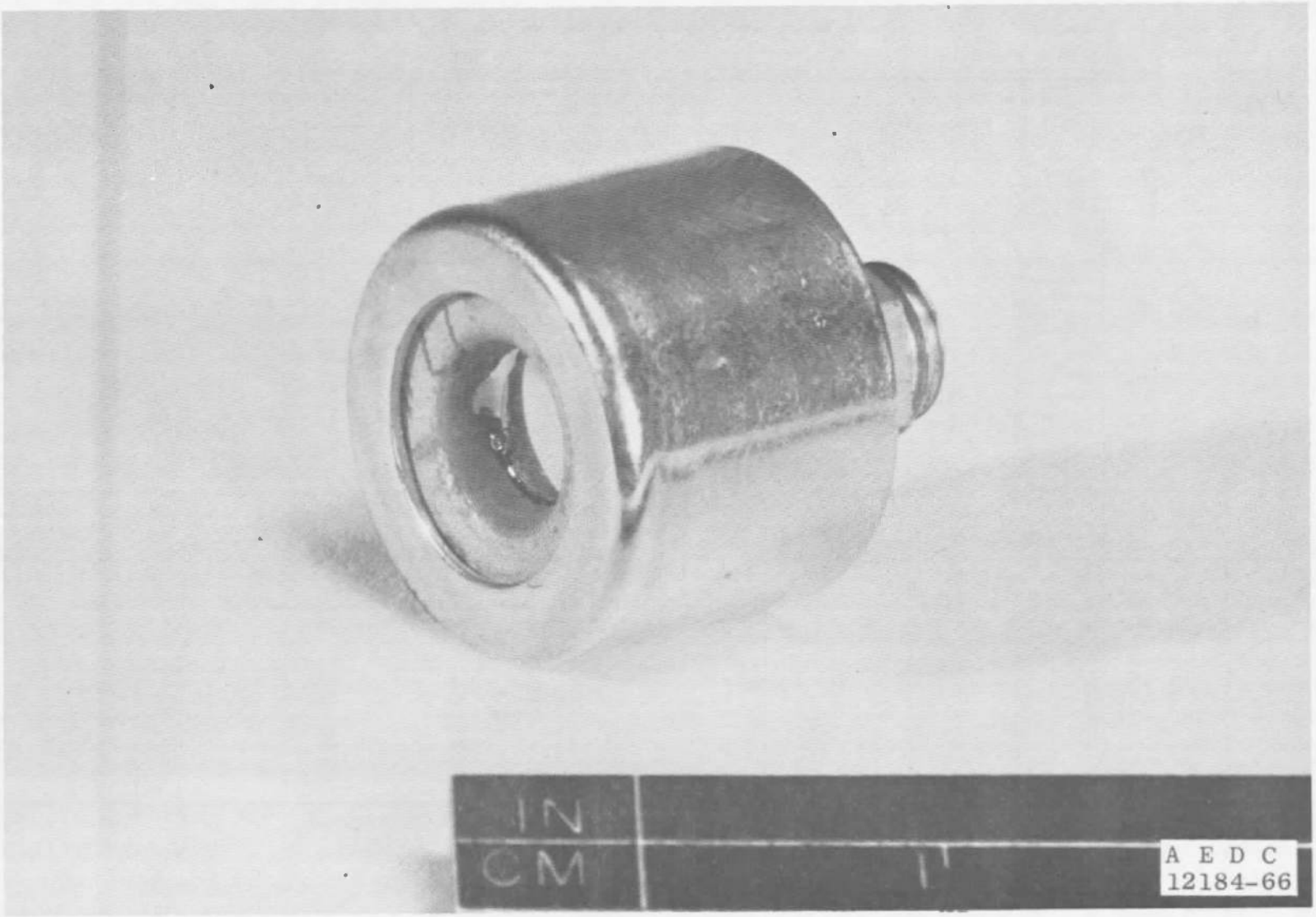

Fig. 17 Photograph of Silicon Surface Barrier Detector

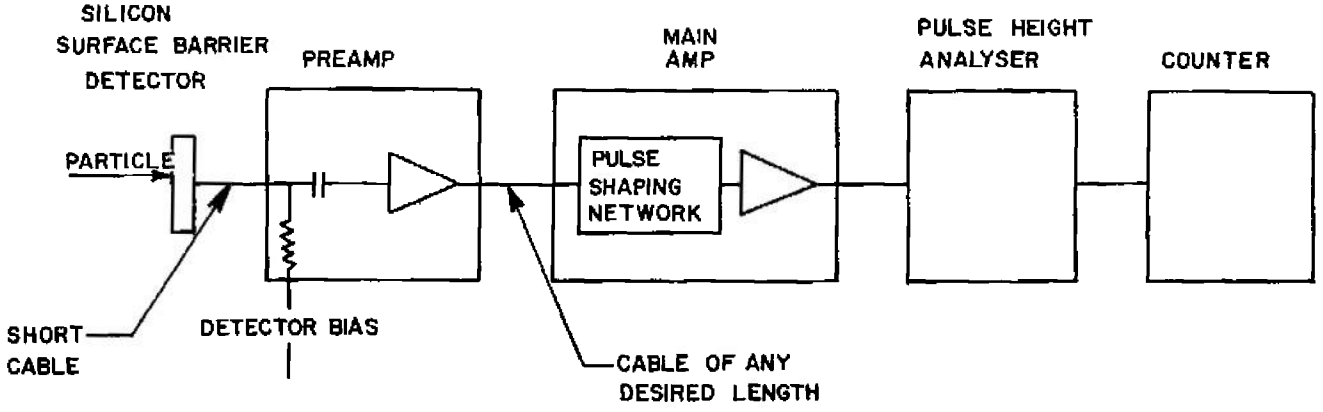

Fig. 18 Instrumentation Used with Silicon Surface Barrier Detector

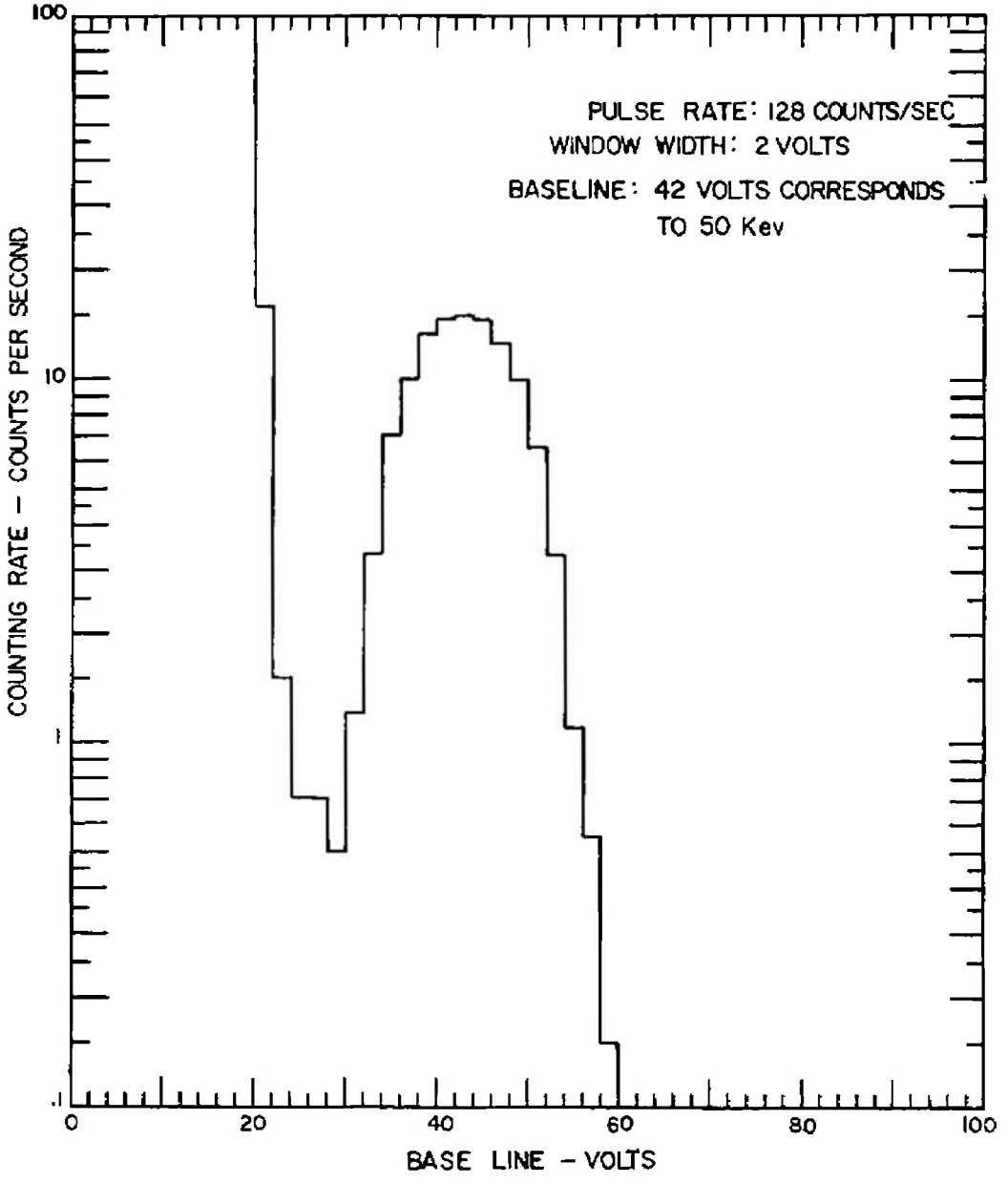

Fig. 19 Differential Spectrum of Pulse Generator Output

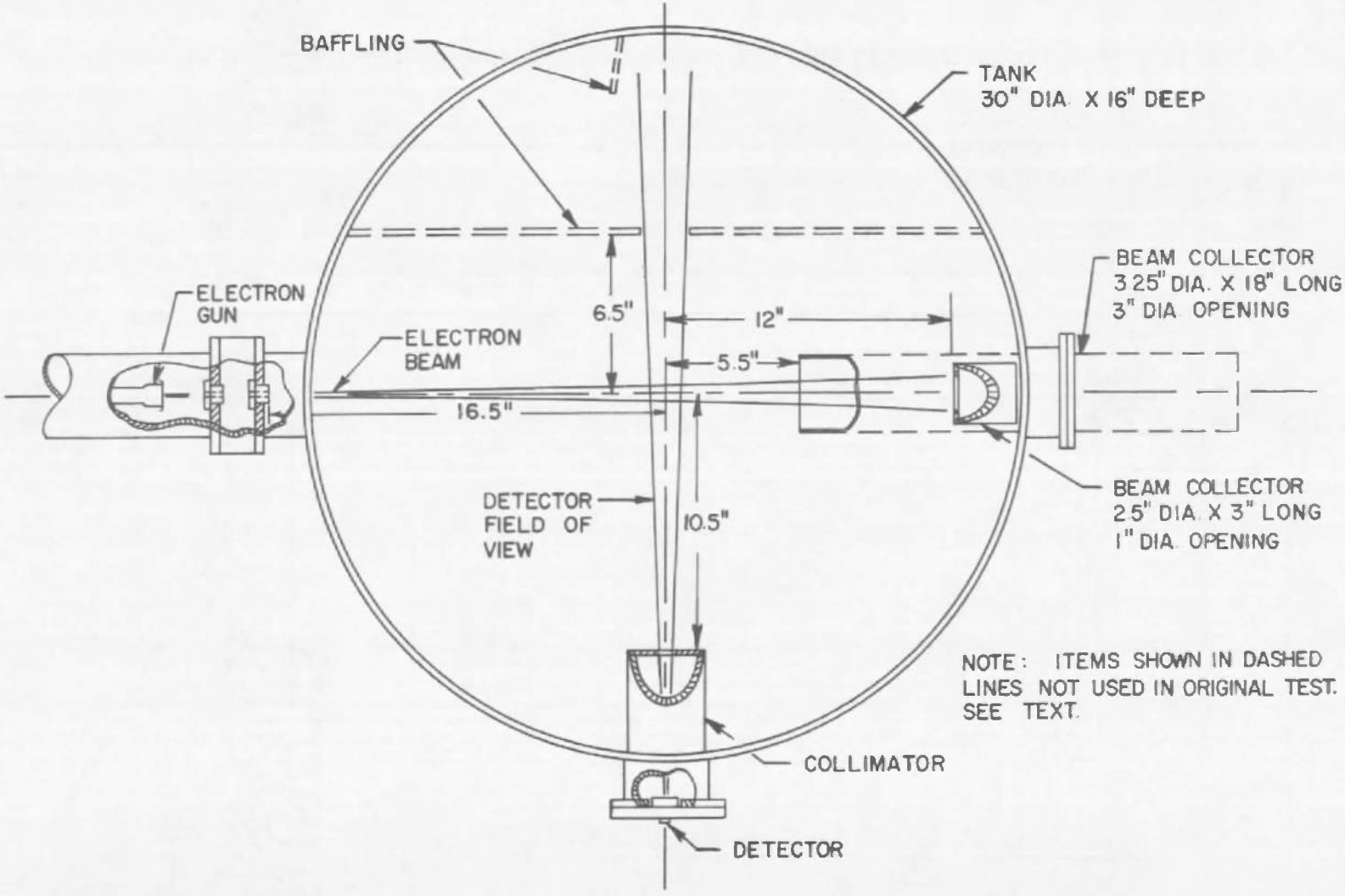

Fig. 20 Arrangement of Scattering Equipment in Tank

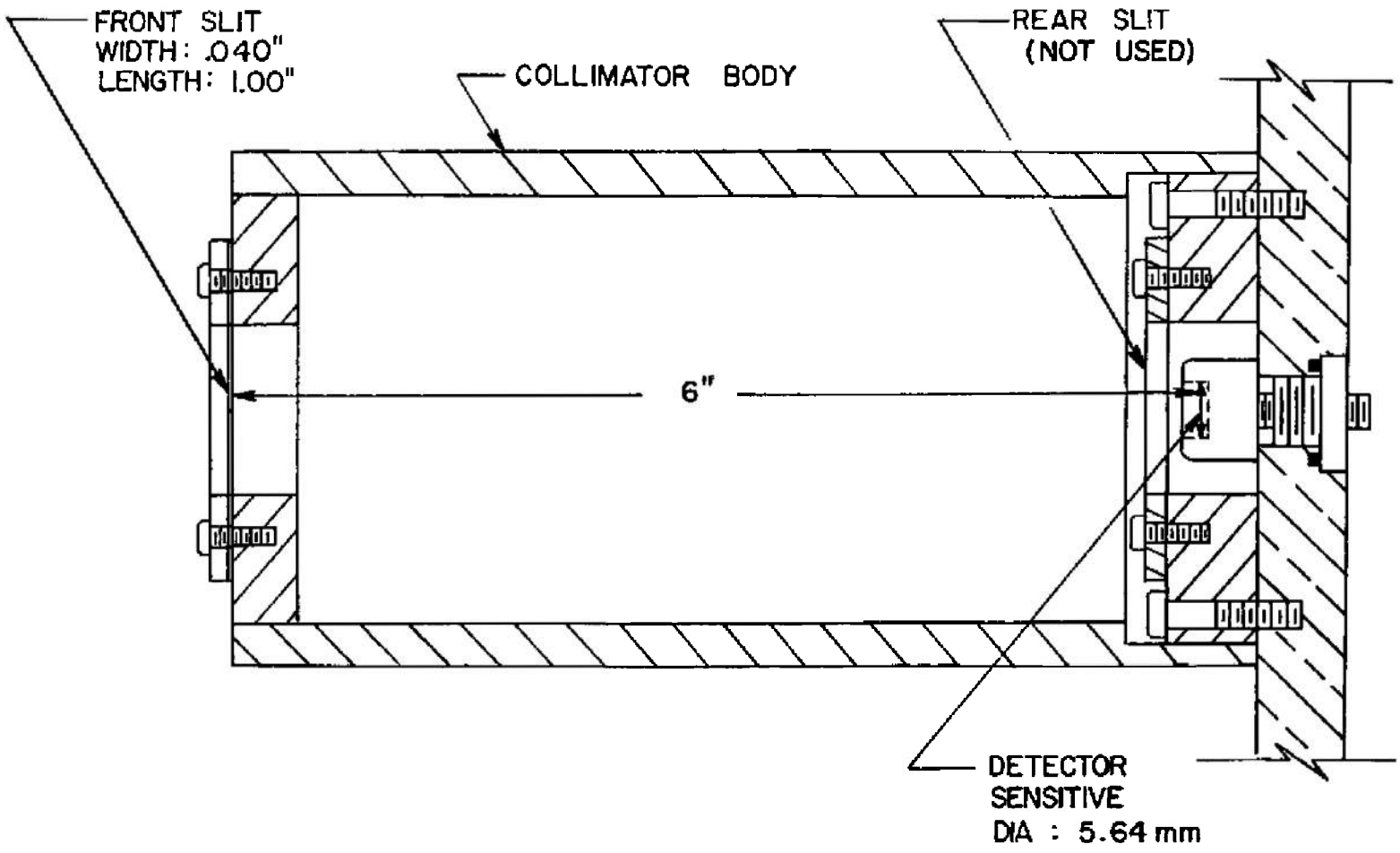

Fig. 21 Drawing of Collimator Used in Experiments in Tank

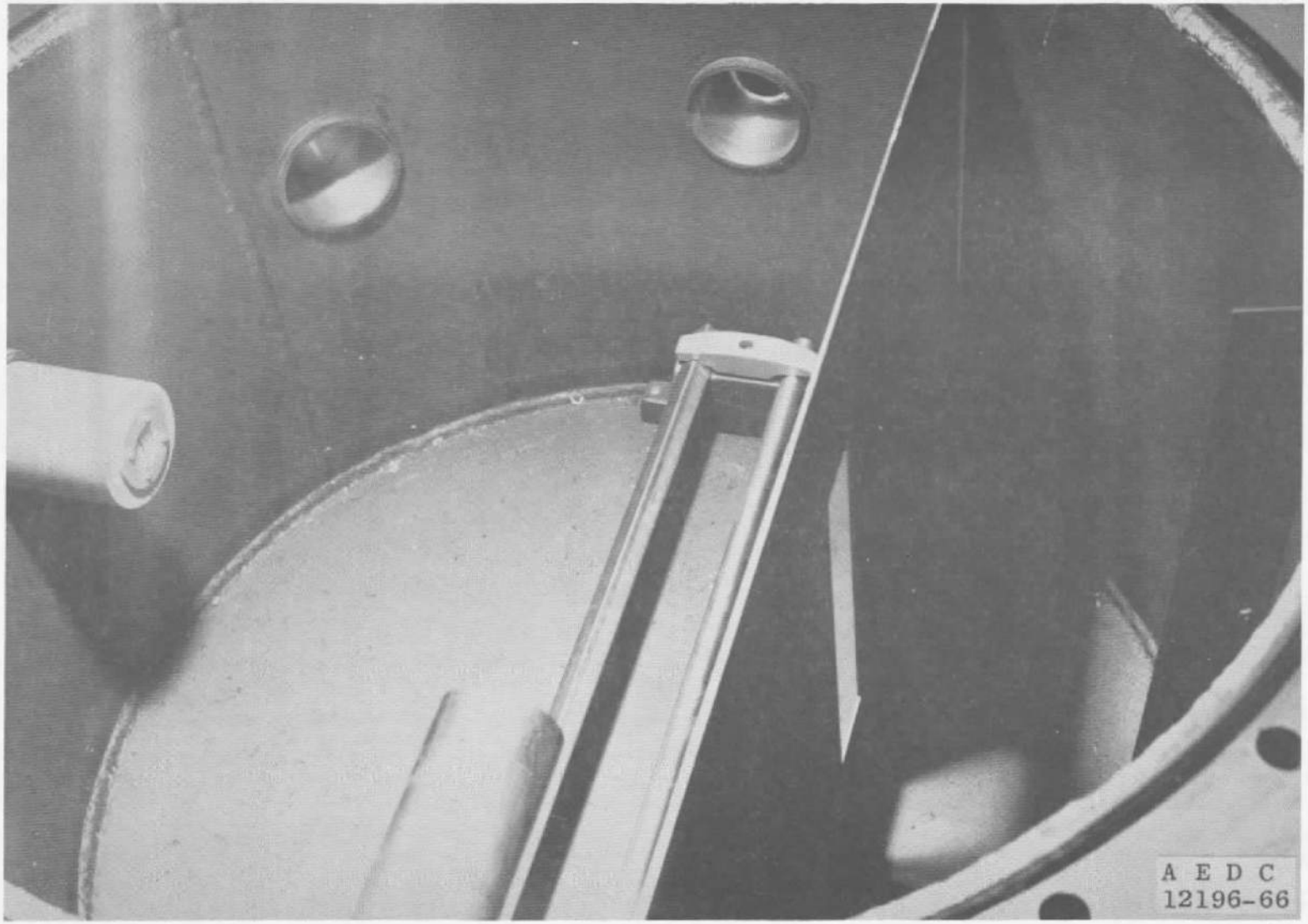

Fig. 22 Photograph of Tank Showing Collector, Collimator, and Baffles

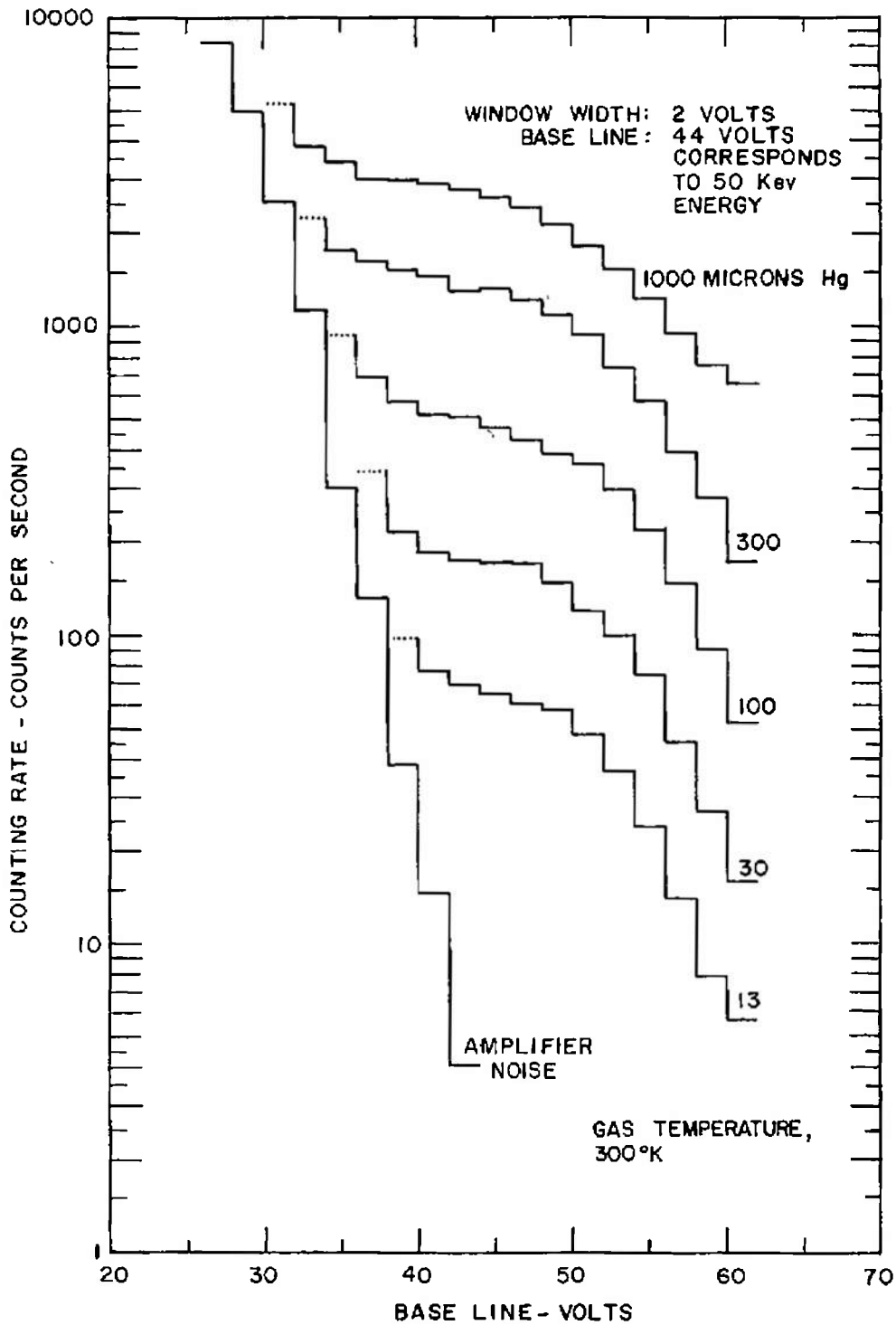

Fig. 23 Differential Spectra Obtained in Tank

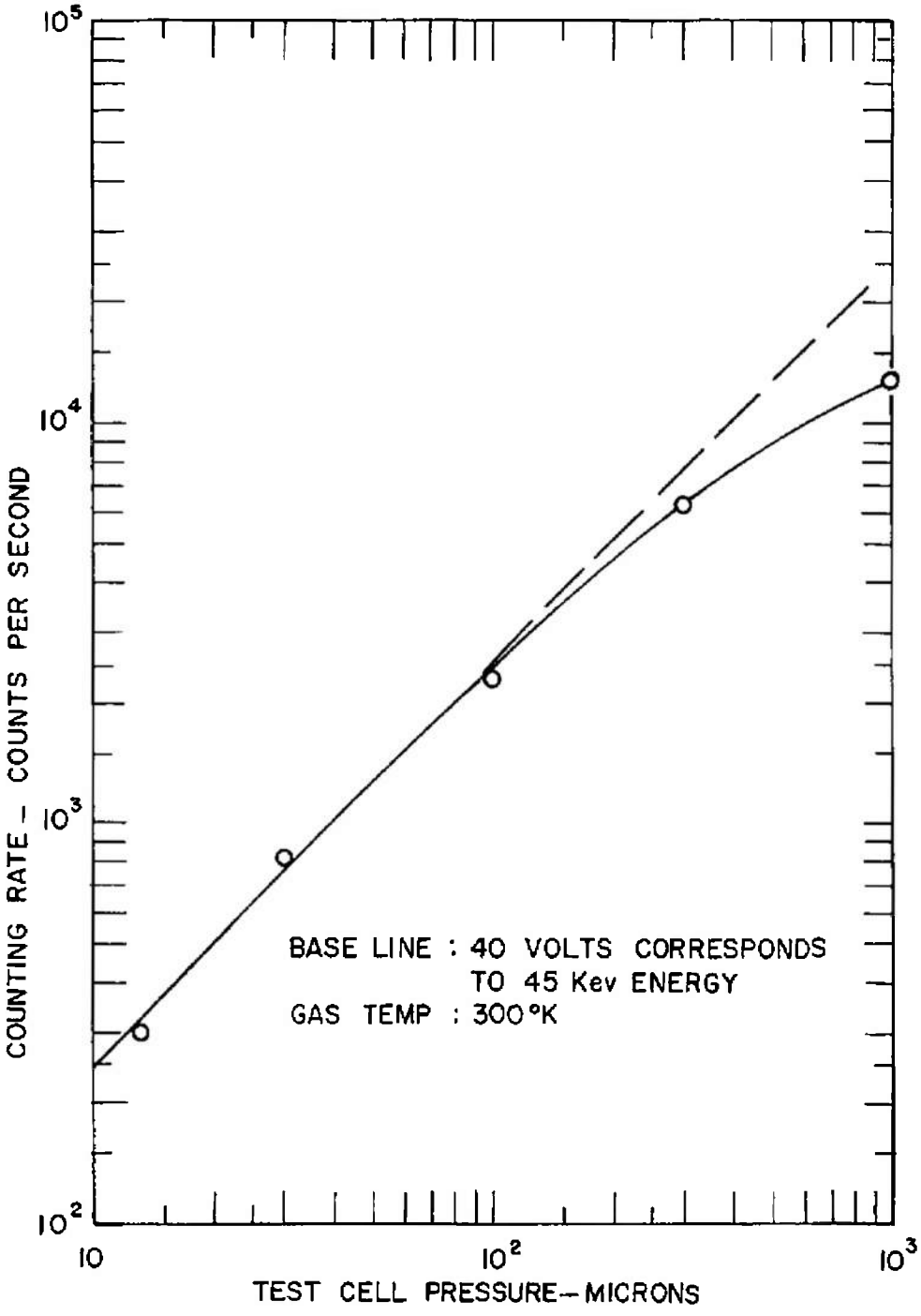

Fig. 24 Calibration Curve Obtained in Tank

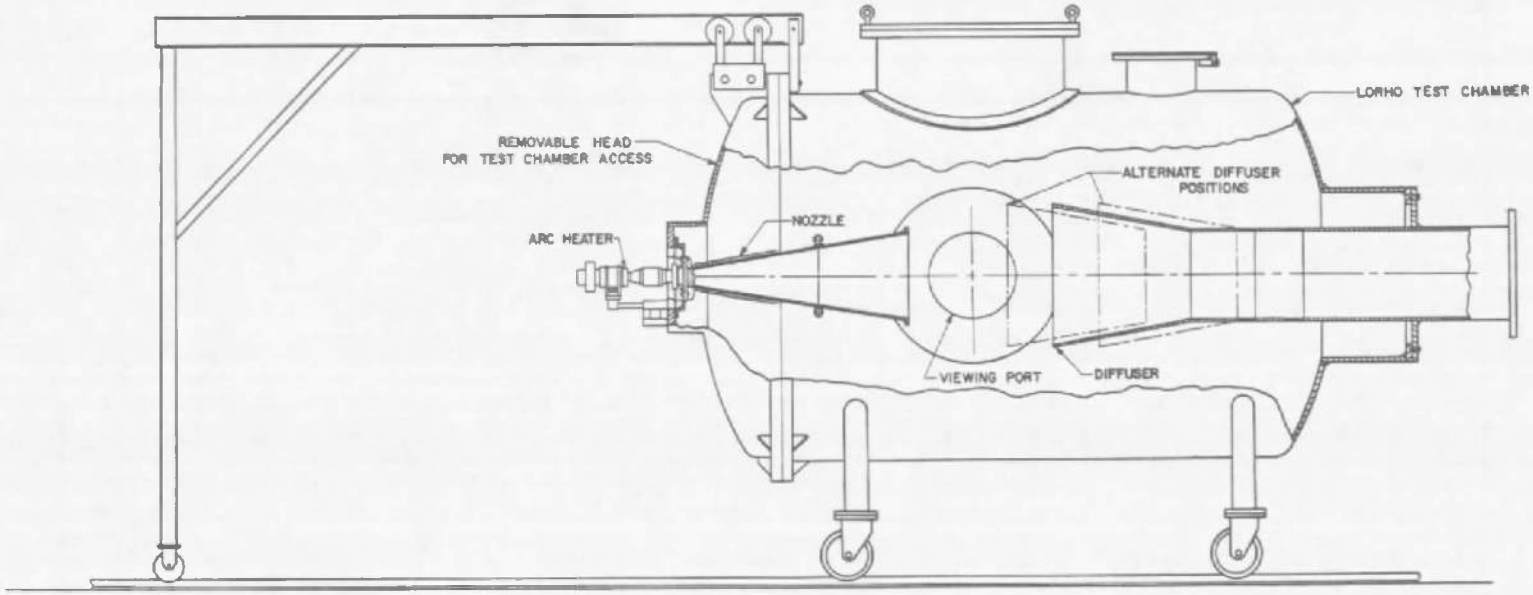

Fig. 25 General Arrangement of the Low Density Wind Tunnel

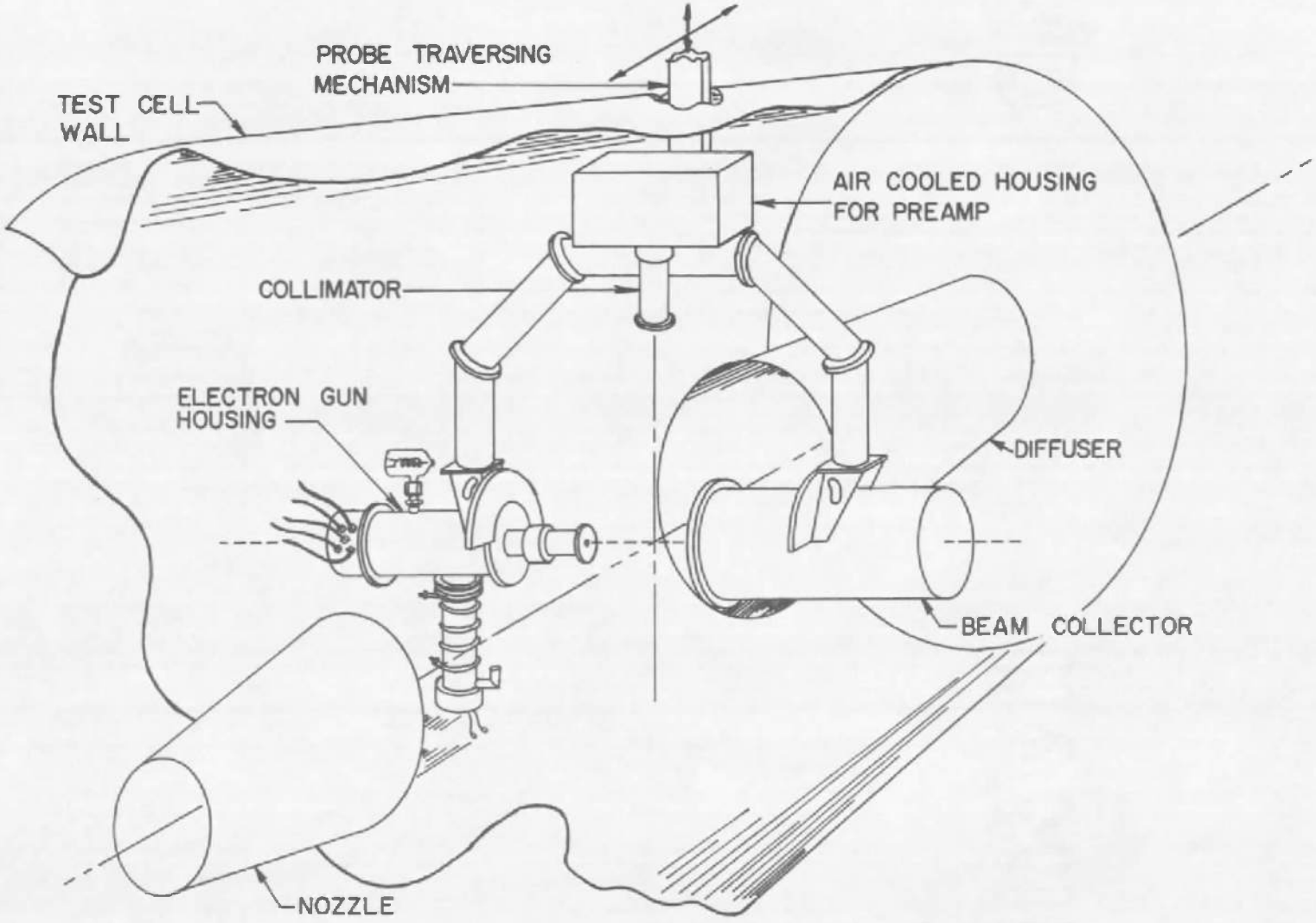

Fig. 26 Installation of Density Measuring Apparatus in the Low Density Wind Tunnel

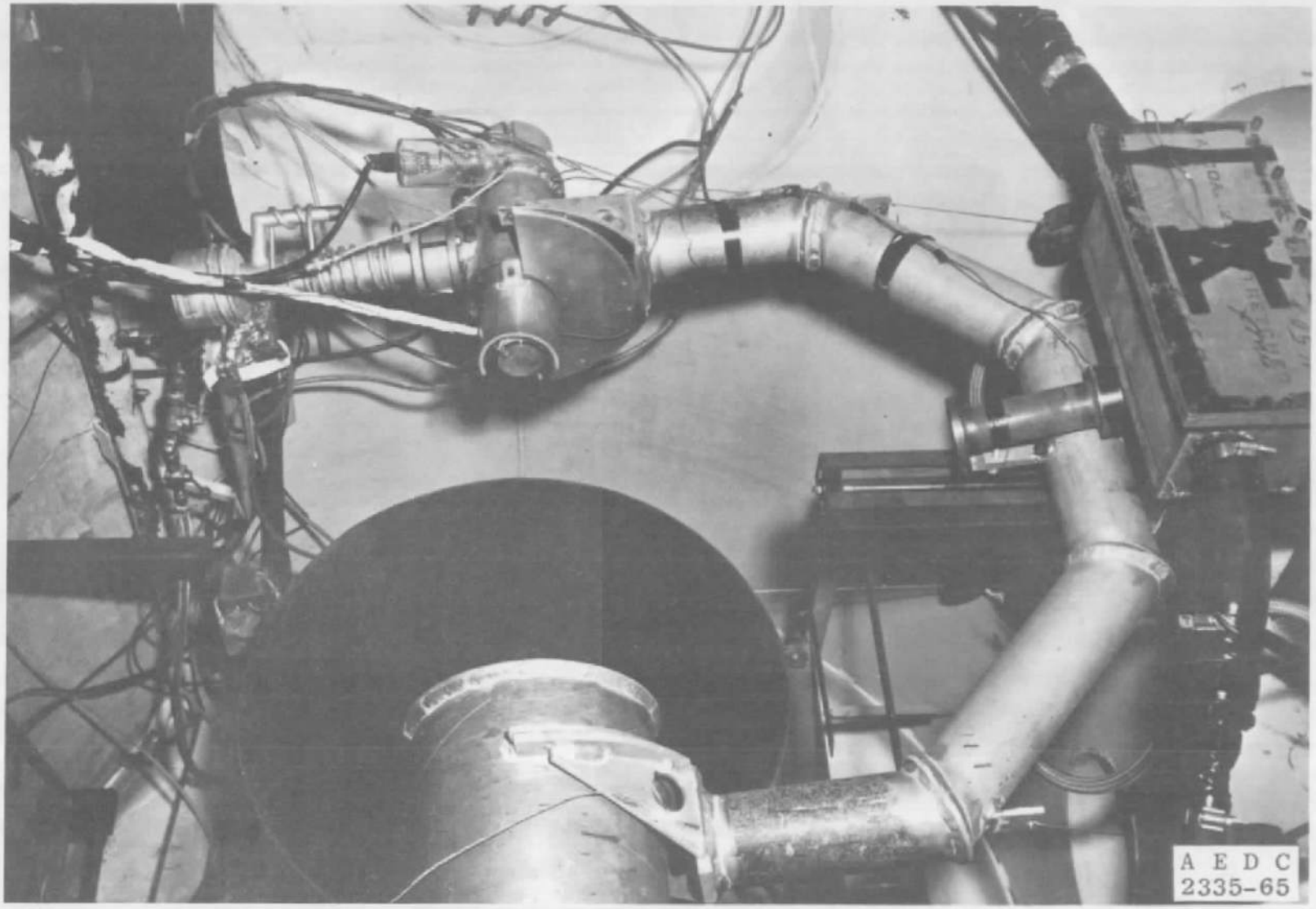

Fig. 27 Photograph of Installation in the Low Density Wind Tunnel

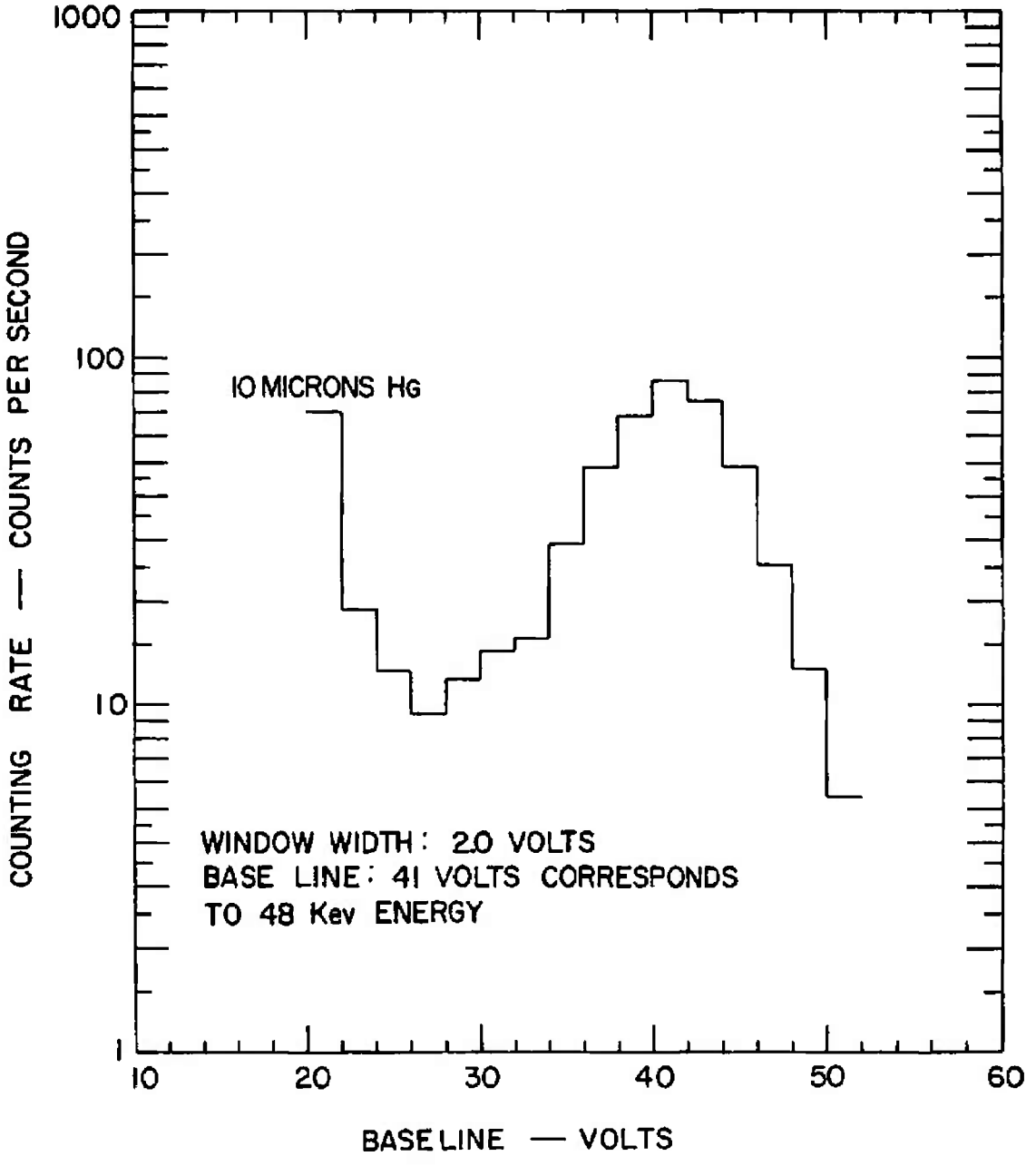

Fig. 28 Differential Spectrum Obtained in the Low Density Wind Tunnel at a Pressure of 10 μ

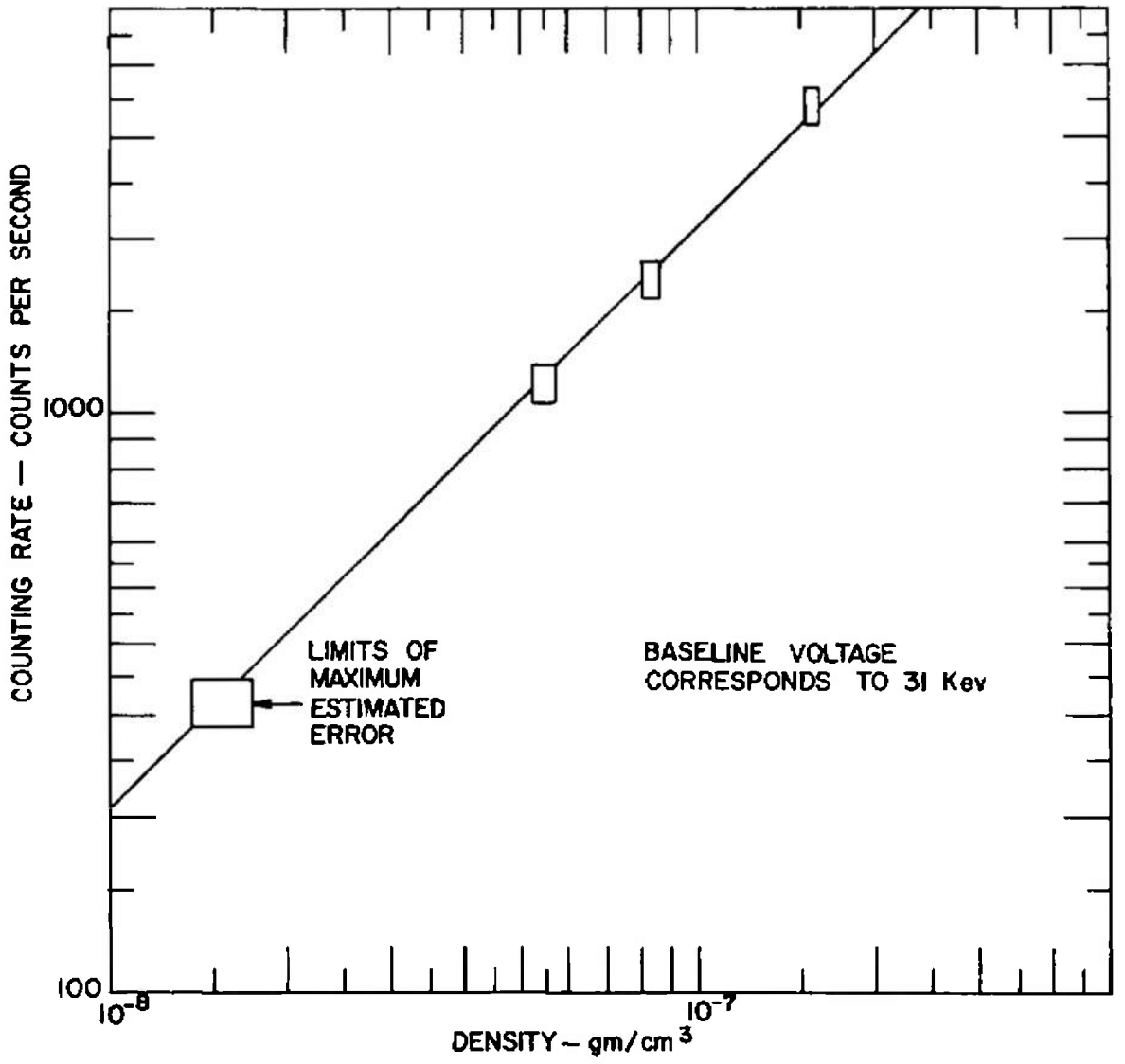

Fig. 29 Calibration Curve Obtained in the Low Density Wind Tunnel

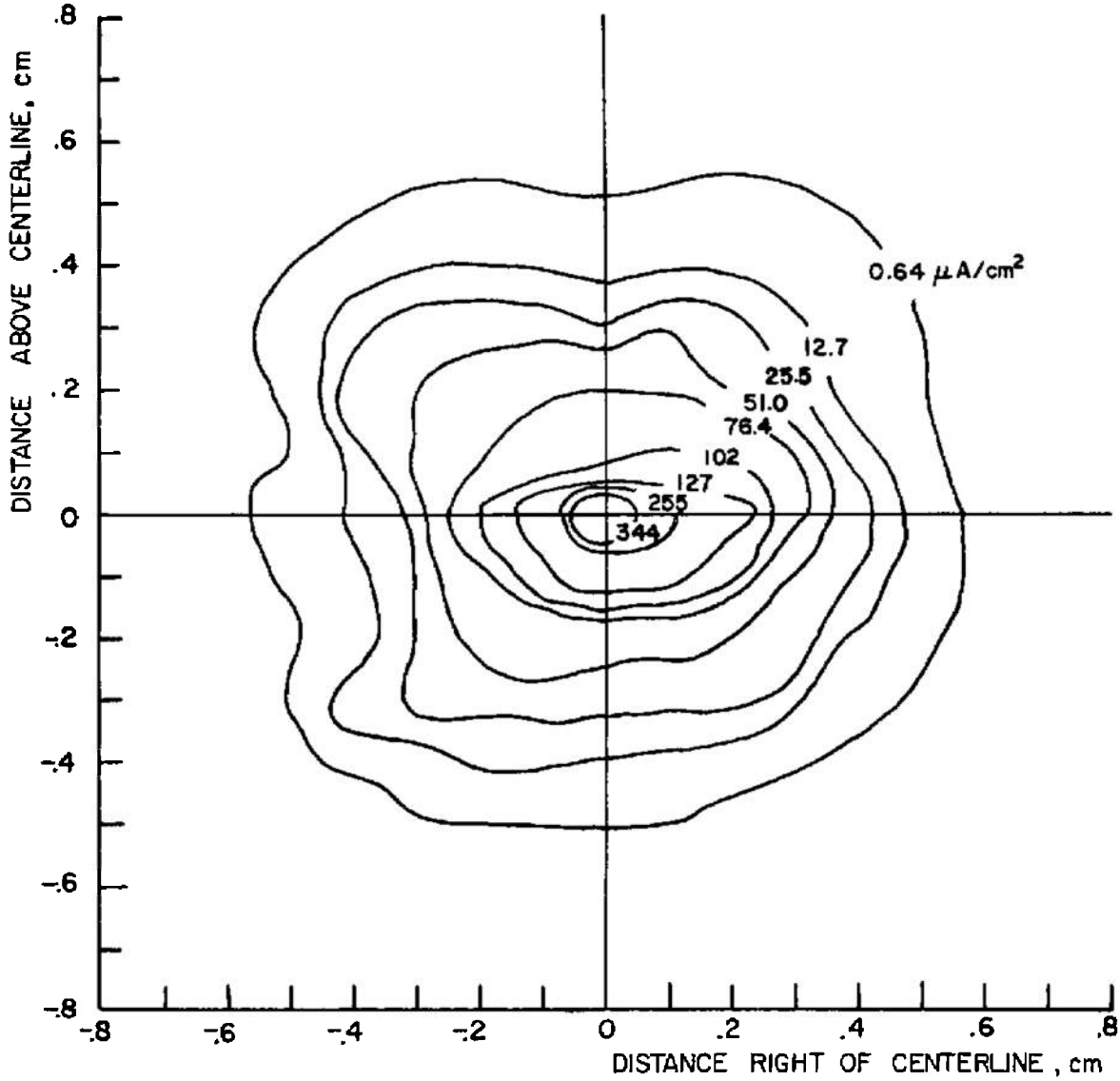

Fig. 30 Typical Map of Current Density in the Beam

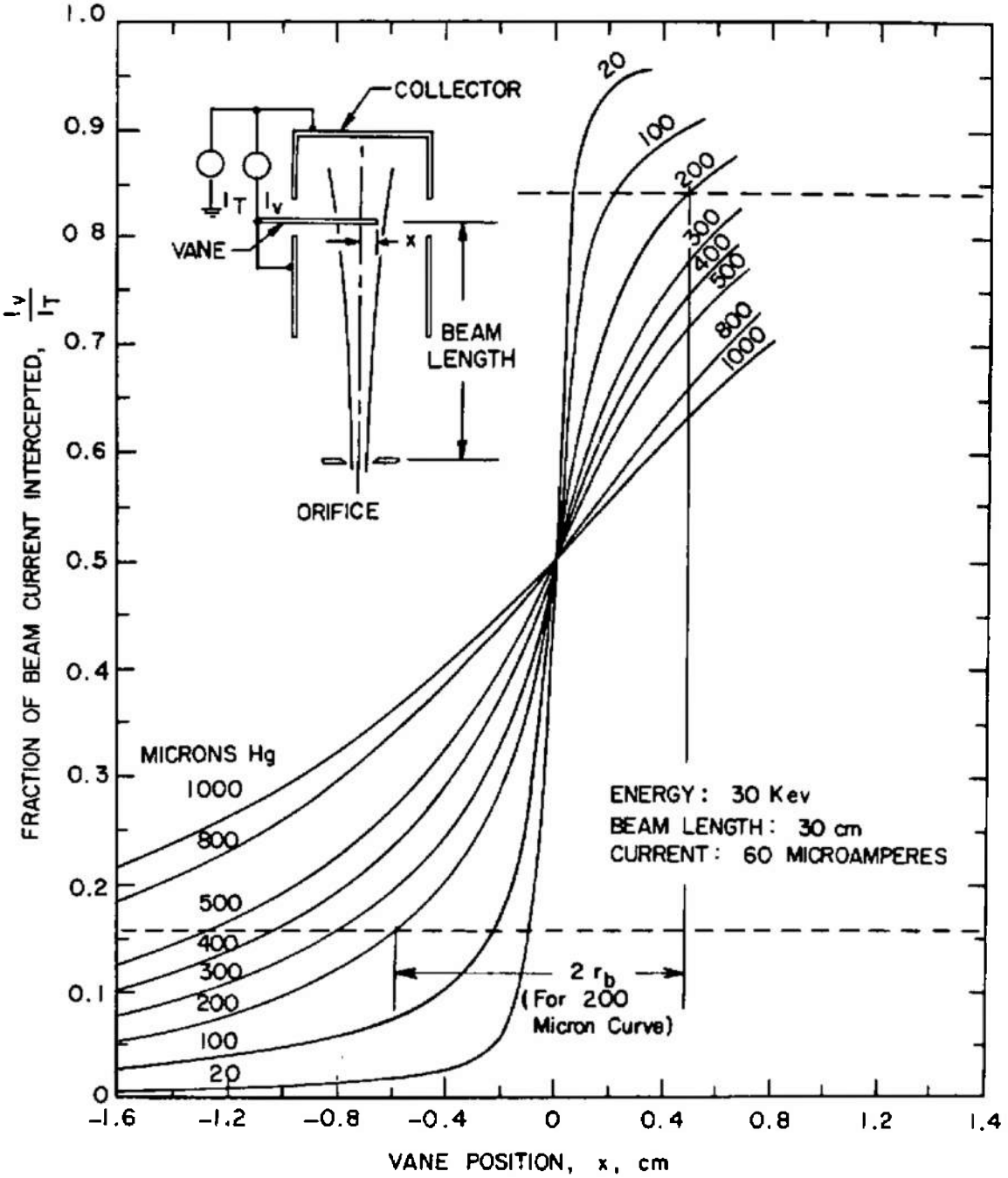

Fig. 31 Plot of Current Distribution in the Beam

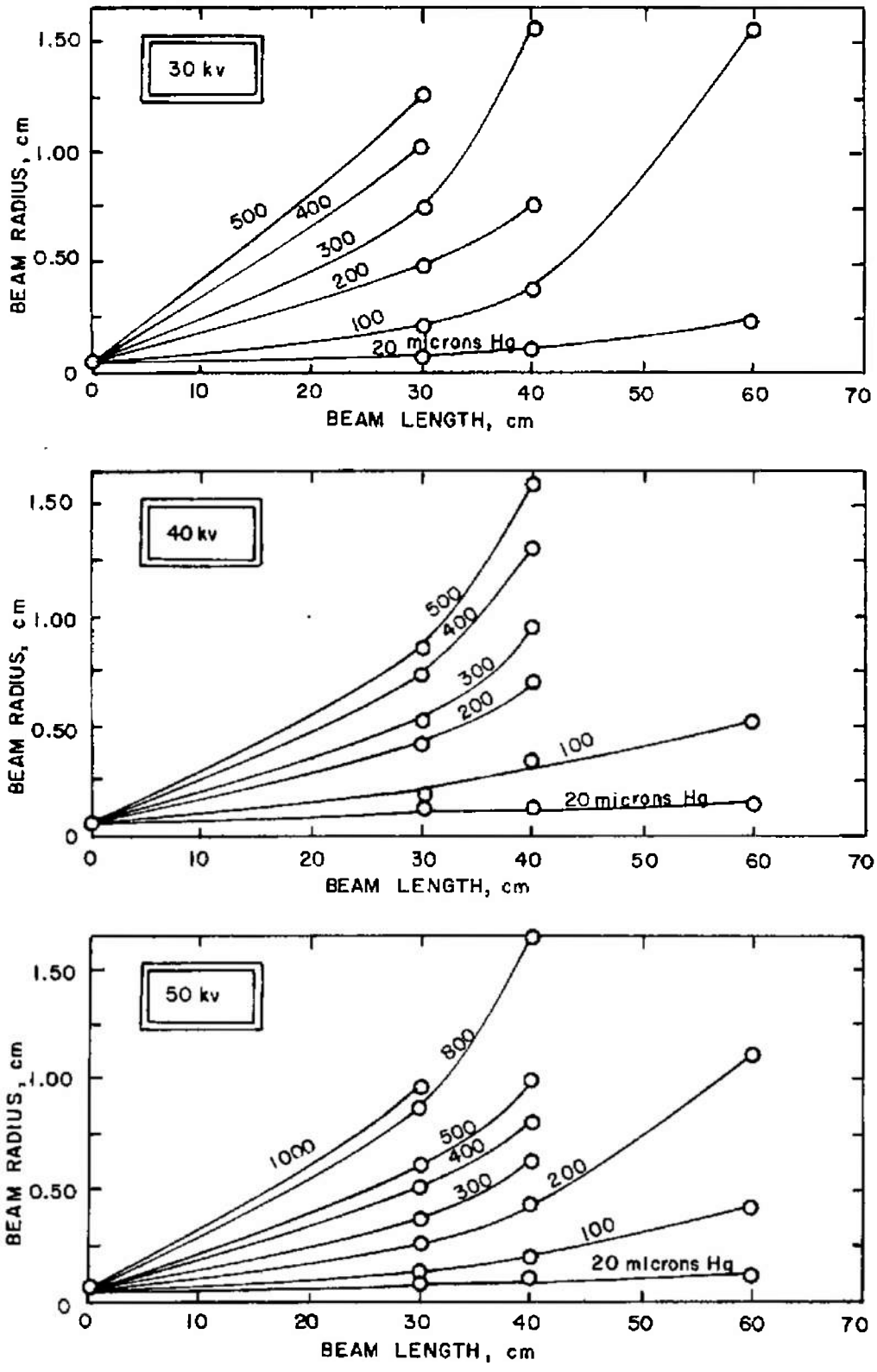

Fig. 32 Experimentally Measured Beam Radius

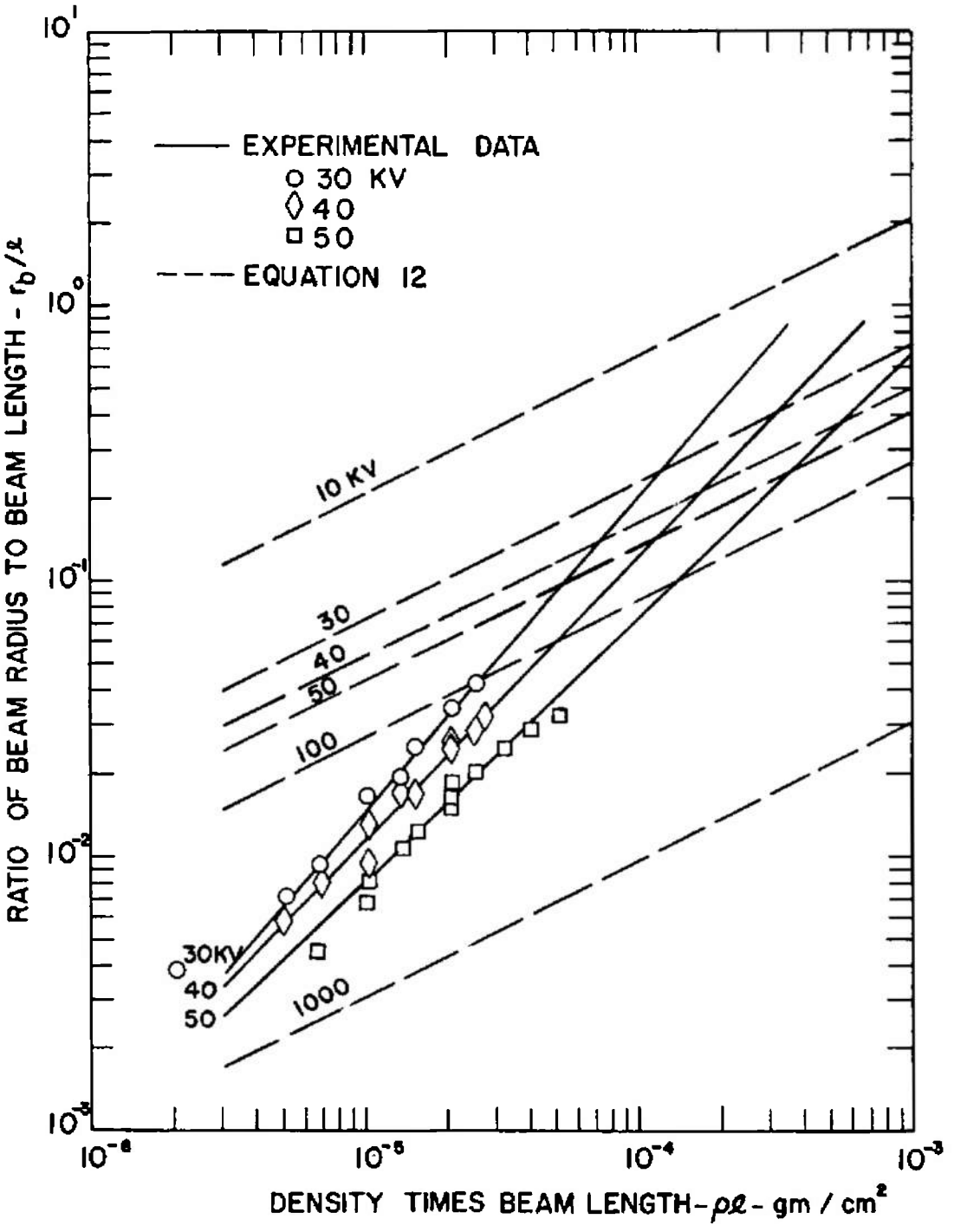

Fig. 33 Comparison of Measured Beam Radius with Radius Predicted by Eq. (12)

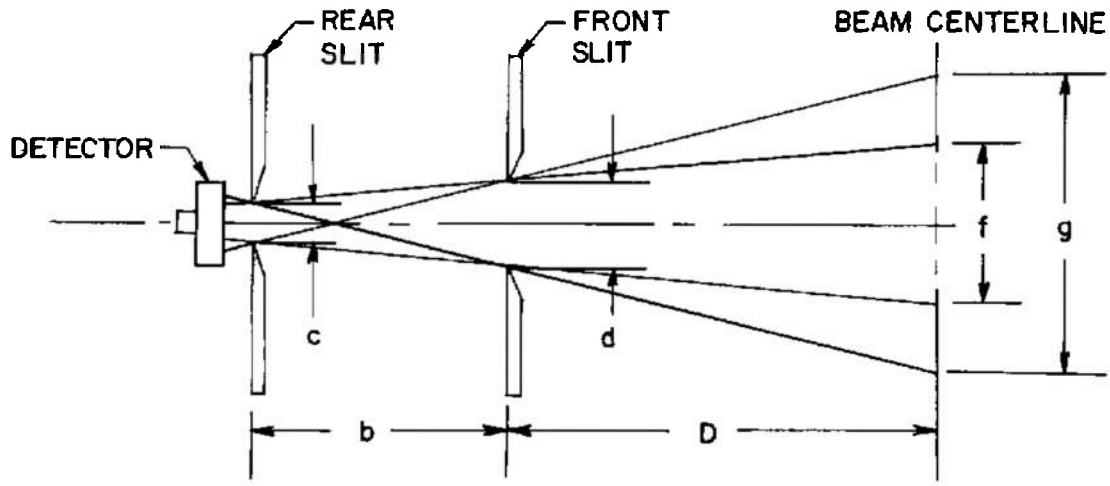

a. Collimator Arrangement and Dimensions

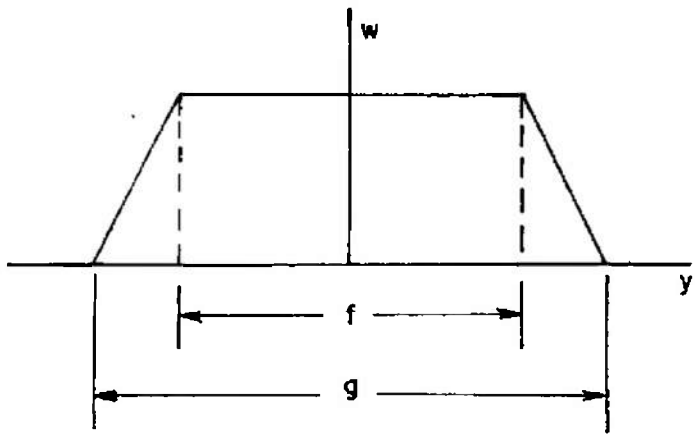

b. Variation of Detector Width with Position in the Beam

Fig. 34 Geometry of Slit Collimator

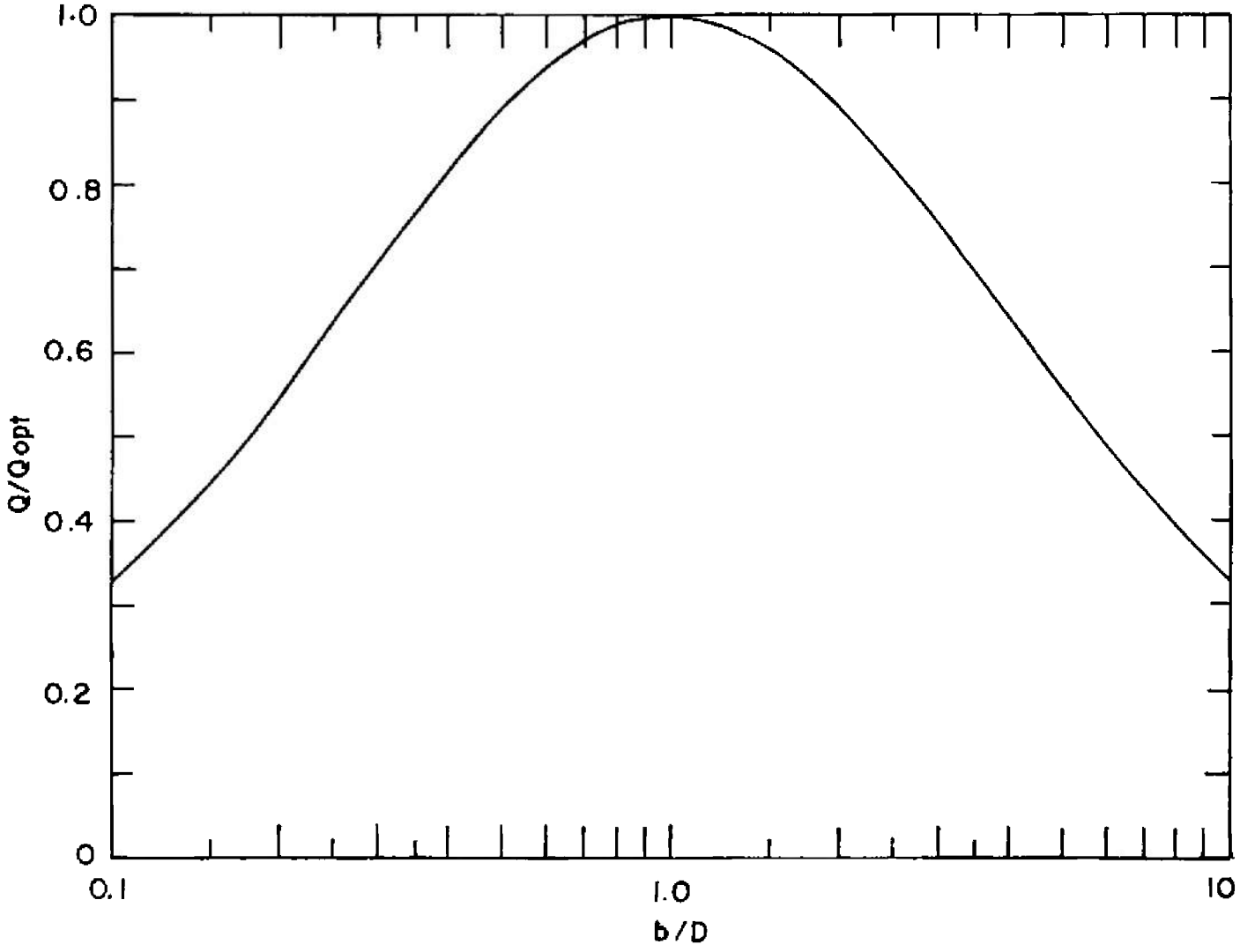

Fig. 35 Variation of Q of a Slit Collimator with Change in Collimator Length

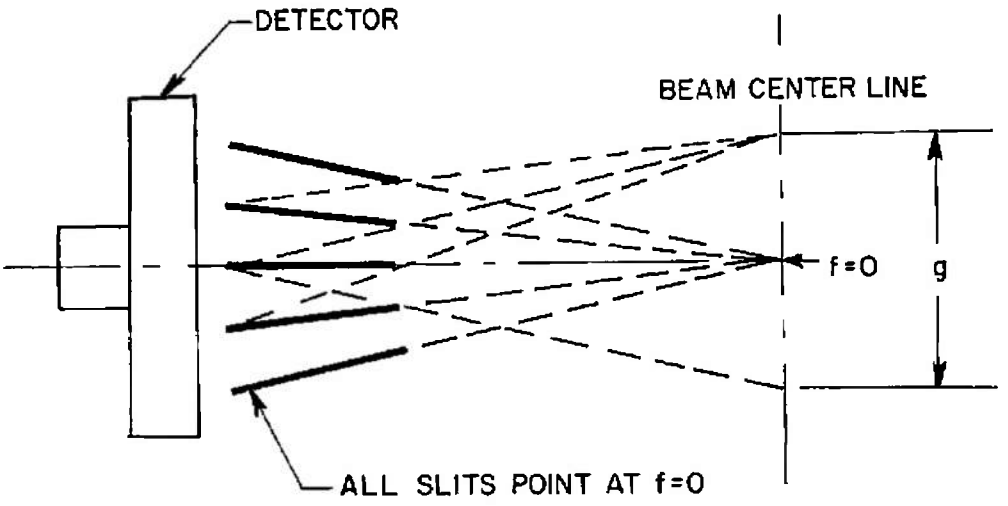

Fig. 36 Geometry of Venetian Blind Collimator

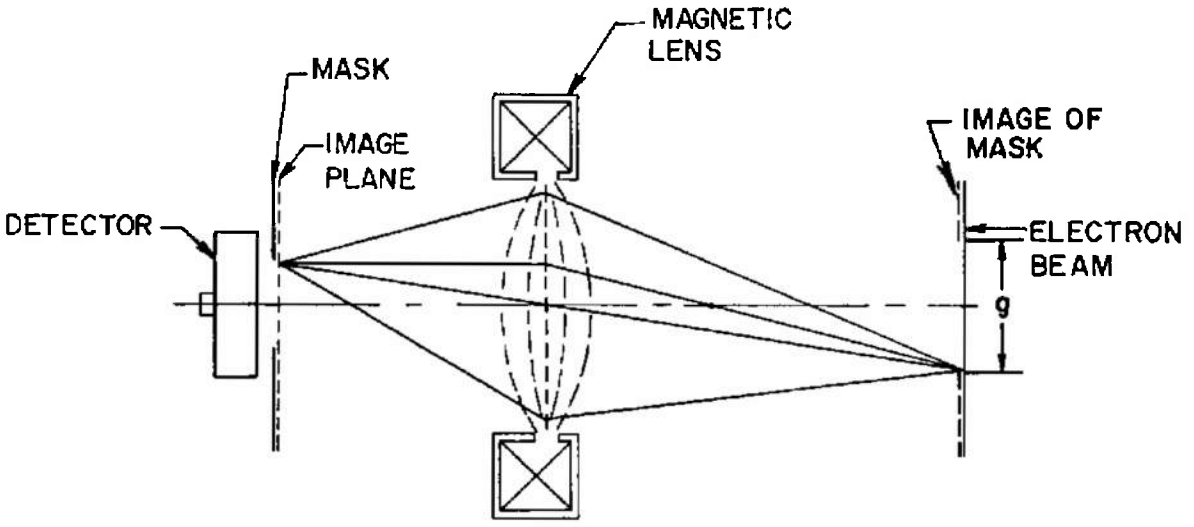

Fig. 37 Geometry of Lens Collimator

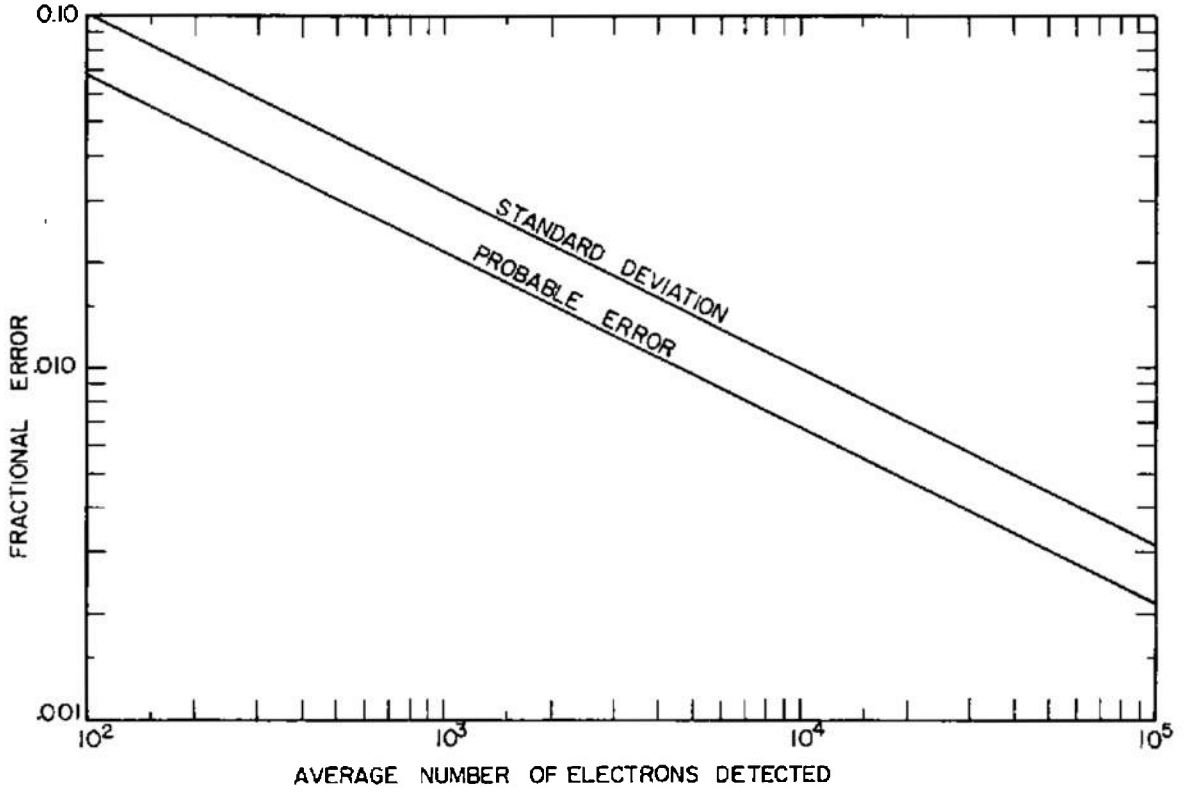

Fig. 38 Relationship of Standard Deviation and Probable Error to Number of Electrons Counted

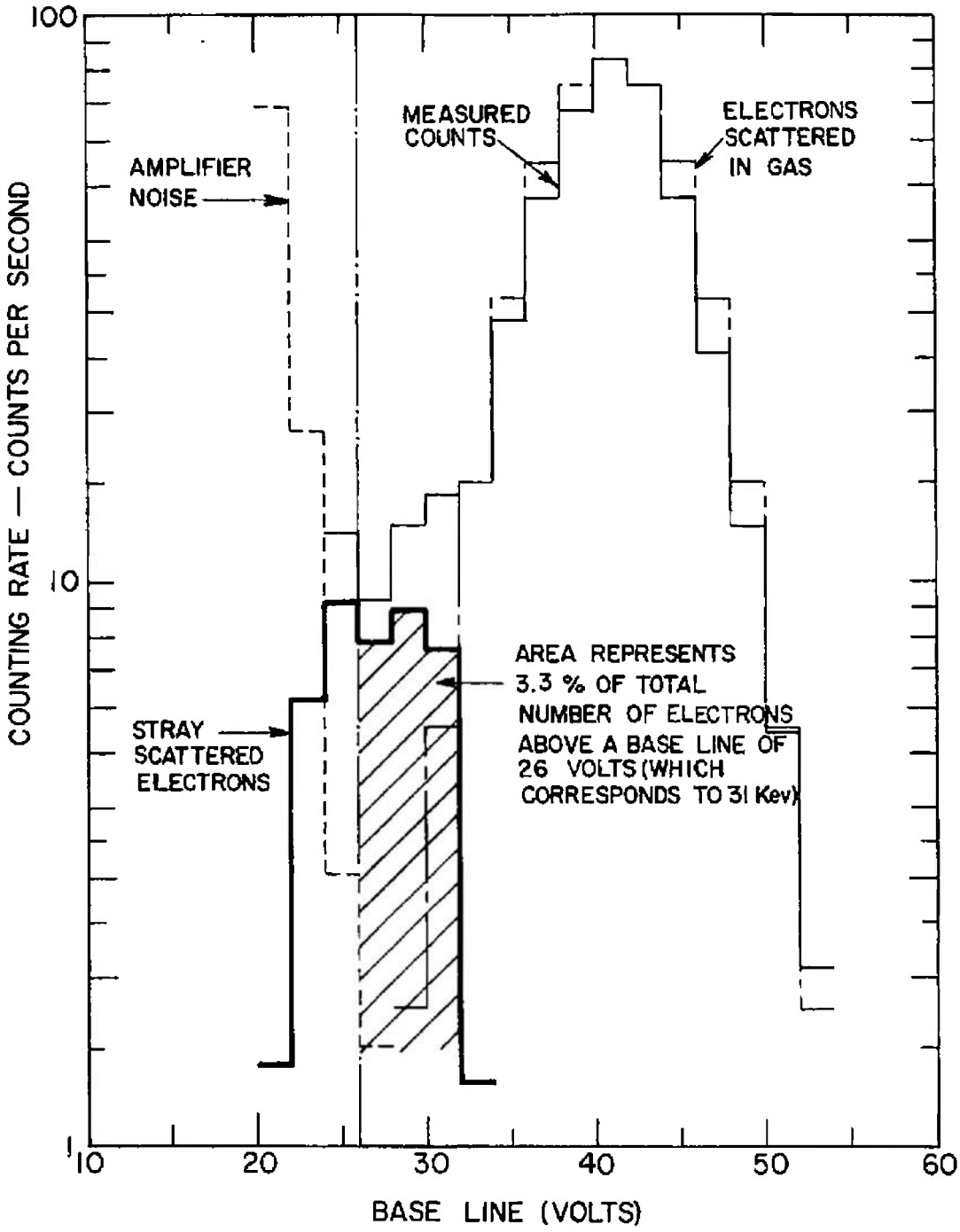

Fig. 39 Estimate of Stray Electron Spectrum

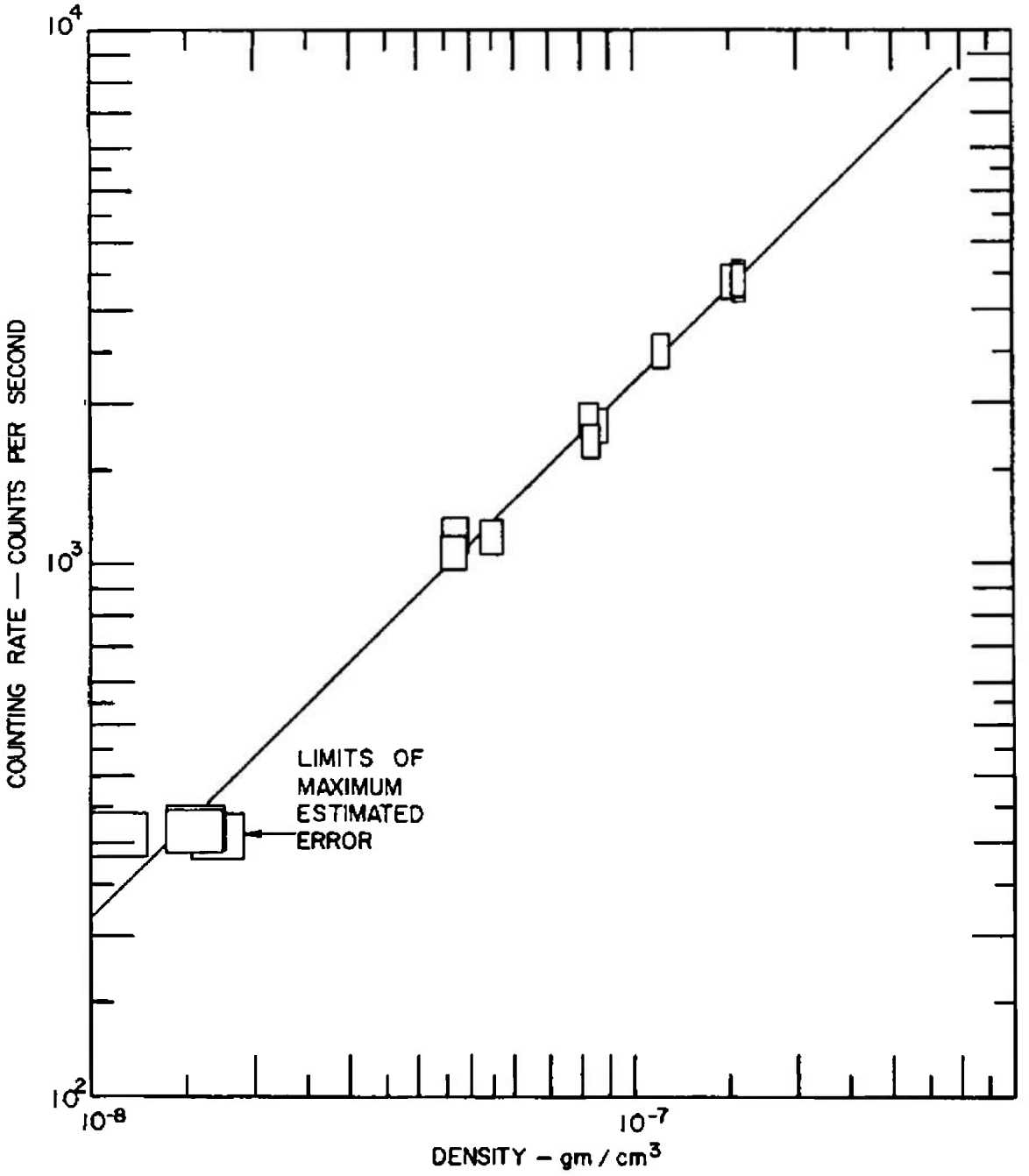

Fig. 40 Group of Calibrations Obtained in the Low Density Wind Tunnel

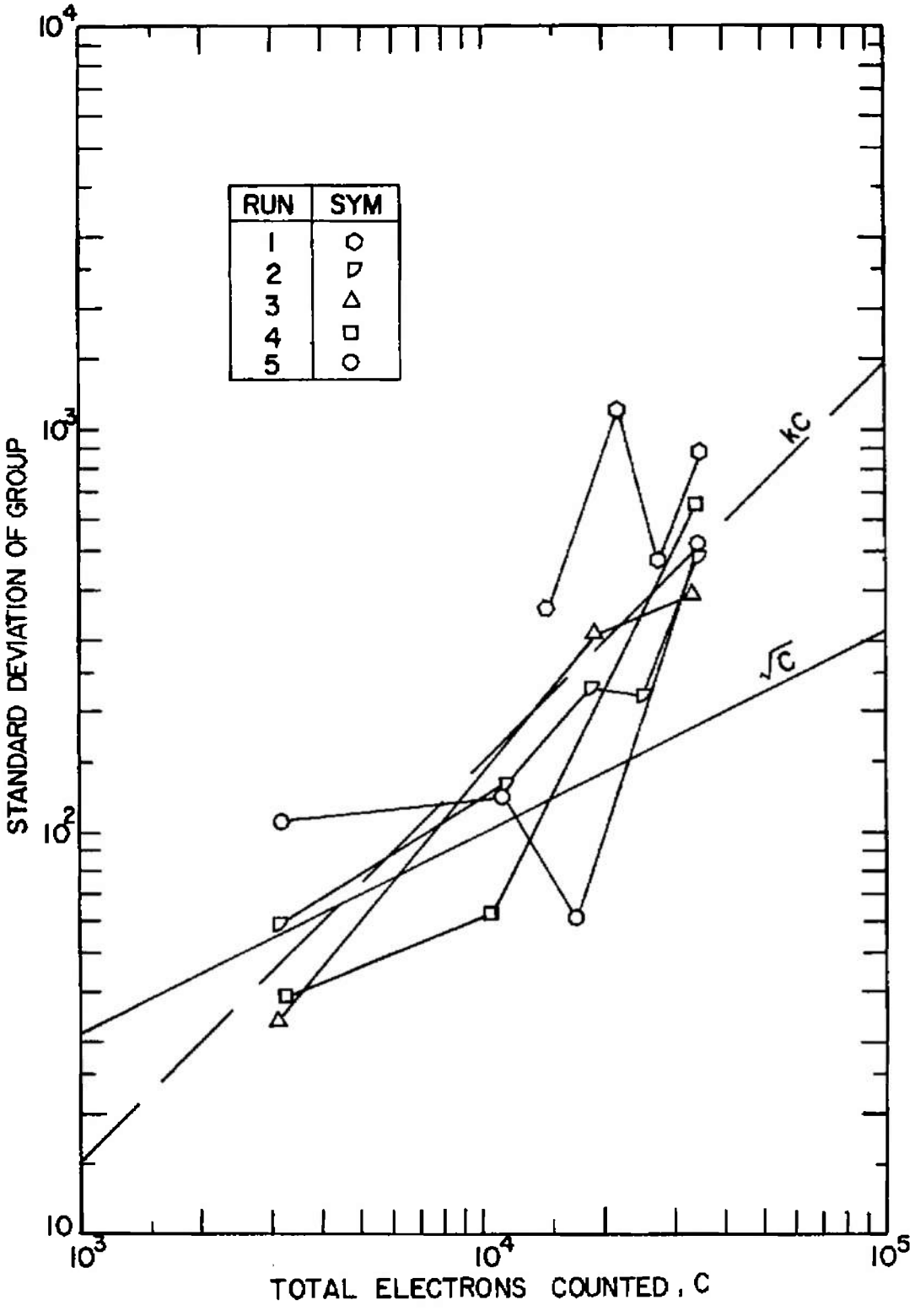

Fig. 41 Plot of Standard Deviations of Measurements of Fig. 40

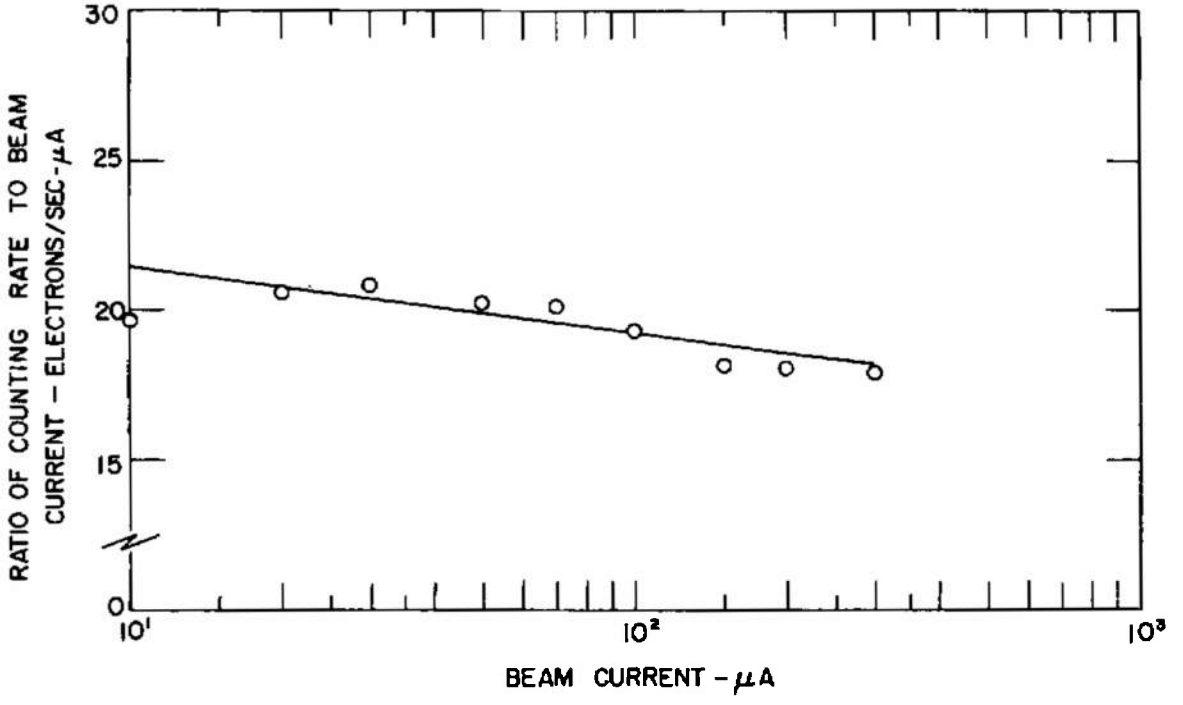

Fig. 42 Effect of Beam Current on Calibration Factor

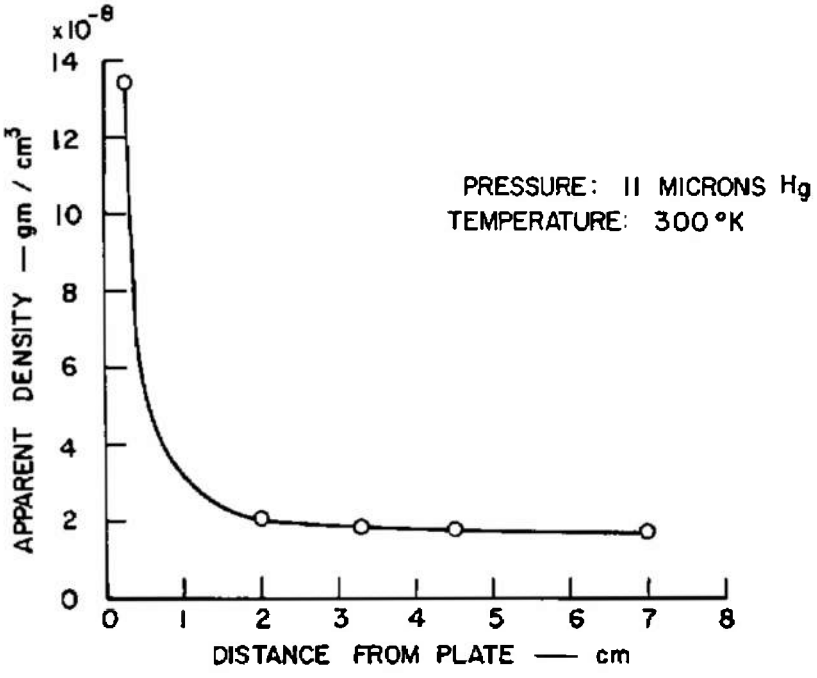

Fig. 43 Effect of a Solid Object near the Sensitive Volume

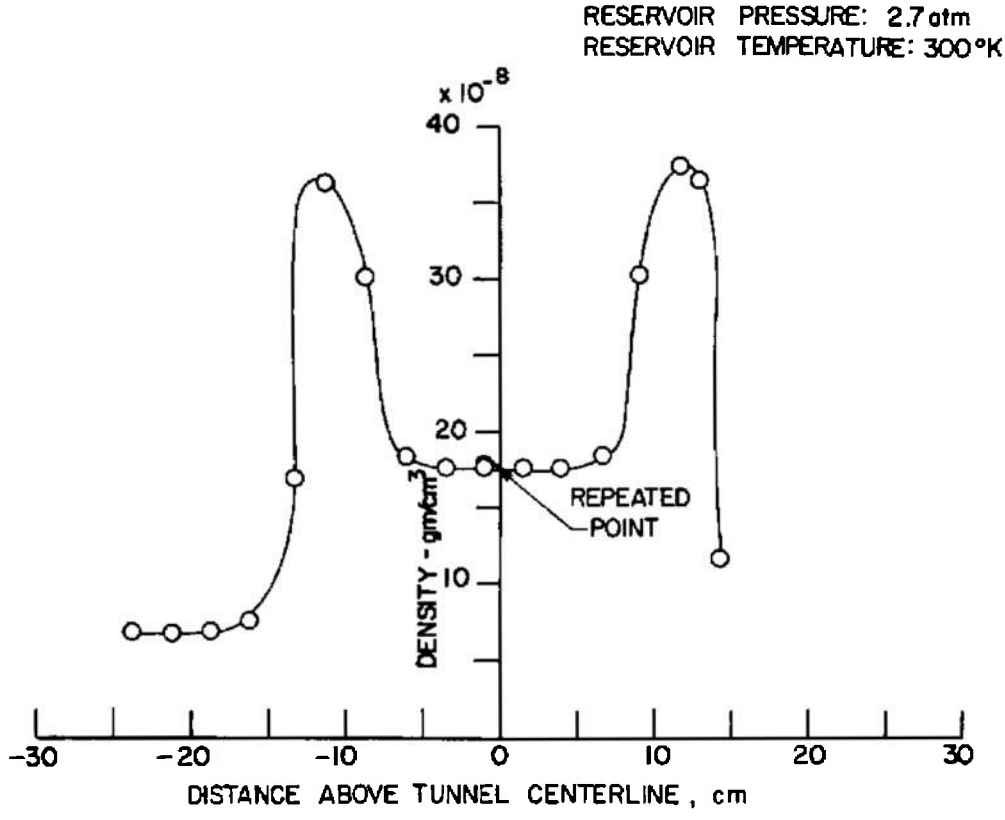

Fig. 44 Cold-Flow Density Profile Measured in the Low Density Wind Tunnel

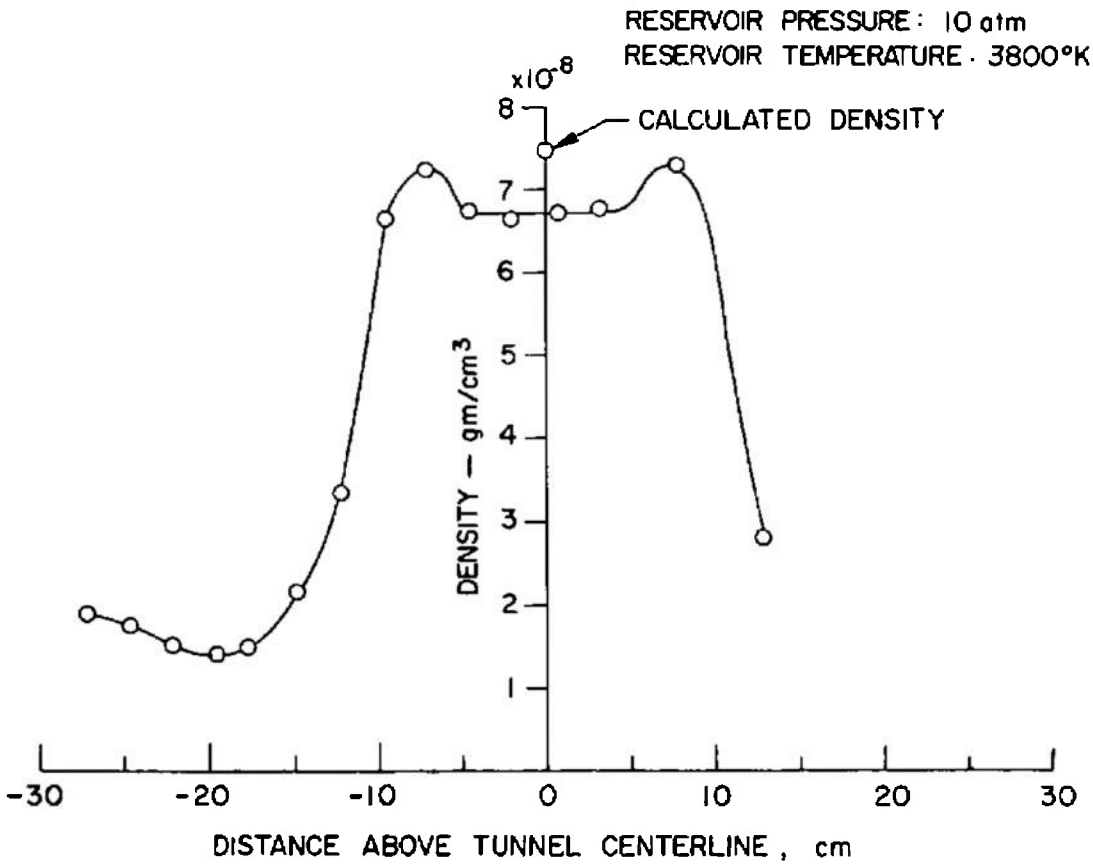

Fig. 45 Hot-Flow Density Profile Measured in the Low Density Wind Tunnel

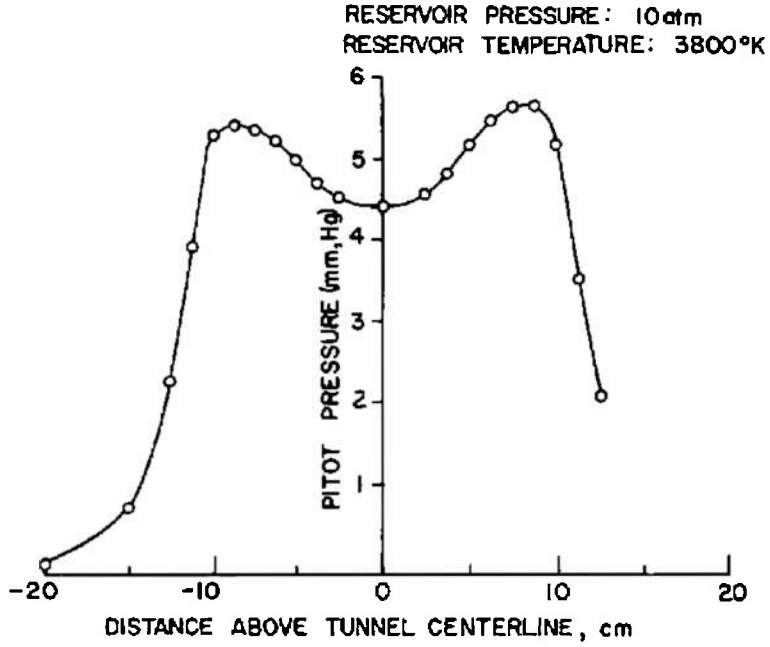

Fig. 46 Hot-Flow Pitot Pressure Profile Measured in the Low Density Wind Tunnel

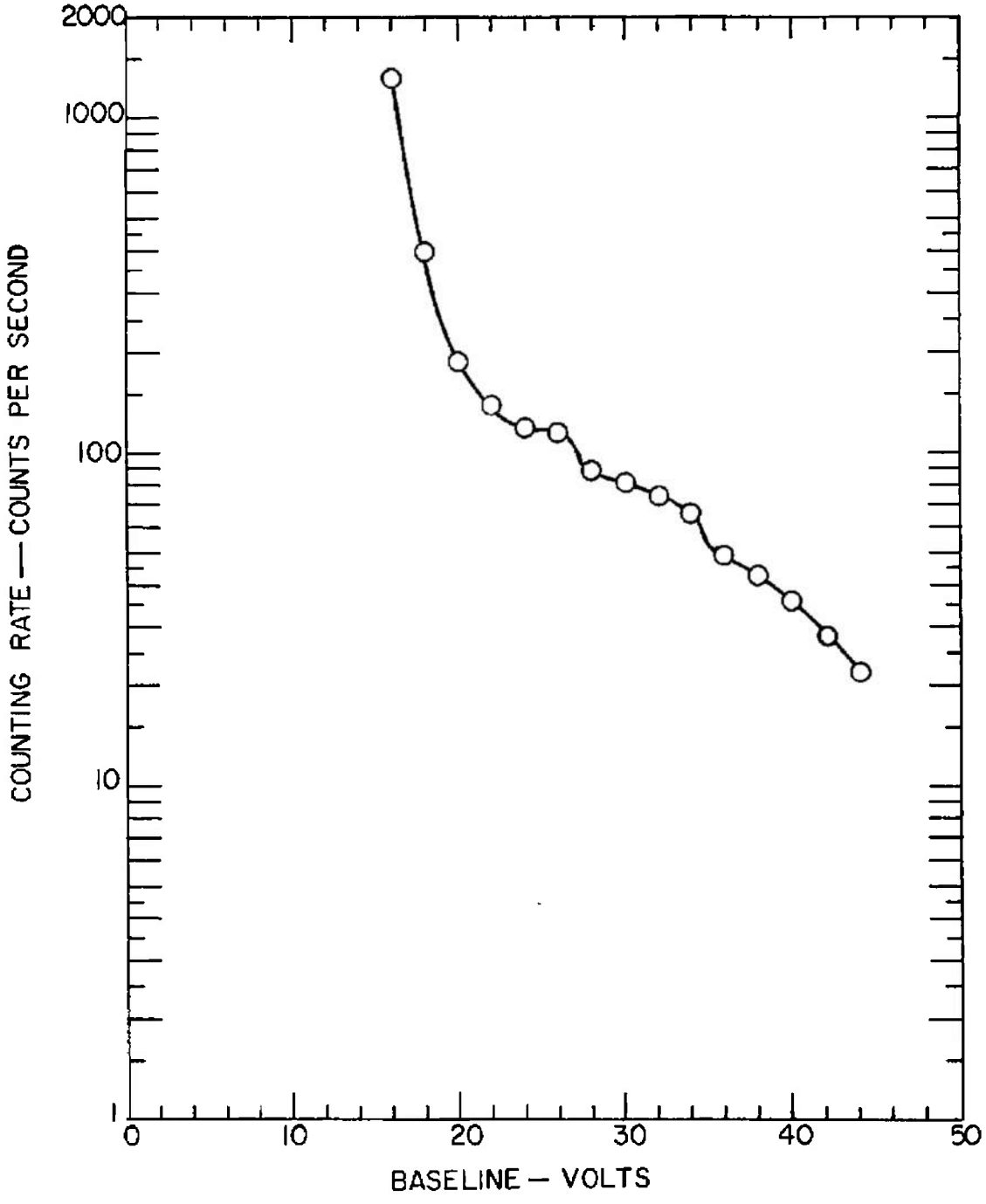

Fig. 47 Integral Spectrum of Noise Picked Up from the Arc Heater

a. Volume Flow versus Pressure Map

Fig. 48 Design Chart for Dynamic Pumping Systems

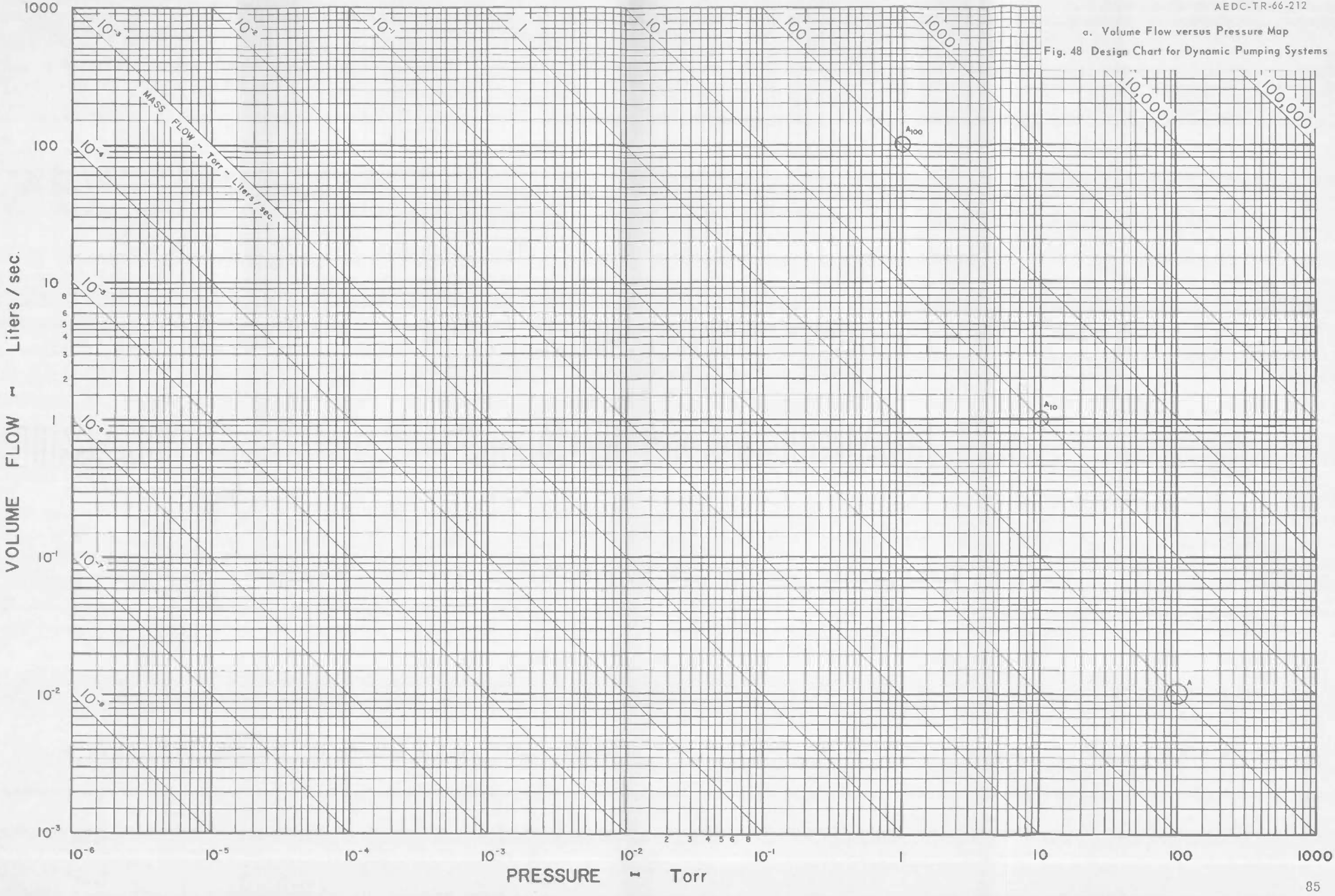

INSTRUCTIONS

TO TRANSFER THE CONDUCTION CURVE FOR A SPECIFIC ORIFICE TO THE VOLUME FLOW VS. PRESSURE CHART (SHEET NO. 1):

1. LOCATE ORIFICE DIAMETER (d) ON DIAGONAL LINE.
2. SUPERIMPOSE THIS POINT WITH POINT "A" OF SHEET NO. 1.
3. TRACE THE CURVE CORRESPONDING TO THE PROPER ℓ/d RATIO.
   THESE CURVES ARE ASYMPTOTES, AND ARE INACCURATE AT CORNERS.
   THE CURVES ARE BASED ON AIR AT 300°K, AND ASSUME THAT UPSTREAM PRESSURE IS MUCH GREATER THAN DOWNSTREAM PRESSURE.
4. TO USE THESE CURVES WITH LARGER DIAMETERS:
   MULTIPLY VALUES ON d SCALE BY 10 (or 100), AND SUPERIMPOSE WITH POINT A_{10} (or A_{100}) ON SHEET NO. 1.

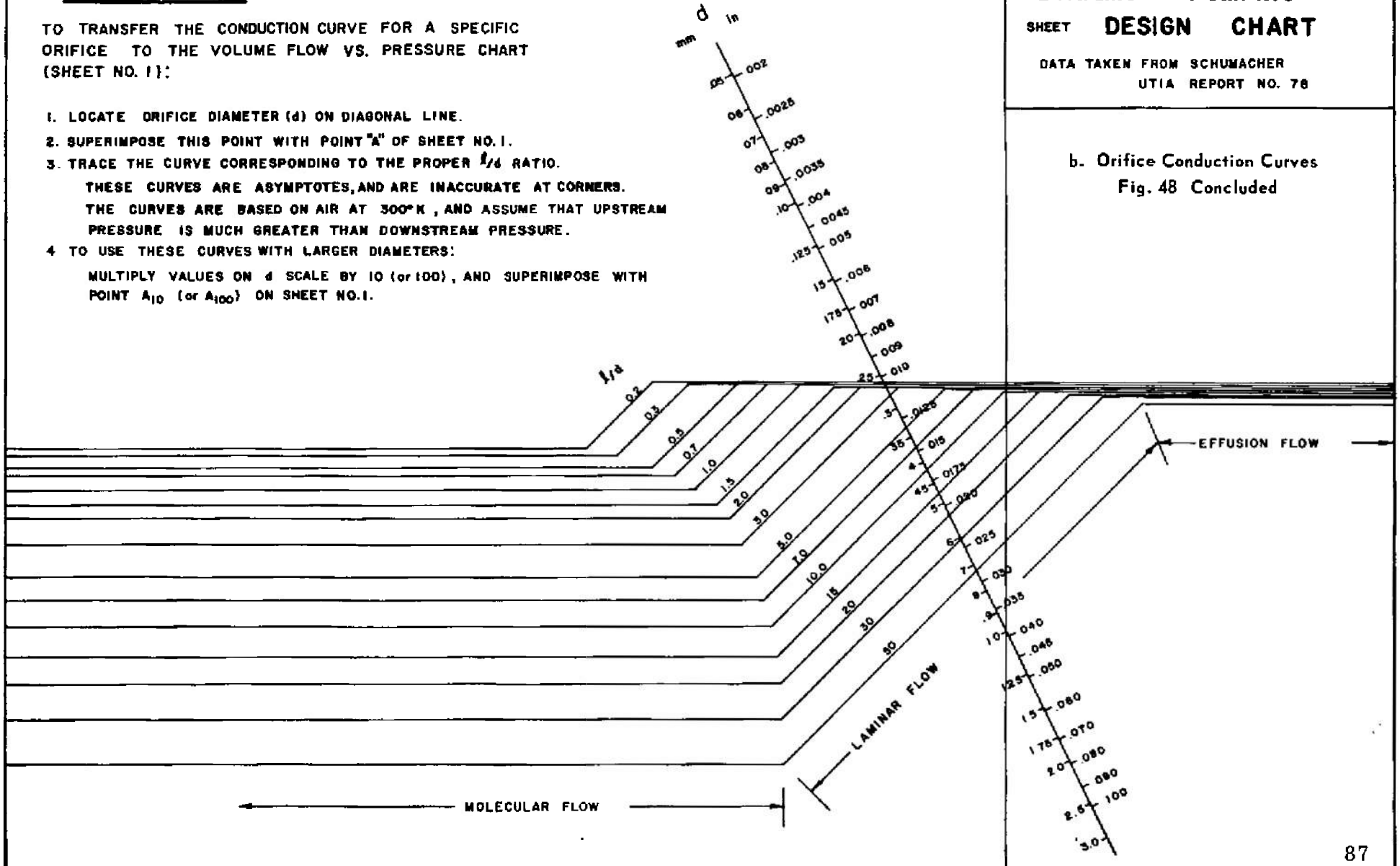

DYNAMIC PUMPING SHEET DESIGN CHART

DATA TAKEN FROM SCHUMACHER UTIA REPORT NO. 78

b. Orifice Conduction Curves
Fig. 48 Concluded

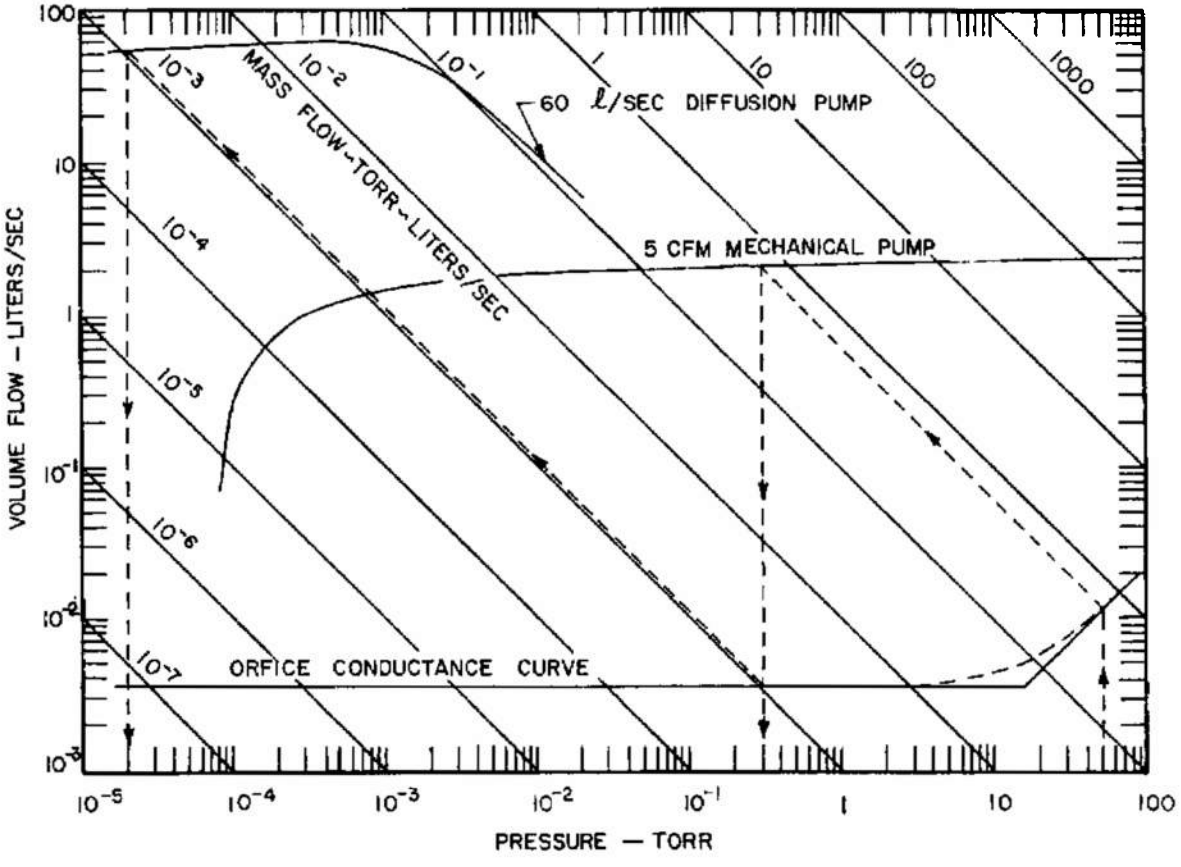

Fig. 49 Illustrative Dynamic Pumping Design Problem

APPENDIX II
TABLES

TABLE I
FUNCTION F(β)

V (kv)	β	F(β)
10	0.1954	660.1
12	0.2134	460.2
15	0.2376	296.2
18	0.2591	206.8
22	0.2849	139.5
27	0.3134	93.46
33	0.3436	63.25
39	0.3705	45.77
47	0.4024	31.95
56	0.4341	22.86
68	0.4710	15.81
82	0.5082	11.12
100	0.5491	7.685
120	0.5875	5.495
150	0.6352	3.664
180	0.6740	2.644
220	0.7159	1.856
270	0.7570	1.300
330	0.7950	0.9213
390	0.8243	0.6942
470	0.8542	0.5075
560	0.8794	0.3790
680	0.9038	0.2746
820	0.9238	0.2014
1000	0.9414	0.1448

TABLE II
FUNCTION G(θ)

θ (deg)	G(θ)
5	2.762×10^5
10	1.733×10^4
15	3.445×10^3
20	1.100×10^3
25	4.557×10^2
30	2.229×10^2
35	1.223×10^2
40	7.308×10^1
45	4.663×10^1
50	3.135×10^1
55	2.200×10^1
60	1.600×10^1
65	1.200×10^1
70	9.239
75	7.281
80	5.858
85	4.800
90	4.000
95	3.384
100	2.904
105	2.524
110	2.221
115	1.976
120	1.778
125	1.615
130	1.482
135	1.373
140	1.282
145	1.209
150	1.149
155	1.101
160	1.063
165	1.035
170	1.015
175	1.004
180	1.000

TABLE III
SCATTERING CROSS SECTIONS
a. Hydrogen, Z = 1

V, kv \ θ, deg	15	30	45	60	75	90	105	120	135	150	165	180
10	4.514-20	2.915-21	6.082-22	2.079-22	9.416-23	5.146-23	3.231-23	2.264-23	1.741-23	1.452-23	1.305-23	1.260-23
12	3.146-20	2.031-21	4.236-22	1.447-22	6.546-23	3.574-23	2.241-23	1.569-23	1.205-23	1.005-23	9.031-24	8.718-24
15	2.025-20	1.307-21	2.722-22	9.287-23	4.197-23	2.288-23	1.433-23	1.002-23	7.684-24	6.399-24	5.747-24	5.547-24
18	1.414-20	9.119-22	1.898-22	6.469-23	2.919-23	1.589-23	9.936-24	6.937-24	5.315-24	4.422-24	3.969-24	3.830-24
22	9.533-21	6.145-22	1.278-22	4.348-23	1.959-23	1.064-23	6.640-24	4.627-24	3.539-24	2.941-24	2.637-24	2.544-24
27	6.386-21	4.113-22	8.541-23	2.901-23	1.304-23	7.068-24	4.399-24	3.058-24	2.334-24	1.936-24	1.735-24	1.673-24
33	4.320-21	2.780-22	5.764-23	1.953-23	8.759-24	4.734-24	2.938-24	2.036-24	1.551-24	1.284-24	1.149-24	1.107-24
39	3.126-21	2.009-22	4.159-23	1.407-23	6.292-24	3.391-24	2.098-24	1.450-24	1.102-24	9.102-25	8.134-25	7.838-25
47	2.182-21	1.401-22	2.894-23	9.761-24	4.352-24	2.337-24	1.440-24	9.919-25	7.509-25	6.188-25	5.520-25	5.316-25
56	1.560-21	1.000-22	2.062-23	6.935-24	3.081-24	1.648-24	1.011-24	6.935-25	5.230-25	4.297-25	3.826-25	3.682-25
68	1.078-21	6.905-23	1.420-23	4.757-24	2.103-24	1.119-24	6.830-25	4.658-25	3.495-25	2.860-25	2.540-25	2.442-25
82	7.580-22	4.844-23	9.930-24	3.314-24	1.458-24	7.709-25	4.676-25	3.169-25	2.364-25	1.925-25	1.705-25	1.637-25
100	5.236-22	3.339-23	6.820-24	2.264-24	9.900-25	5.198-25	3.128-25	2.103-25	1.557-25	1.260-25	1.111-25	1.066-25
120	3.741-22	2.381-23	4.845-24	1.600-24	6.951-25	3.622-25	2.161-25	1.440-25	1.057-25	8.499-26	7.459-26	7.142-26
150	2.493-22	1.582-23	3.203-24	1.051-24	4.523-25	2.331-25	1.374-25	9.040-26	6.556-26	5.214-26	4.543-26	4.339-26
180	1.797-22	1.138-23	2.293-24	7.476-25	3.192-25	1.629-25	9.494-26	6.168-26	4.418-26	3.477-26	3.007-26	2.864-26
220	1.260-22	7.952-24	1.595-24	5.162-25	2.183-25	1.101-25	6.323-26	4.043-26	2.850-26	2.210-26	1.892-26	1.795-26
270	8.818-23	5.547-24	1.107-24	3.554-25	1.487-25	7.399-26	4.181-26	2.624-26	1.813-26	1.381-26	1.166-26	1.101-26
330	6.246-23	3.917-24	7.775-25	2.477-25	1.026-25	5.031-26	2.794-26	1.717-26	1.159-26	8.633-27	7.172-27	6.730-27
390	4.703-23	2.942-24	5.815-25	1.841-25	7.552-26	3.661-26	2.002-26	1.207-26	7.969-27	5.804-27	4.738-27	4.417-27
470	3.435-23	2.144-24	4.217-25	1.326-25	5.386-26	2.576-26	1.383-26	8.149-27	5.234-27	3.701-27	2.949-27	2.723-27
560	2.564-23	1.596-24	3.127-25	9.771-26	3.935-26	1.858-26	9.810-27	5.649-27	3.525-27	2.413-27	1.869-27	1.705-27
680	1.856-23	1.153-24	2.250-25	6.987-26	2.788-26	1.299-26	6.734-27	3.778-27	2.277-27	1.494-27	1.113-27	9.989-28
820	1.361-23	8.436-25	1.640-25	5.065-26	2.005-26	9.238-27	4.706-27	2.576-27	1.499-27	9.392-28	6.676-28	5.862-28
1000	9.779-24	6.053-25	1.173-25	3.605-26	1.416-26	6.455-27	3.234-27	1.726-27	9.669-28	5.740-28	3.839-28	3.270-28

TABLE III (Continued)

b. Helium, Z = 2

θ, deg / V, kv	15	30	45	60	75	90	105	120	135	150	165	180
10	1.806-19	1.167-20	2.435-21	8.325-22	3.771-22	2.060-22	1.293-22	9.061-23	6.964-23	5.808-23	5.222-23	5.041-23
12	1.259-19	8.133-21	1.696-21	5.794-22	2.622-22	1.431-22	8.973-23	6.281-23	4.824-23	4.020-23	3.613-23	3.487-23
15	8.104-20	5.232-21	1.090-21	3.720-22	1.681-22	9.162-23	5.736-23	4.009-23	3.075-23	2.560-23	2.299-23	2.219-23
18	5.659-20	3.652-21	7.604-22	2.591-22	1.169-22	6.365-23	3.978-23	2.777-23	2.127-23	1.769-23	1.588-23	1.532-23
22	3.816-20	2.461-21	5.119-22	1.742-22	7.847-23	4.263-23	2.659-23	1.852-23	1.416-23	1.177-23	1.055-23	1.018-23
27	2.557-20	1.647-21	3.422-22	1.162-22	5.225-23	2.831-23	1.762-23	1.224-23	9.342-24	7.748-24	6.940-24	6.692-24
33	1.730-20	1.114-21	2.310-22	7.829-23	3.510-23	1.897-23	1.177-23	8.153-24	6.206-24	5.136-24	4.595-24	4.429-24
39	1.251-20	8.050-22	1.667-22	5.639-23	2.522-23	1.359-23	8.406-24	5.808-24	4.409-24	3.642-24	3.254-24	3.135-24
47	8.735-21	5.613-22	1.160-22	3.914-23	1.745-23	9.366-24	5.771-24	3.972-24	3.006-24	2.476-24	2.208-24	2.126-24
56	6.246-21	4.009-22	8.288-23	2.781-23	1.235-23	6.605-24	4.053-24	2.778-24	2.094-24	1.720-24	1.531-24	1.473-24
68	4.319-21	2.768-22	5.693-23	1.908-23	8.436-24	4.487-24	2.738-24	1.866-24	1.399-24	1.145-24	1.016-24	9.769-25
82	3.036-21	1.942-22	3.993-23	1.330-23	5.848-24	3.092-24	1.875-24	1.270-24	9.466-25	7.705-25	6.819-25	6.548-25
100	2.097-21	1.339-22	2.736-23	9.088-24	3.973-24	2.086-24	1.234-24	8.427-25	6.235-25	5.044-25	4.445-25	4.262-25
120	1.499-21	9.546-23	1.944-23	6.425-24	2.791-24	1.454-24	8.669-25	5.772-25	4.235-25	3.402-25	2.954-25	2.857-25
150	9.988-22	6.345-23	1.286-23	4.219-24	1.816-24	9.360-25	5.514-25	3.625-25	2.626-25	2.087-25	1.818-25	1.736-25
180	7.202-22	4.564-23	9.209-24	3.003-24	1.283-24	6.544-25	3.811-25	2.474-25	1.770-25	1.392-25	1.203-25	1.146-25
220	5.050-22	3.191-23	6.407-24	2.075-24	8.774-25	4.423-25	2.539-25	1.622-25	1.142-25	8.849-26	7.370-26	7.182-26
270	3.534-22	2.227-23	4.447-24	1.429-24	5.980-25	2.974-25	1.650-25	1.053-25	7.269-26	5.529-26	4.666-26	4.405-26
330	2.504-22	1.573-23	3.125-24	9.962-25	4.125-25	2.024-25	1.123-25	6.896-26	4.650-26	3.458-26	2.870-26	2.692-26
390	1.885-22	1.181-23	2.337-24	7.404-25	3.039-25	1.473-25	8.049-26	4.848-26	3.198-26	2.326-26	1.896-26	1.767-26
470	1.377-22	8.609-24	1.696-24	5.335-25	2.168-25	1.037-25	5.565-26	3.276-26	2.101-26	1.483-26	1.180-26	1.089-26
560	1.028-22	6.411-24	1.259-24	3.933-25	1.584-25	7.484-26	3.949-26	2.272-26	1.416-26	9.673-27	7.461-27	6.822-27
680	7.444-23	4.632-24	9.051-25	2.813-25	1.123-25	5.235-26	2.712-26	1.521-26	9.152-27	5.995-27	4.457-27	3.996-27
820	5.455-23	3.389-24	6.599-25	2.040-25	8.078-26	3.723-26	1.896-26	1.037-26	6.027-27	3.769-27	2.674-27	2.345-27
1000	3.921-23	2.432-24	4.720-25	1.452-25	5.709-26	2.603-26	1.304-26	6.957-27	3.892-27	2.306-27	1.538-27	1.308-27

TABLE III (Continued)

c. Carbon, Z = 6

V, kv \ θ, deg	15	30	45	60	75	90	105	120	135	150	165	180
10	1.629-18	1.054-19	2.201-20	7.526-21	3.408-21	1.551-21	1.167-21	8.172-22	6.276-22	5.231-22	4.700-22	4.537-22
12	1.136-18	7.347-20	1.534-20	5.240-21	2.371-21	1.293-21	8.103-22	5.666-22	4.347-22	3.621-22	3.252-22	3.139-22
15	7.312-19	4.728-20	9.865-21	3.366-21	1.521-21	8.284-22	5.181-22	3.618-22	2.772-22	2.306-22	2.070-22	1.997-22
18	5.107-19	3.302-20	6.892-21	2.346-21	1.059-21	5.757-22	3.595-22	2.506-22	1.918-22	1.594-22	1.429-22	1.379-22
22	3.445-19	2.226-20	4.636-21	1.578-21	7.108-22	3.858-22	2.404-22	1.672-22	1.277-22	1.060-22	9.497-23	9.159-23
27	2.308-19	1.491-20	3.101-21	1.054-21	4.736-22	2.564-22	1.594-22	1.106-22	8.427-23	6.980-23	6.248-23	6.023-23
33	1.562-19	1.008-20	2.094-21	7.103-22	3.184-22	1.719-22	1.065-22	7.367-23	5.599-23	4.628-23	4.137-23	3.986-23
39	1.131-19	7.293-21	1.513-21	5.120-22	2.289-22	1.232-22	7.611-23	5.250-23	3.979-23	3.282-23	2.930-23	2.822-23
47	7.895-20	5.088-21	1.053-21	3.556-22	1.585-22	8.499-23	5.229-23	3.593-23	2.713-23	2.232-23	1.988-23	1.914-23
56	5.647-20	3.633-21	7.513-22	2.529-22	1.123-22	5.998-23	3.674-23	2.513-23	1.891-23	1.550-23	1.378-23	1.326-23
68	3.906-20	2.512-21	5.178-22	1.737-22	7.677-23	4.079-23	2.484-23	1.690-23	1.264-23	1.032-23	9.150-24	8.792-24
82	2.747-20	1.764-21	3.626-22	1.211-22	5.328-23	2.814-23	1.703-23	1.150-23	8.555-24	6.949-24	6.140-24	5.893-24
100	1.898-20	1.217-21	2.493-22	8.290-23	3.624-23	1.900-23	1.140-23	7.641-24	5.638-24	4.550-24	4.003-24	3.836-24
120	1.357-20	8.684-22	1.773-22	5.867-23	2.548-23	1.326-23	7.889-24	5.239-24	3.832-24	3.070-24	2.668-24	2.571-24
150	9.049-21	5.775-22	1.174-22	3.859-23	1.661-23	8.551-24	5.026-24	3.294-24	2.378-24	1.884-24	1.637-24	1.562-24
180	6.528-21	4.157-22	8.417-23	2.750-23	1.175-23	5.986-24	3.478-24	2.251-24	1.605-24	1.257-24	1.084-24	1.031-24
220	4.579-21	2.909-22	5.852-23	1.902-23	8.047-24	4.053-24	2.321-24	1.478-24	1.036-24	7.997-25	6.821-25	6.463-25
270	3.206-21	2.031-22	4.073-23	1.312-23	5.494-24	2.730-24	1.539-24	9.613-25	6.605-25	5.000-25	4.205-25	3.964-25
330	2.272-21	1.436-22	2.865-23	9.153-24	3.796-24	1.881-24	1.031-24	6.305-25	4.251-25	3.131-25	2.587-25	2.423-25
390	1.711-21	1.079-22	2.145-23	6.814-24	2.800-24	1.357-24	7.400-25	4.441-25	2.914-25	2.107-25	1.710-25	1.590-25
470	1.251-21	7.870-23	1.557-23	4.915-24	2.001-24	9.567-25	5.126-25	3.007-25	1.919-25	1.346-25	1.065-25	9.802-26
560	9.336-22	5.853-23	1.170-23	3.627-24	1.464-24	6.916-25	3.645-25	2.090-25	1.295-25	8.788-26	6.752-26	6.159-26
680	6.763-22	4.239-23	8.525-24	2.597-24	1.039-24	4.847-25	2.508-25	1.402-25	8.393-26	5.457-26	4.026-26	3.596-26
820	4.957-22	3.102-23	6.073-24	1.884-24	7.482-25	3.452-25	1.757-25	9.587-26	5.542-26	3.439-26	2.417-26	2.110-26
1000	3.664-22	2.227-23	4.347-24	1.343-24	5.293-25	2.416-25	1.211-25	6.446-26	3.589-26	2.109-26	1.392-26	1.177-26

TABLE III (Continued)

d. Nitrogen, Z = 7

θ, deg / V, kv	15	30	45	60	75	90	105	120	135	150	165	180
10	2.218-18	1.436-19	2.999-20	1.026-20	4.644-21	2.536-21	1.590-21	1.113-21	8.545-22	7.121-22	6.398-22	6.176-22
12	1.547-18	1.001-19	2.090-20	7.141-21	3.231-21	1.762-21	1.104-21	7.717-22	5.919-22	4.929-22	4.426-22	4.272-22
15	9.958-19	6.443-20	1.344-20	4.588-21	2.073-21	1.129-21	7.059-22	4.927-22	3.774-22	3.139-22	2.817-22	2.718-22
18	6.956-19	4.499-20	9.381-21	3.198-21	1.443-21	7.846-22	4.898-22	3.414-22	2.611-22	2.169-22	1.945-22	1.877-22
22	4.692-19	3.034-20	6.319-21	2.152-21	9.690-22	5.258-22	3.276-22	2.278-22	1.739-22	1.443-22	1.293-22	1.247-22
27	3.145-19	2.032-20	4.228-21	1.437-21	6.458-22	3.496-22	2.172-22	1.507-22	1.148-22	9.503-23	8.504-23	8.198-23
33	2.128-19	1.375-20	2.856-21	9.686-22	4.342-22	2.344-22	1.451-22	1.004-22	7.626-23	6.301-23	5.631-23	5.425-23
39	1.540-19	9.942-21	2.053-21	6.904-22	3.122-22	1.680-22	1.038-22	7.194-23	5.420-23	4.469-23	3.988-23	3.840-23
47	1.076-19	6.937-21	1.437-21	4.852-22	2.162-22	1.159-22	7.129-23	4.896-23	3.696-23	3.039-23	2.705-23	2.605-23
56	7.695-20	4.958-21	1.023-21	3.451-22	1.533-22	8.183-23	5.010-23	3.426-23	2.576-23	2.111-23	1.876-23	1.804-23
68	5.324-20	3.426-21	7.066-22	2.371-22	1.048-22	5.565-23	3.388-23	2.303-23	1.722-23	1.405-23	1.246-23	1.197-23
82	3.744-20	2.406-21	4.949-22	1.654-22	7.274-23	3.840-23	2.323-23	1.568-23	1.166-23	9.463-24	8.359-24	8.021-24
100	2.588-20	1.660-21	3.404-22	1.132-22	4.949-23	2.594-23	1.556-23	1.042-23	7.683-24	6.196-24	5.449-24	5.221-24
120	1.850-20	1.185-21	2.421-22	8.015-23	3.481-23	1.811-23	1.077-23	7.145-24	5.223-24	4.181-24	3.659-24	3.499-24
150	1.234-20	7.883-22	1.604-22	5.273-23	2.270-23	1.168-23	6.862-24	4.494-24	3.242-24	2.557-24	2.229-24	2.126-24
180	8.900-21	5.676-22	1.150-22	3.799-23	1.606-23	8.181-24	4.751-24	3.072-24	2.188-24	1.713-24	1.476-24	1.403-24
220	6.244-21	3.972-22	8.012-23	2.601-23	1.100-23	5.541-24	3.172-24	2.018-24	1.413-24	1.090-24	9.286-25	8.797-25
270	4.372-21	2.774-22	5.568-23	1.794-23	7.515-24	3.735-24	2.103-24	1.313-24	9.011-25	6.814-25	5.726-25	5.396-25
330	3.099-21	1.961-22	3.918-23	1.253-23	5.105-24	2.547-24	1.410-24	8.616-25	5.775-25	4.267-25	3.523-25	3.298-25
390	2.334-21	1.474-22	2.933-23	9.325-24	3.833-24	1.857-24	1.012-24	6.071-25	3.979-25	2.873-25	2.329-25	2.164-25
470	1.706-21	1.075-22	2.130-23	6.728-24	2.740-24	1.310-24	7.018-25	4.112-25	2.621-25	1.835-25	1.450-25	1.334-25
560	1.274-21	8.012-23	1.582-23	4.966-24	2.005-24	9.475-25	4.992-25	2.860-25	1.770-25	1.199-25	9.197-26	8.356-26
680	9.227-22	5.793-23	1.139-23	3.556-24	1.424-24	6.642-25	3.437-25	1.920-25	1.148-25	7.448-26	5.484-26	4.895-26
820	6.764-22	4.240-23	8.312-24	2.582-24	1.026-24	4.733-25	2.409-25	1.313-25	7.583-26	4.696-26	3.293-26	2.873-26
1000	4.863-22	3.044-23	5.950-24	1.840-24	7.257-25	3.314-25	1.660-25	8.836-26	4.914-26	2.882-26	1.897-26	1.602-26

TABLE III (Continued)

e. Oxygen, Z = 8

γ, kv \ θ, deg	15	30	45	60	75	90	105	120	135	150	165	180
10	2.899-18	1.577-19	3.922-20	1.341-20	6.072-21	3.315-21	2.078-21	1.434-21	1.116-21	9.302-22	8.396-22	8.066-22
12	2.021-18	1.309-19	2.733-20	9.339-21	4.224-21	2.304-21	1.443-21	1.009-21	7.734-22	6.439-22	5.782-22	5.560-22
15	1.301-18	8.424-20	1.758-20	6.001-21	2.711-21	1.476-21	9.228-22	6.440-22	4.932-22	4.101-22	3.660-22	3.550-22
18	9.091-19	5.883-20	1.227-20	4.184-21	1.887-21	1.026-21	6.404-22	4.462-22	3.412-22	2.824-22	2.541-22	2.451-22
22	6.135-19	3.967-20	8.267-21	2.815-21	1.268-21	6.878-22	4.283-22	2.978-22	2.273-22	1.885-22	1.689-22	1.628-22
27	4.111-19	2.658-20	5.532-21	1.880-21	8.449-22	4.573-22	2.840-22	1.969-22	1.500-22	1.242-22	1.111-22	1.071-22
33	2.782-19	1.795-20	3.737-21	1.268-21	5.682-22	3.066-22	1.898-22	1.312-22	9.966-23	8.232-23	7.355-23	7.086-23
39	2.014-19	1.301-20	2.700-21	9.142-22	4.087-22	2.199-22	1.357-22	9.354-23	7.084-23	5.839-23	5.209-23	5.016-23
47	1.406-19	9.077-21	1.881-21	6.352-22	2.830-22	1.517-22	9.327-23	6.402-23	4.831-23	3.970-23	3.535-23	3.402-23
56	1.006-19	6.488-21	1.342-21	4.519-22	2.007-22	1.071-22	6.556-23	4.480-23	3.367-23	2.758-23	2.451-23	2.356-23
68	6.962-20	4.484-21	9.252-22	3.105-22	1.372-22	7.287-23	4.434-23	3.013-23	2.252-23	1.836-23	1.627-23	1.563-23
82	4.896-20	3.150-21	6.482-22	2.167-22	9.529-23	5.029-23	3.040-23	2.052-23	1.524-23	1.237-23	1.092-23	1.048-23
100	3.385-20	2.174-21	4.459-22	1.484-22	6.485-23	3.398-23	2.037-23	1.363-23	1.005-23	8.098-24	7.118-24	6.820-24
120	2.420-20	1.552-21	3.173-22	1.051-22	4.563-23	2.375-23	1.410-23	9.352-24	6.831-24	5.464-24	4.780-24	4.571-24
150	1.614-20	1.033-21	2.102-22	6.914-23	2.977-23	1.531-23	8.991-24	5.883-24	4.241-24	3.355-24	2.912-24	2.777-24
180	1.165-20	7.435-22	1.508-22	4.930-23	2.105-23	1.073-23	6.226-24	4.023-24	2.863-24	2.239-24	1.928-24	1.833-24
220	8.171-21	5.205-22	1.051-22	3.412-23	1.444-23	7.269-24	4.159-24	2.644-24	1.850-24	1.423-24	1.213-24	1.149-24
270	5.722-21	3.636-22	7.305-23	2.355-23	9.866-24	4.901-24	2.759-24	1.721-24	1.180-24	8.911-25	7.481-25	7.048-25
330	4.056-21	2.571-22	5.140-23	1.645-23	6.822-24	3.344-24	1.850-24	1.130-24	7.564-25	5.582-25	4.603-25	4.307-25
390	3.055-21	1.933-22	3.850-23	1.225-23	5.036-24	2.440-24	1.329-24	7.963-25	5.213-25	3.759-25	3.043-25	2.827-25
470	2.233-21	1.410-22	2.796-23	8.836-24	3.600-24	1.722-24	9.218-25	5.397-25	3.435-25	2.402-25	1.895-25	1.743-25
560	1.667-21	1.051-22	2.076-23	6.525-24	2.636-24	1.246-24	6.560-25	3.755-25	2.322-25	1.570-25	1.202-25	1.091-25
680	1.208-21	7.597-23	1.496-23	4.674-24	1.872-24	8.736-25	4.519-25	2.522-25	1.506-25	9.755-26	7.170-26	6.393-26
820	8.856-22	5.561-23	1.092-23	3.394-24	1.349-24	6.226-25	3.169-25	1.727-25	9.957-26	6.154-26	4.306-26	3.752-26
1000	6.367-22	3.992-23	7.815-24	2.419-24	9.547-25	4.361-25	2.185-25	1.162-25	6.457-26	3.779-26	2.481-26	2.093-26

TABLE III (Continued)

f. Neon, Z = 10

V, kv \ θ, deg	15	30	45	60	75	90	105	120	135	150	165	180
10	4.534-18	2.938-19	6.140-20	2.100-20	9.508-21	5.190-21	3.232-21	2.275-21	1.746-21	1.454-21	1.306-21	1.260-21
12	3.162-18	2.048-19	4.230-20	1.463-20	6.616-21	3.608-21	2.258-21	1.578-21	1.209-21	1.006-21	9.034-22	8.718-22
15	2.036-18	1.319-19	2.734-20	9.402-21	4.247-21	2.312-21	1.445-21	1.008-21	7.712-22	6.410-22	5.750-22	5.547-22
18	1.422-18	9.213-20	1.922-20	6.556-21	2.957-21	1.607-21	1.003-21	6.982-22	5.335-22	4.430-22	3.971-22	3.830-22
22	9.597-19	6.214-20	1.295-20	4.413-21	1.987-21	1.078-21	6.707-22	4.660-22	3.555-22	2.947-22	2.639-22	2.544-22
27	6.483-19	4.164-20	8.673-21	2.949-21	1.325-21	7.167-22	4.449-22	3.083-22	2.346-22	1.941-22	1.736-22	1.673-22
33	4.359-19	2.818-20	5.862-21	1.989-21	8.913-22	4.807-22	2.975-22	2.055-22	1.559-22	1.287-22	1.149-22	1.107-22
39	3.153-19	2.039-20	4.236-21	1.435-21	6.412-22	3.446-22	2.127-22	1.465-22	1.105-22	9.129-23	8.140-23	7.838-23
47	2.202-19	1.423-20	2.952-21	9.972-22	4.443-22	2.380-22	1.462-22	1.003-22	7.589-23	6.208-23	5.525-23	5.316-23
56	1.576-19	1.018-20	2.107-21	7.098-22	3.151-22	1.681-22	1.028-22	7.019-23	5.269-23	4.312-23	3.830-23	3.682-23
68	1.090-19	7.035-21	1.453-21	4.879-22	2.156-22	1.144-22	6.956-23	4.721-23	3.525-23	2.872-23	2.543-23	2.442-23
82	7.571-20	4.943-21	1.013-21	3.406-22	1.498-22	7.901-23	4.772-23	3.217-23	2.386-23	1.934-23	1.707-23	1.637-23
100	5.503-20	3.413-21	7.010-22	2.334-22	1.020-22	5.341-23	3.199-23	2.138-23	1.574-23	1.267-23	1.113-23	1.066-23
120	3.795-20	2.437-21	4.990-22	1.653-22	7.180-23	3.731-23	2.216-23	1.467-23	1.070-23	8.549-24	7.471-24	7.142-24
150	2.530-20	1.622-21	3.309-22	1.069-22	4.688-23	2.410-23	1.414-23	9.236-24	6.648-24	5.250-24	4.532-24	4.339-24
180	1.626-20	1.169-21	2.374-22	7.758-23	3.319-23	1.690-23	9.796-24	6.319-24	4.489-24	3.504-24	3.013-24	2.864-24
220	1.281-20	8.185-22	1.655-22	5.380-23	2.277-23	1.146-23	6.548-24	4.155-24	2.902-24	2.231-24	1.897-24	1.795-24
270	8.976-21	5.720-22	1.151-22	3.715-23	1.557-23	7.733-24	4.348-24	2.707-24	1.852-24	1.396-24	1.170-24	1.101-24
330	6.363-21	4.046-22	8.105-23	2.597-23	1.078-23	5.280-24	2.918-24	1.779-24	1.188-24	8.747-25	7.199-25	6.730-25
390	4.794-21	3.042-22	6.073-23	1.934-23	7.959-24	3.855-24	2.099-24	1.255-24	8.196-25	5.893-25	4.729-25	4.417-25
470	3.505-21	2.220-22	4.413-23	1.397-23	5.694-24	2.723-24	1.457-24	8.515-25	5.405-25	3.764-25	2.965-25	2.723-25
560	2.617-21	1.655-22	3.278-23	1.032-23	4.171-24	1.971-24	1.038-24	5.931-25	3.657-25	2.464-25	1.881-25	1.705-25
680	1.896-21	1.197-22	2.362-23	7.393-24	2.964-24	1.384-24	7.154-25	3.988-25	2.375-25	1.533-25	1.122-25	9.989-26
820	1.390-21	8.761-23	1.724-23	5.370-24	2.137-24	9.869-25	5.021-25	2.733-25	1.572-25	9.680-26	6.743-26	5.862-26
1000	9.997-22	6.291-23	1.235-23	3.829-24	1.513-24	6.917-25	3.465-25	1.842-25	1.021-25	5.951-26	3.889-26	3.270-26

TABLE III (Continued)

g. Argon, Z = 18

V, kv \ θ, deg	15	30	45	60	75	90	105	120	135	150	165	180
10	1.475-17	9.583-19	2.006-19	6.865-20	3.107-20	1.694-20	1.060-20	7.402-21	5.670-21	4.716-21	4.232-21	4.083-21
12	1.029-17	6.687-19	1.399-19	4.786-20	2.164-20	1.178-20	7.364-21	5.135-21	3.929-21	3.265-21	2.926-21	2.825-21
15	6.629-18	4.309-19	9.014-20	3.079-20	1.390-20	7.559-21	4.715-21	3.282-21	2.507-21	2.080-21	1.864-21	1.797-21
18	4.633-18	3.012-19	6.298-20	2.150-20	9.692-21	5.260-21	3.275-21	2.275-21	1.735-21	1.438-21	1.287-21	1.241-21
22	3.128-18	2.033-19	4.250-20	1.448-20	6.519-21	3.530-21	2.193-21	1.520-21	1.156-21	9.565-22	8.554-22	8.243-22
27	2.098-18	1.364-19	2.848-20	9.692-21	4.352-21	2.351-21	1.456-21	1.006-21	7.634-22	6.302-22	5.627-22	5.421-22
33	1.421-18	9.240-20	1.927-20	6.547-21	2.932-21	1.579-21	9.743-22	6.710-22	5.076-22	4.180-22	3.726-22	3.587-22
39	1.029-18	6.692-20	1.394-20	4.728-21	2.112-21	1.134-21	6.974-22	4.787-22	3.610-22	2.965-22	2.639-22	2.539-22
47	7.194-19	4.676-20	9.731-21	3.292-21	1.466-21	7.838-22	4.800-22	3.280-22	2.464-22	2.017-22	1.791-22	1.722-22
56	5.151-19	3.347-20	6.955-21	2.346-21	1.041-21	5.544-22	3.379-22	2.298-22	1.719-22	1.402-22	1.242-22	1.193-22
68	3.567-19	2.317-20	4.805-21	1.616-21	7.138-22	3.780-22	2.290-22	1.548-22	1.151-22	9.338-23	8.247-23	7.913-23
82	2.511-19	1.630-20	3.373-21	1.130-21	4.966-22	2.615-22	1.574-22	1.056-22	7.796-23	6.292-23	5.535-23	5.304-23
100	1.738-19	1.127-20	2.326-21	7.760-22	3.391-22	1.772-22	1.057-22	7.031-23	5.146-23	4.123-23	3.609-23	3.452-23
120	1.244-19	8.059-21	1.659-21	5.509-22	2.392-22	1.241-22	7.337-23	4.833-23	3.504-23	2.784-23	2.424-23	2.314-23
150	8.305-20	5.374-21	1.102-21	3.637-22	1.567-22	8.037-23	4.694-23	3.049-23	2.180-23	1.711-23	1.477-23	1.406-23
180	5.998-20	3.876-21	7.922-22	2.601-22	1.112-22	5.649-23	3.261-23	2.091-23	1.475-23	1.143-23	9.782-24	9.260-24
220	4.213-20	2.719-21	5.535-22	1.806-22	7.650-23	3.842-23	2.186-23	1.379-23	9.554-24	7.286-24	6.159-24	5.817-24
270	2.954-20	1.903-21	3.858-22	1.250-22	5.246-23	2.602-23	1.457-23	9.011-24	6.112-24	4.566-24	3.800-24	3.568-24
330	2.095-20	1.348-21	2.721-22	8.760-23	3.641-23	1.782-23	9.812-24	5.942-24	3.933-24	2.867-24	2.340-24	2.181-24
390	1.580-20	1.015-21	2.042-22	6.537-23	2.696-23	1.305-23	7.078-24	4.205-24	2.721-24	1.935-24	1.548-24	1.431-24
470	1.156-20	7.410-22	1.486-22	4.730-23	1.934-23	9.246-24	4.931-24	2.864-24	1.801-24	1.240-24	9.651-25	8.822-25
560	8.633-21	5.529-22	1.105-22	3.500-23	1.420-23	6.713-24	3.524-24	2.003-24	1.223-24	8.132-25	6.129-25	5.525-25
680	6.258-21	4.003-22	7.976-23	2.513-23	1.011-23	4.726-24	2.439-24	1.352-24	7.978-25	5.077-25	3.662-25	3.236-25
820	4.590-21	2.932-22	5.828-23	1.828-23	7.304-24	3.379-24	1.718-24	9.307-25	5.305-25	3.219-25	2.204-25	1.899-25
1000	3.302-21	2.107-22	4.178-23	1.305-23	5.182-24	2.374-24	1.189-24	6.298-25	3.463-25	1.989-25	1.274-25	1.059-25

TABLE III (Concluded)

h. Air, Z = 7.3105

V, kv \ θ, deg	15	30	45	60	75	90	105	120	135	150	165	180
10	2.420-18	1.567-19	3.273-20	1.119-20	5.068-21	2.767-21	1.735-21	1.214-21	9.322-22	7.767-22	6.978-22	6.735-22
12	1.688-18	1.092-19	2.281-20	7.794-21	3.526-21	1.923-21	1.204-21	8.419-22	6.457-22	5.376-22	4.828-22	4.659-22
15	1.086-18	7.031-20	1.467-20	5.008-21	2.262-21	1.232-21	7.703-22	5.376-22	4.117-22	3.424-22	3.073-22	2.965-22
18	7.589-19	4.910-20	1.024-20	3.491-21	1.575-21	8.564-22	5.345-22	3.725-22	2.849-22	2.366-22	2.122-22	2.047-22
22	5.120-19	3.311-20	6.898-21	2.349-21	1.058-21	5.739-22	3.575-22	2.486-22	1.897-22	1.574-22	1.410-22	1.360-22
27	3.431-19	2.218-20	4.616-21	1.569-21	7.050-22	3.816-22	2.370-22	1.644-22	1.252-22	1.037-22	9.276-23	8.941-23
33	2.322-19	1.500-20	3.116-21	1.058-21	4.741-22	2.558-22	1.584-22	1.095-22	8.320-23	6.873-23	6.142-23	5.917-23
39	1.681-19	1.085-20	2.253-21	7.626-22	3.409-22	1.835-22	1.133-22	7.807-23	5.913-23	4.875-23	4.350-23	4.189-23
47	1.174-19	7.573-21	1.569-21	5.299-22	2.361-22	1.266-22	7.782-23	5.343-23	4.032-23	3.315-23	2.957-23	2.841-23
56	8.398-20	5.413-21	1.119-21	3.770-22	1.674-22	8.936-23	5.470-23	3.739-23	2.810-23	2.302-23	2.046-23	1.968-23
68	5.810-20	3.741-21	7.717-22	2.590-22	1.145-22	6.078-23	3.699-23	2.514-23	1.879-23	1.533-23	1.359-23	1.305-23
82	4.086-20	2.627-21	5.406-22	1.807-22	7.946-23	4.195-23	2.536-23	1.712-23	1.272-23	1.032-23	9.117-24	8.748-24
100	2.825-20	1.813-21	3.719-22	1.237-22	5.407-23	2.834-23	1.699-23	1.138-23	8.385-24	6.760-24	5.944-24	5.694-24
120	2.020-20	1.294-21	2.646-22	8.759-23	3.804-23	1.978-23	1.176-23	7.802-24	5.701-24	4.562-24	3.991-24	3.817-24
150	1.347-20	8.611-22	1.753-22	5.763-23	2.481-23	1.277-23	7.498-24	4.908-24	3.539-24	2.801-24	2.431-24	2.319-24
180	9.717-21	6.201-22	1.257-22	4.109-23	1.755-23	8.943-24	5.191-24	3.355-24	2.389-24	1.869-24	1.609-24	1.531-24
220	6.818-21	4.340-22	8.758-23	2.844-23	1.203-23	6.058-24	3.467-24	2.205-24	1.543-24	1.189-24	1.013-24	9.595-25
270	4.774-21	3.032-22	6.088-23	1.962-23	8.220-24	4.084-24	2.300-24	1.435-24	9.841-25	7.437-25	6.246-25	5.885-25
330	3.384-21	2.143-22	4.284-23	1.371-23	5.683-24	2.786-24	1.541-24	9.417-25	6.308-25	4.658-25	3.843-25	3.597-25
390	2.549-21	1.611-22	3.208-23	1.020-23	4.194-24	2.032-24	1.107-24	6.637-25	4.347-25	3.136-25	2.540-25	2.360-25
470	1.863-21	1.175-22	2.330-23	7.362-24	2.998-24	1.434-24	7.678-25	4.498-25	2.864-25	2.004-25	1.582-25	1.455-25
560	1.391-21	8.758-23	1.730-23	5.435-24	2.195-24	1.037-24	5.463-25	3.129-25	1.935-25	1.309-25	1.003-25	9.114-26
680	1.008-21	6.333-23	1.246-23	3.892-24	1.558-24	7.273-25	3.763-25	2.101-25	1.255-25	8.136-26	5.985-26	5.338-26
820	7.387-22	4.635-23	9.093-24	2.826-24	1.123-24	5.183-25	2.638-25	1.438-25	8.295-26	5.131-26	3.594-26	3.133-26
1000	5.311-22	3.328-23	6.510-24	2.014-24	7.947-25	3.630-25	1.819-25	9.675-26	5.378-26	3.150-26	2.071-26	1.748-26

APPENDIX III
DESIGN OF DYNAMIC PUMPING SYSTEMS

The problem in designing a pumping system such as that shown in Fig. 10 is to predict the pressure in the gun volume as a function of the pressure in the test cell. The orifice dimensions and the characteristics of the pumps are known. In the usual case, the pressure ratio across each orifice is so high that the downstream pressure has an insignificant effect on the flow through the orifice. The flow is then a function only of the upstream pressure.

The ratio between the mass flow and the upstream pressure depends upon the mechanism controlling the flow, and three regimes may be distinguished. At high densities, the orifice behaves as a choked nozzle, and the mass flow is proportional to upstream pressure. There is a small effect on the flow caused by the length of the orifice, because of the boundary layer which builds up on the orifice walls. At lower densities, the boundary layer becomes thicker and eventually merges, and the flow becomes laminar. Mass flow is then proportional to the square of the upstream pressure. At still lower densities, collisions between molecules become infrequent, and the mass flow is governed by the probability that a molecule will enter the orifice in the correct direction to pass through. The mass flow in the molecular flow regime is again proportional to the upstream pressure.

The design becomes simpler if it is assumed that the gas flows at constant temperature. Since only modest accuracy is required of the solution, this assumption is often justified. In many cases the gas upstream of the orifice is at room temperature. In the molecular flow regime (and perhaps also in the laminar flow regime) the gas temperature may be taken as the temperature of the orifice walls, which are usually at room temperature. The design procedure presented here assumes that the gas temperature remains at 300°K. Schumacher (Ref. 22) discusses corrections to be applied if significantly different conditions are encountered.

If the gas temperature remains constant, the mass flow is proportional to the volume flow past a point and to the pressure at that point, and mass flow may then be measured in units of pressure times volume flow (e.g., torr - liters per second). The state of the gas at any point in the system may be plotted on full logarithmic paper, with pressure on the abcissa and volume flow on the ordinate (Fig. 48a). As the gas expands through an orifice, the state of the gas will shift along a line with a slope of -1.

The volume flow through a pump is a function only of the inlet pressure, so the characteristic of a pump may be specified by a single curve (the "conduction curve") on the volume flow versus pressure chart. The same is true of an orifice of given dimensions. Although the conduction curve of a pump may be obtained from the manufacturer's literature, no such convenient source is available for orifice conduction curves.

The conduction curve of an orifice (volume flow versus pressure) may be approximated by three straight line asymptotes, one for each of the flow regimes. In the choked flow and molecular flow regimes, the asymptotes are lines of constant volume flow (slope of zero). In the laminar flow regime, volume flow is proportional to pressure (slope of +1). A graphical construction is described in Ref. 22 which allows one point on each asymptote to be determined, for any given orifice.

An alternative method of obtaining the orifice conduction curve is to use an overlay such as that shown in Fig. 48b. It can be shown that for a given ℓ/d ratio, volume flow is proportional to d^2 in the choked flow and molecular flow regimes, and to d^3 in the laminar flow regime. As a result, the conduction curves of all orifices of the same ℓ/d ratio are geometrically similar. It is then possible to draw a family of conduction curves on an overlay, one curve for each ℓ/d ratio. The curves can be used with orifices of any diameter by properly positioning the overlay on the volume flow versus pressure chart. Figures 48a and b present the same data which is available in Ref. 22, but in a more convenient form. In particular, the effect upon the entire curve of a change in orifice length or diameter is immediately apparent. Instructions for positioning the overlay are given in Fig. 48b. Figures 48a and b cover a large range of diameters and can be used to determine the conductance of large pipes and hoses, as well as small orifices.

The complete solution of a two-stage pumping problem is shown in Fig. 49. The system consists of two identical orifices 0.016-in. diameter by 0.060 in. long. The volume between the orifices is pumped by a 5-cfm mechanical pump, and the volume behind the downstream orifice is pumped by a 60-ℓ/sec diffusion pump. The solution for an inlet pressure of 50 torr is shown. The mass flow through the first orifice is determined by the intersection of the orifice conduction curve with the 50 torr line. This entire mass flow enters the mechanical pump (the mass flow through the second orifice being negligible), and thus determines the pressure between the orifices (0.3 torr). The pressure behind the second orifice is determined by an identical construction to be 2×10^{-5} torr. The procedure may easily be repeated for a number of inlet pressures.

Several errors are inherent in this simplified procedure. The error caused by the assumption of constant temperature flow has been mentioned. There will also be an error caused by the use of the asymptotic curve if the construction intersects the curve near a corner. The actual curve is rounded at the corners as is shown by the dashed curve in Fig. 49. There may also be an error if the jet from the first orifice impinges upon the second orifice with an appreciable total pressure. Each of these errors is discussed in Ref. 22.

Security Classification

DOCUMENT CONTROL DATA - R&D

(Security classification of title, body of abstract and indexing annotation must be entered when the overall report is classified)

1 ORIGINATING ACTIVITY (Corporate author) Arnold Engineering Development Center ARO, Inc., Operating Contractor Arnold Air Force Station, Tennessee	2a REPORT SECURITY CLASSIFICATION UNCLASSIFIED 2b GROUP N/A

3 REPORT TITLE

MEASUREMENT OF GAS DENSITY BY ELECTRON SCATTERING

4 DESCRIPTIVE NOTES (Type of report and inclusive dates)

N/A

5 AUTHOR(S) (Last name, first name, initial)

Cunningham, J. W. and Fisher, C. H., ARO, Inc.

6 REPORT DATE	7a TOTAL NO OF PAGES	7b NO OF REFS
February 1967	118	26

8a CONTRACT OR GRANT NO.	9a ORIGINATOR'S REPORT NUMBER(S)
AF40(600)-1200 b PROJECT NO. 8951	AEDC-TR-66-212
c Program Element 61440514 d Task 895105	9b OTHER REPORT NO(S) (Any other numbers that may be assigned this report) N/A

10 AVAILABILITY/LIMITATION NOTICES

Distribution of this document is unlimited.

11 SUPPLEMENTARY NOTES	12 SPONSORING MILITARY ACTIVITY
Available in DDC	Arnold Engineering Development Center Air Force Systems Command Arnold Air Force Station, Tennessee

13 ABSTRACT It is theoretically possible to infer the density of a gas from the rate at which particles are scattered out of a beam of subatomic particles which is passed through the gas. This technique offers the possibility of a probeless density measurement which is independent of the state of the gas. Previous research verified that this technique could be implemented using a gamma ray beam, but that the best spatial resolution and measuring time which could be achieved were inadequate to allow the technique to be applied to a low density test facility. In the research reported herein, the technique was applied using a 50,00-v electron beam. It was found that excellent spatial resolution and measuring time could be achieved at densities as low as 6 x 10^{-8} gm/cm^3. Density profiles were measured in a low density wind tunnel with a nozzle exit diameter of 18 in. and an open jet test section. A spatial resolution of about 1 cm was achieved, and measurements required 10 sec per point. This measuring time can probably be reduced by several orders of magnitude if necessary. The densities measured were repeatable within 1 percent. Accuracy, spatial resolution, and measuring time are found to be interrelated. The constraint on the combination is discussed in detail. The design of equipment is discussed.

DD FORM 1 JAN 64 1473

Security Classification

14 KEY WORDS	LINK A		LINK B		LINK C	
	ROLE	WT	ROLE	WT	ROLE	WT
density						
electron scattering						
subatomic particles						

INSTRUCTIONS

1. ORIGINATING ACTIVITY: Enter the name and address of the contractor, subcontractor, grantee, Department of Defense activity or other organization *(corporate author)* issuing the report.

2a. REPORT SECURITY CLASSIFICATION: Enter the overall security classification of the report. Indicate whether "Restricted Data" is included. Marking is to be in accordance with appropriate security regulations.

2b. GROUP: Automatic downgrading is specified in DoD Directive 5200.10 and Armed Forces Industrial Manual. Enter the group number. Also, when applicable, show that optional markings have been used for Group 3 and Group 4 as authorized.

3. REPORT TITLE: Enter the complete report title in all capital letters. Titles in all cases should be unclassified. If a meaningful title cannot be selected without classification, show title classification in all capitals in parenthesis immediately following the title.

4. DESCRIPTIVE NOTES: If appropriate, enter the type of report, e.g., interim, progress, summary, annual, or final. Give the inclusive dates when a specific reporting period is covered.

5. AUTHOR(S): Enter the name(s) of author(s) as shown on or in the report. Enter last name, first name, middle initial. If military, show rank and branch of service. The name of the principal author is an absolute minimum requirement.

6. REPORT DATE: Enter the date of the report as day, month, year, or month, year. If more than one date appears on the report, use date of publication.

7a. TOTAL NUMBER OF PAGES: The total page count should follow normal pagination procedures, i.e., enter the number of pages containing information.

7b. NUMBER OF REFERENCES: Enter the total number of references cited in the report.

8a. CONTRACT OR GRANT NUMBER: If appropriate, enter the applicable number of the contract or grant under which the report was written.

8b, 8c, & 8d. PROJECT NUMBER: Enter the appropriate military department identification, such as project number, subproject number, system numbers, task number, etc.

9a. ORIGINATOR'S REPORT NUMBER(S): Enter the official report number by which the document will be identified and controlled by the originating activity. This number must be unique to this report.

9b. OTHER REPORT NUMBER(S): If the report has been assigned any other report numbers *(either by the originator or by the sponsor)*, also enter this number(s).

10. AVAILABILITY/LIMITATION NOTICES: Enter any limitations on further dissemination of the report, other than those imposed by security classification, using standard statements such as:

(1) "Qualified requesters may obtain copies of this report from DDC."

(2) "Foreign announcement and dissemination of this report by DDC is not authorized."

(3) "U. S. Government agencies may obtain copies of this report directly from DDC. Other qualified DDC users shall request through _____."

(4) "U. S. military agencies may obtain copies of this report directly from DDC. Other qualified users shall request through _____."

(5) "All distribution of this report is controlled. Qualified DDC users shall request through _____."

If the report has been furnished to the Office of Technical Services, Department of Commerce, for sale to the public, indicate this fact and enter the price, if known.

11. SUPPLEMENTARY NOTES: Use for additional explanatory notes.

12. SPONSORING MILITARY ACTIVITY: Enter the name of the departmental project office or laboratory sponsoring *(paying for)* the research and development. Include address.

13 ABSTRACT. Enter an abstract giving a brief and factual summary of the document indicative of the report, even though it may also appear elsewhere in the body of the technical report. If additional space is required, a continuation sheet shall be attached.

It is highly desirable that the abstract of classified reports be unclassified. Each paragraph of the abstract shall end with an indication of the military security classification of the information in the paragraph, represented as *(TS), (S), (C), or (U)*.

There is no limitation on the length of the abstract. However, the suggested length is from 150 to 225 words.

14. KEY WORDS: Key words are technically meaningful terms or short phrases that characterize a report and may be used as index entries for cataloging the report. Key words must be selected so that no security classification is required. Identifiers, such as equipment model designation, trade name, military project code name, geographic location, may be used as key words but will be followed by an indication of technical context. The assignment of links, rules, and weights is optional.